Aerodynamic design of Vertical Axis Wind Turbines

by

R.A.McD. Galbraith
F.N. Coton
D. Jiang

GU Aero Report No. 9246 December 1992

FINAL REPORT

for SERC Award No. GR/F63466

AERODYNAMIC DESIGN OF VERTICAL AXIS WIND TURBINES

BY

R.A.MCD. GALBRAITH
F.N. COTON
JIANG DACHUN

GU. Aero. Rpt. No. 9246

December, 1992

SUMMARY

This is the final report of research project GR/F 63466 on the Aerodynamic Design of Vertical Axis Wind Turbines. It is divided into two main sections. First, a general overview of the content, management and success of the work. Second, detailed technical information describing the design tools developed and experiments performed.

Although the experimental programme, to test three appropriate aerofoil sections, had minor modification for reasons explained, three aerofoils were tested and the data distributed before archiving. Likewise, the proposed design code was subject to minor modification but a successful distorted wake model, including unsteady viscous effects, with typical run times well within designers requirements, was developed and is in current use. The package permits a wide range of blade designs that include taper, pitch, twist and change of aerofoil section along the span. The code has been delivered to Vertical Axis Wind Turbines Ltd.

CONTENTS

SECTION 1

OVERVIEW

1.1 INTRODUCTION

For many years, the wind energy community within Britain have had an active interest in the design and development of large-scale vertical axis wind turbines. The prime motivation for this was an anticipation that, for multi-megawatt machines, the economics of the vertical axis wind turbine would be more favourable than that of its horizontal axis counterpart. In addition, the apparent simplicity of their mechanical design and their omnidirectional capability augured well for their placement in large offshore wind farms.

Although, as mentioned above, there was an apparent simplicity of mechanical design, the aerodynamic environment and operation of the blades is indeed complex, for the turbine operation relies on the apparent unsteady flow past the aerofoil. As a consequence of this and a lack of detailed knowledge, little was known as to the manner in which the choice of aerofoil section or blade geometry should be made. Several research programmes were addressing this problem and included detailed pressure measurements on wind turbines, two-dimensional dynamic stall of typical turbine sections, and aerofoil design procedures.

Albeit much was gained from the research, designers were still without codes for the detailed aerodynamic design of the blades. They required an aerodynamic performance model which could produce useful information in minutes rather than many hours. After all, the design process is predominantly iterative and heuristically based so that, for any one design, the code may be required to run several hundred times. The present study was specifically designed to provide some of the necessary tools.

Glasgow University, under the Department of Energy funding, had already developed an aerofoil design code and had the skills to produce codes for assessing the unsteady aerodynamic performance of the designed aerofoil. In addition, they were also at the early stages of developing a prescribed wake model for vertical axis wind turbines. The technique had the potential of a greatly reduced execution time when compared to that of a free-wake model. Early indications were that a target of under ten minutes per run, with the then available computers, was possible. The first model, however, required detailed extension and the inclusion of an unsteady aerodynamic coefficient assessment (e.g. the Beddoes model).

The combining of these two codes (i.e., the prescribed wake and the Beddoes model) was an interesting and successful activity resulting in a design tool which relaxed previous geometric constraints placed upon the turbine blades. It also elevated the level of aerodynamic analysis of such machines to that of its horizontal axis equivalent. For any new turbine, the designer is now free to include the effects of pitch angle, blade taper, blade twist and the use of different aerofoil sections along the span. The code is also useful to structural designers because the detailed output may be the input to an aeroelastic code.

In parallel with the above, it was clear that a form of validation would be required using experimental data. An appropriate programme to test three new programme aerofoils was proposed but this was modified to account for changing circumstances. Three aerofoils were tested and confirmed not only the appropriateness

of the test technique, but also the design procedures. The prime objective of the test was to ensure that our procedures would allow the designer to choose the approximate stalling angle is important for passively stall regulated machines. Two new aerofoils were designed and tested and achieved the design specification. The third aerofoil, however, was of a standard section previously assessed at Glasgow University but with only half the chord length of its predecessor. The undoubted purpose of this test was to verify and validate that our testing technique with the larger models was adequate for the purpose intended. This was necessary because of observed peculiarities in the measured data and so it became incumbent upon us to ensure that our extant procedures were not responsible. The fact that we did proceed with the old set-up on the third test session, is evidence that all was well.

In conclusion, therefore, all the main goals of the project were achieved and the test results distributed to industry together with delivery of the design codes to Vertical Axis Wind Turbine Ltd.

1.2. ACHIEVEMENT OF GOALS AND PROGRAMME ALTERATIONS

Figure 1 is a copy of Figure 5 from the original proposal in which the anticipated flow of work throughout the project was given. It will be observed that there were three main activities, two of which were dominant and the third, although successfully completed, of less importance. The main two were, the development of a prescribed wake model for use in the design of vertical axis wind turbines, and the wind tunnel testing of three chosen aerofoils.

The prescribed wake code was successfully completed although, in the final version, we chose to ignore the effects of tower shadow and ground proximity. We did, however, include losses associated with the crossarm and the blade crossarm junction. At an early stage it was realised that the inclusion of the Tom Beddoes code for the assessment of unsteady aerofoil behaviour would be more difficult than first appreciated. Accordingly, a fixed wake model was constructed to test its implementation so working in parallel with the development of the prescribed wake model. This proved to be an exceptionally useful procedure and facilitated a relatively easy implementation of the Beddoes model in the full prescribed wake code. The Beddoes code, however, required a re-specification of the thrust coefficient to render it appropriate. The codes developed are now capable of modifying the aerofoil shape to give a specified stall angle and the wind turbine blades may be designed to have the prescribed pitch, twist, taper and specified aerofoil sections along the blade.

As mentioned in the Introduction, the experimental phase of the work was altered in the light of anomalies observed in other data. These were a disharmony between Glasgow data and that from other test facilities in America, and an unforeseen negative lift at high incidence during rapid pitch down motions not, so far, evident elsewhere.

To assess the appropriateness of the Glasgow facility, the second aerofoil tested was a NACA 0015 with half the chord length of a previous model with the same section. This gave a large change in the wind tunnel blockage, making the test conditions marginally more favourable than those in America the data from which were at odds with those from Glasgow. Fortunately, for these new tests, little change to the aerodynamic performance of the aerofoil could be observed when compared to the larger model tests. The results were so convincing that, for practical reasons, we returned to our original set up for the final aerofoil test of the programme. Analysed data from the NACA 0015 tests were presented at the International Congress of Aerospace Science in Beijing in 1992.

In collaboration with Vertical Axis Wind Turbines Ltd., a third model was tested and finally closed the loop in our verification procedures. All test data have been distributed and archived on the Glasgow University database in standard form and published as test reports. A summary of these is included with this report.

1.3 CONCLUDING REMARKS

All the main project goals have been achieved. Although vertical axis wind turbines no longer receive the interest they had when the project started, their aerodynamic analysis is now at a comparable level to HAWT's. Additionally, the techniques developed are now being applied to HAWT's for the consideration of yaw and dynamic inflow. (SERC GR/H 82105)

SECTION 2

TECHNICAL

2.1. INTRODUCTION

The following sections outline the areas of technical achievement associated with the present study. There are three main sections, these deal with performance prediction methods, blade design parameters and wind tunnel testing. Finally, an overall assessment of the work is made and future prospects are outlined.

2.2 VAWT PERFORMANCE PREDICTION METHODS

It is well known that a vertical axis wind turbine (VAWT), which generally has a simple geometric configuration, experiences a very complicated flow field environment as shown in Figure 2.1. When calculating the flow field around a VAWT many parameters have to be considered.

Historically, the performance of vertical axis wind turbines has been satisfactorily assessed by momentum methods in the form of multiple stream tubes with either single or double actuation discs. Such methods are both adequate and fast for the purpose intended but, when time-dependent details of the local flow states are required, other methods must be employed. Currently, detailed aerodynamics can be provided by vortex wake methods and they represent the most sophisticated tools available for aerodynamic design. The purest application of the vortex method is the so-called free wake method in which the turbine is represented by filaments of shed and trailing vorticity that are free to convect at will. The associated computation time, unfortunately, renders the technique inappropriate for day to day design practice and, consequently, hybrid methods which blend elements of momentum theory and vortex theory are generally preferred. One such technique is the Fixed Wake approach of Wilson and Walker.

As with most vortex based techniques, the Fixed Wake method inherently includes some of the unsteady aspects of the turbine flowfield. In particular, the inclusion of the vortex system automatically accounts for the induced 'history effect' from the circulation in the turbine wake. This results in a more accurate specification of instantaneous blade loadings but the technique suffers from the simplistic nature of its wake model.

Another hybrid method is the Prescribed Wake technique of Basuno et al. The Prescribed Wake model again uses a combination of vortex and momentum theory to obtain a solution for the flow around a vertical axis wind turbine. In the technique vortex elements, corresponding to the spanwise and azimuthal blade loading variations, are shed from the turbine and follow a path prescribed by consideration of momentum theory. The induced effect which the wake has on the blade loadings is then calculated according to vortex theory. This technique can be extremely accurate if the wake is correctly prescribed.

A particular feature of vortex methods, however, is that the detailed information relating to the aerodynamic coefficients of the blade aerofoil section are normally taken to be those from steady experiments. In other words, it is the standard aerodynamic data which can be obtained from most aerofoil catalogues. Thus, whilst the prescribed or indeed the free-wake methods provide unsteady aerodynamic information from the wake,

the aerodynamic data for the aerofoil is derived from static data. It is because of this that such methods may be classified as quasi-steady.

Where a vertical axis wind turbine operates at low tip speed ratios, the aerofoil environment is truly unsteady and, indeed, may exhibit excursions in incidence far beyond the static stall incidence and an associated reduced frequency which places it firmly in the full dynamic stall domain. The differences between the static and dynamic aerofoil coefficients are illustrated in Fig. 2.2. where it may be seen that, in the critical low tip speed ratio region, the use of static data could lead to significant predictive inaccuracies. The obvious deficiency, however, can be alleviated by the inclusion of an aerofoil unsteady-performance code.

Whilst there are several such predictive codes available, that chosen in the present study is attributable to Leishman and Beddoes and was developed for helicopter rotor performance assessments. The vertical axis wind turbine is not a helicopter rotor and so, as anticipated, a few modifications have been incorporated to render it more appropriate to the current application.

In the following sections, several predictive configurations are described. Initially, the fundamental Prescribed Wake technique is detailed. This is followed by a combined Fixed Wake - dynamic stall model which was used to assess the influence of dynamic aerofoil performance on the low tip speed ratio regime. The final method is the combined Prescribed Wake - dynamic stall technique which is the most sophisticated aerodynamic model of a VAWT currently available. This technique is then used to examine the influence of blade pitch, twist, taper and aerofoil profile on the operating characteristics of an H-configured vertical axis wind turbine.

2.2.1. The Prescribed Wake Method

The Prescribed Wake method follows the philosophy of a fixed wake approach in that the influence which the wake has on itself is not directly considered during a calculation. Instead, it is considered that accurate prescription of the wake shape should adequately account for this effect. This form of wake modelling also removes the requirement to build up the wake in a step-by-step manner and so it is possible to prescribe a wake consisting of many cycles at the outset of the calculation. In addition, the existence of unrepresentative vortex filament strengths at the rear of the wake has been removed by updating all filament strengths in the wake as the calculation progresses. By constantly updating wake elements in this way, it has been possible to accelerate convergence and thus significantly reduce the computation time associated with the model.

The vortex method which forms the core of the prescribed wake model is illustrated in Fig. 2.3. In it, the spanwise blade loading distribution is approximated by a series of bound vortex segments of constant strength. In this way, a vorticity imbalance is created between adjoining bound vortex segments. This is resolved by the creation of trailing vortex filaments whose strengths are defined by the difference in vorticity from one bound vortex element to the next. The strengths of the vortex filaments trailing from the blade tips are simply equivalent to those of the corresponding bound vorticity segments.

The change of turbine blade incidence with time necessitates inclusion of the influence of the associated variation of blade bound vorticity. This is achieved by considering the blade incidence variation in discrete time steps and producing shed vortices, equivalent to the resulting change in circulation, from each blade segment at every time step. In this way, a lattice of shed and trailing vortex elements is generated behind the turbine blade.

As indicated above, the vortex systems which trail from the turbine blade, are constrained to follow a pre-determined path derived from momentum theory. Thus, in the initial stages of the calculation procedure, although the wake shape is known, the strengths of the vortex elements in the wake and on the blades must be calculated. It is, therefore necessary to adopt an iterative procedure in which the wake shape is fixed and the values of shed and trailing vorticity in the wake are systematically adjusted to correspond to the variations in circulation and spanwise bound vorticity on the turbine blades. The starting values for the iteration process are determined from the loadings associated with the variation of blade geometric incidence. The particular scheme adopted involves considering the induced effect of the wake at a given blade position, via the Biot-Savart relationship, and then updating the corresponding shed and trailing vorticity terms before moving to the next blade position. By only changing the specific vorticity values which correspond to the azimuthal position under consideration, the remainder of the vortex wake effectively damps the iteration process and so enhances the convergence characteristics of the system.

The purpose of the momentum model in the prescribed wake method is to provide initial estimates of convection velocities at each azimuthal position on the turbine. These velocities are then used to construct a basic wake shape which, in turn, is used to provide more accurate estimates of blade loadings. A further application of momentum theory, is then employed to provide a final wake shape. It is, therefore, essential that the momentum model used is sufficiently accurate to permit a realistic estimate of the actual wake shape to be generated. A double-multiple streamtube model was ultimately incorporated into the prescribed wake scheme. The main advantage which this type of momentum model has over the simpler methods is its ability to differentiate between the induced velocities on the upwind and downwind passes of the turbine blade. This feature was found to be crucial when vortex convection in the near-wake region is being considered.

To develop a first estimate of the wake shape associated with a vertical axis wind turbine, it is necessary to model the rate of convection of vorticity elements downstream. In the prescribed wake method, a first approximation to the induced velocities at each blade position is provided by the double-multiple streamtube model. This allows a simple wake geometry to be derived by convecting vortex elements downstream at the resultant of the incoming and the calculated induced streamwise velocities. Although this approach is not strictly in keeping with momentum theory, since the calculated wake velocity is not used, the estimated wake shape compares favourably with that of the free-vortex model.

The predicted variation of turbine power coefficient versus tip-speed ratio from this basic wake model compares well with that predicted by the free-wake method. The corresponding variations in instantaneous blade loadings, however, are not modelled quite as well. A detailed comparison with the free-wake method indicates that the poor loading predictions of this wake model stem from its inability to account for near and far wake convection velocities. In particular, the near wake from the upstream blade pass, which often lies within the turbine swept perimeter and has a strong influence on the induced velocity field at the turbine, is badly modelled. This problem is alleviated by the next stage of the wake prescription process which consists of modifications to the above wake geometry based on momentum considerations and observations made by extracting pertinent information from the free-vortex method. Also, at this stage, wake expansion is included.

In this second level modification, the calculated estimates of induced velocities at the blades are used, via the expressions derived from momentum theory, to modify the wake in both the streamwise and cross-stream directions. New induced velocities are then calculated by iteration. The overall procedure is outlined in Fig 2.4 and Fig. 2.5 illustrates the quality of agreement obtained between the prescribed wake model and the free wake method at tip-speed ratio five. The technique achieves the same accuracy

levels as the free vortex model but with a reduction in computation time of approximately two orders of magnitude.

The main purpose behind the development of the prescribed wake model was to provide an accurate and computationally efficient three-dimensional modelling tool for use in the design of both Darrieus and straight bladed vertical axis wind turbines. It was envisaged that the model would be used primarily to provide estimates of instantaneous blade forces and moments for aerodynamic-structural interaction analyses. As such, power predictions obtained from the prescribed wake method are subject to errors associated with the omission of features such as crossarms, towers or support wires from the model. The configuration of the Darrieus turbine, however, is approximated reasonably well by the 'clean' model and so it is possible to compare the predicted power coefficients with those obtained in field tests.

In Fig. 2.6. the power coefficient predictions from the prescribed wake model are compared with field data obtained from the Sandia 17 meter Darrieus turbine at a rotational speed of 38.7 revolutions per minute. As can be observed from the figure, the prediction compares reasonably well with the field data over the entire range of tip-speed ratios. It is clear, however, that the predictions obtained at high tip speed ratios show the greatest discrepancies with the field data. This is a likely consequence of the sensitivity of the high tip speed ratio cases to the accuracy with which the shape of the closely packed near wake structure, which may partially be contained within the turbine swept volume, is prescribed. Comparison of the prescribed wake shapes with those of the free vortex method indicate that a slight under-prediction of wake convection velocities occurs at high tip speed ratios. Although this difference is small, it produces a lower power coefficient. Additionally, the solution is particularly sensitive to differences between the input two-dimensional aerofoil tangential force coefficients and those actually experienced by the turbine blade profile. This is especially true at high tip speed ratios where the effective incidence range of the turbine blades is low.

2.2.2 The Fixed Wake Method with Unsteady Aerodynamics

The particular Fixed Wake analysis technique used in this study was originally developed by Walker and Wilson Again, this method is a combination of vortex theory and momentum theory. In the technique, the air flowing through a turbine is divided into a number of streamtubes, as shown in Fig.2.7. From momentum theory, it is possible to determine an interference factor 'a' which gives an indication of the decrement in freestream velocity resulting from the action of the turbine blades. This information, in isolation, is insufficient to provide a closed solution to the VAWT problem. In particular, the differential loading on the front and rear blade passes must be resolved. This is achieved by consideration of vortex theory.

The particular scheme adopted by Wilson and Walker involves considering each streamtube as a vortex cell which is bounded by the upwind and downwind blade passes and from which a shed vortex system emanates. The vortex cell is generated by assuming that the aerofoil travels along the edges of the cell and sheds circulation at each of the corner points. By then considering each vortex cell in isolation, the induced velocity on the upwind blade is related only to the semi-infinite wake shed from the upwind portion of the vortex cell. In a similar manner, the velocity induced on the downwind blade pass is obtained by consideration of the shed vortex systems from both the front and the rear of the vortex cell.

As a result of this analysis, it is possible to divide the total interference factor for the turbine into components representing the upwind and downwind blade passes respectively which are related to the streamwise velocities experienced on the turbine blades.

With the vortex system configured in this way, a relationship between the upwind and downwind interference factors and the strength of the shed vorticity elements can be established. This relationship, via the Kutta-Joukowski theorem, provides closure of the system of equations.

In the original Fixed Wake method of Wilson & Walker, some contributions resulting from the dynamic motion of the aerofoil were taken into account. These terms did not fully address the dynamic nature of the flow and so were withdrawn from the present scheme to facilitate implementation of a more comprehensive dynamic model.

As indicated in the introduction, the influence of unsteady aerodynamics on wind turbines can be profound especially at low tip-speed ratios. Under these conditions, predictions of both power coefficients and instantaneous force are often in error when quasi-steady aerodynamics are used for the blade section characteristics; usually values are under estimated. Veers showed that an error of 30% in the prediction of dynamic air loads on V.A.W.Ts can result in a reduction by a factor of 70 in the expected life span of wind turbines. Since dynamic-stall effects can, in the extreme case, produce a difference from static results of up to 100% in air loads, the development of prediction techniques which incorporate unsteady aerodynamics has become an important area in the advancement of wind-turbine technology.

The unsteady aerodynamic response of an airfoil to a specific time history of forcing can now be determined in considerable detail and accuracy using numerical solutions of the Navier-stokes equations. Unfortunately, the required computational resources for this kind of solution method are so extreme that it will not be suitable as a design tool for some time. For this type of application, semi-empirical dynamic stall models are currently more appropriate. One such technique is that due to Leishman and Beddoes.

The main features of this technique may be summarised as follows:

(1) Unsteady effects during attached flow conditions are represented by an indicial formulation.
(2) Nonlinearities in the aerofoil behaviour, related to small amounts of trailing edge separation, are represented using a Kirchhoff flow model.
(3) The onset of vortex shedding during dynamic stall is identified using a criterion for leading edge or shock induced separation based on the attainment of a critical leading edge pressure.
(4) The induced vortex lift and the associated pitching moment are represented empirically in a time dependent manner during dynamic stall.

The model has been validated for the prediction of rotorcraft airloads as part of an overall aeroelastic analysis and is also very efficient due to its explicit algebraic format.

In the model, the attached flow behaviour is simulated by the superposition of indicial aerodynamic responses. These indicial responses result from a step change in, for example, incidence and can be decomposed into non-circulatory and circulatory parts. The non-circulatory component represents the initial response of the flow to the applied step change. This initial loading, which is obtained via piston theory, decays rapidly with time. Conversely, the circulatory loading, on application of the step input, builds up rapidly towards a steady state value in a manner analagous to a body experiencing a sharp-edged gust.

In order to extend this approach to consider the continually varying incidence experienced by, for example, helicopter and wind turbine blades, it is necessary to

break the motion down into a series of step inputs. The cumulative response to the aerofoil motion is then calculated using an appropriate superposition technique.

As has been observed from experiment, an aerofoil moving in air may experience either leading or trailing edge separation, in varying degrees, depending on incidence, Reynolds number, Mach number and aerofoil geometry. In the dynamic case, aerofoil behaviour is further complicated by the suppression of trailing edge separation due to the pitching motion. It is, however, generally the case that even very sudden leading edge stalling is preceded by some limited trailing edge separation and, hence, non-linearity in the force and moment characteristics.

In order to model the loading patterns in the non-linear regime, the dynamic stall technique utilises the dependency of the separation point on the aerofoil motion. Firstly, the method invokes the Kirchhoff flow relations to derive a curve of static separation point versus incidence from experimental data. During a dynamic stall calculation this curve is used, in conjunction with a deficiency function to obtain estimates of the unsteady flow separation point. This new separation point is then used to provide unsteady loads via the Kirchhoff flow relations.

As indicated above, the forward movement of the trailing edge separation point of an aerofoil experiencing high pitching rates will be suppressed. Under these conditions, it follows that the localised boundary-layer behaviour at the leading edge may become the determining factor in the stalling process. In particular, if the pitching rate is sufficiently high, circulation is retained near the leading edge of the aerofoil in the form of a strong vortex. The build up, and subsequent downstream travel of this vortex, termed the dynamic stall vortex, can have significant influence on aerofoil behaviour and represents a formidable modelling problem.

In the technique, leading edge stall onset is indicated by a criterion based on a critical leading edge pressure and associated pressure gradient. The method also models the creation and subsequent downstream travel of the dynamic stall vortex in a time dependent manner.

In the unsteady aerodynamic model, the effect of the shed vorticity, due to the changes in angle of attack and incoming velocity, is automatically considered. Likewise, the Fixed Wake method also includes the influence of the shed wake as an inherent part of the calculation procedure. There is, however, a significant difference between the physical effects modelled by the two techniques. In particular, the Fixed Wake method includes the influence which the vorticity shed by a turbine blade on the upwind pass has on the same blade's downwind pass. In addition, the influence which the vorticity shed by one turbine blade has on another blade is inherently modelled by the technique. These two phenomena, which are peculiar to vertical axis wind turbine flows, are the dominant features of the flow problem under consideration. Thus, whilst there is a small element of duplication of the flow phenomena modelled by the two techniques, the degree of solution overlap was considered small enough to be insignificant in the present analysis.

The overall performance of a vertical axis wind turbine is uniquely related to the azimuthal variation in blade tangential force. For this reason, the manner in which the tangential force coefficient Ct is modelled, within any prediction scheme, assumes particular importance. In this study, considerable emphasis was placed on the derivation of an appropriate Ct formulation. This is discussed in more detail in the following section.

The manner in which the fixed wake method is coupled to the dynamic model is illustrated in Fig.2.8 Initially, the fixed wake model is run using static data. The resulting induced velocity, angle of attack and the reduced pitch rates are then used as the input to the Beddoes model. From the Beddoes model, a first estimate of the

dynamic airloads on the wind turbine is obtained and these airloads are fed back into the fixed wake model to calculate new estimates of induced velocity, angle of attack and pitching rates. This procedure is then repeated until convergence is achieved. Usually a steady state solution can be reached after four iterations.

In Fig. 2.9. predictions of power versus wind speed, with and without dynamic effects, are compared to field data for the VAWT 220. It is clear, from the figure, that the inclusion of dynamic effects has no significant influence on the predicted power for wind speeds below 10m/s. This corresponds to tip speed ratios above approximately three where the range in effective incidence of the blade section is not sufficient to penetrate beyond stall. It is, however, apparent that predicted power levels in this region are too high. This is a likely consequence of the absence of crossarm and parasitic drag terms from the calculation scheme.

At higher wind speeds, however, the results predicted using static aerofoil section data fall considerably below the field data. The trend of this discrepancy is such that it increases as the wind speed and, hence, the effective incidence range of the turbine blade is increased. In contrast, the predictions obtained from the dynamic model appear to correlate well with the field data up to wind speeds of around 18m/s. Above 18m/s, tip speed ratio 1.5, the turbine blade section experiences very high incidence on both the upstream and downstream blade passes. It is likely, that the degree of stall is so severe, under these conditions, that the tangential force coefficient formulation used in the dynamic stall model may be inappropriate.

In Figs. 2.10 & 2.11 the instantaneous force and moment coefficients, corresponding to the above case, are presented for tip speed ratios two and three respectively. These figures provide a particularly good illustration of the influence of dynamic effects on the loading characteristics of a vertical axis wind turbine. Possibly the most significant observation, to be made from comparison of the two figures, is the dramatic influence of the unsteady aerodynamic modelling at the lower tip speed ratio. It is clear, that the improvement in the Cp prediction which the dynamic model shows is accompanied by marked changes in the instantaneous tangential force coefficient values. A second effect, which is structurally more significant, is the increase in the peak normal coefficient values over the static predictions. This increased loading on the turbine blade is of the order of 40% and, on the downstream blade pass, appears as a structurally undesirable sharp peak on the load characteristic. In addition to this effect, it is clear that an enhancement of the force imbalance experienced by blades on the upwind and downwind passes is identified.

In contrast, the dynamic loads for the tip speed ratio 3 case, in Fig. 2.11., are little different from those predicted using static aerofoil data. As indicated in Fig. 2.9. the Cp obtained using static aerofoil data showed good agreement with field data for this case. It, therefore, follows that evidence of dynamic effects in the instantaneous load characteristics would be limited. As may be expected, however, a small amount of load hysteresis is apparent in the dynamic loading characteristics and, at the higher blade incidence values on the upstream blade pass, very light dynamic stall is experienced.

It is clear that the tip speed ratio 3 case almost represents a limit, for this particular machine, below which dynamic effects become significant and above which they are of little consequence. A similar result was reported by Paraschiviou & Delclaux for a Darrieus wind turbine. In that case, however, the limiting tip speed ratio, based on the equatorial radius, was somewhat higher. This may be explained by the fact that, on a Darrieus turbine, blade sections away from the equator experience lower effective tip speed ratios.

2.2.3 The Prescribed Wake method with Unsteady Aerodynamics

In the unsteady aerodynamic model described above, the effect of the shed vorticity, due to changes in angle of attack, is automatically considered. Likewise, the Prescribed Wake method also includes the influence of the shed wake as an inherent part of the calculation procedure. To avoid a duplicative accounting of this effect, part of the influence of the shed vorticity, on the induced velocity, was removed from the Prescribed Wake scheme , i.e. the contribution from a given blade's shed vortex system to the induced velocity at a control point on that blade was not considered.

When applying the dynamic model, it is necessary to input some data, such as the reduced pitching rates, the local relative velocity, the instantaneous angle of attack and so on. These data can be initialized by running the Prescribed Wake program using static aerodynamic characteristics. This stage of the calculation procedure also produces the wake geometry for the subsequent dynamic calculation. The overall procedure for a full dynamic calculation is illustrated in Fig.2.12.

The overall performance of a vertical axis wind turbine is uniquely related to the azimuthal variation in blade tangential force. For this reason, the manner in which the tangential force coefficient Ct is modelled, within any prediction scheme, assumes particular importance. The version of Beddoes' model which was used to account for the unsteady effects was developed in Department of Aerospace engineering of University of Glasgow. In this model, the formula for the coefficient of chordwise force, C_T, is the same as the original Beddoes' model and it can be expressed as

$$C_T = \eta\, C_N^c \,\mathrm{Tan}(\alpha_E)\, \sqrt{f}\, \Phi \qquad (2.1)$$

where C_N^c is the circulatory load and $C_N^c \,\mathrm{Tan}(\alpha_E)$ is its contribution towards chordwise force. f is the trailing edge separation point. $\sqrt{f}$ is the Kirchhoff modification which accounts for the influence of trailing edge separation and $\Phi = f^{RK(CN' - CN)}$. This exponent is suggested by Beddoes and Leishman and has no significance other than to ensure continuity of the behaviour in the equation. η is a recovery factor used to realize the chordwise force which would be attained in potential flow.

When this C_T formula was applied to the calculation of vertical-axis wind turbine (VAWT) performance it was found that there was a significant deficiency in this formula. At low tip-speed ratios where the effect of dynamic stall becomes more important, it gave much lower values of C_T and, consequently, the lower power output than field data as can be seen in Fig.2.13. Even when the values of both Φ and η were taken as 1, this C_T formula still under-predicted the power output at tip-speed ratio 2.0 by about 11% but over-predicted the power output at tip-speed ratio 1.5. Furthermore, it was obvious that this formula did not take the viscous friction into account. This effect should becomes important in performance calculations when the tip-speed ratio is high. Since VAWTs use chordwise force to generate power, it was necessary to improve its representation before incorporating the dynamic model into the wind turbine performance code.

Harris suggested the following formula for C_T,

$$C_T = C_N^2 / C_N^{\alpha} \qquad (2.2)$$

Apparently, this formula considered neither the nonlinear influence of trailing edge separation nor the viscous friction. Although it gave good agreement with field data at tip-speed ratio 2.0, when the tip-speed ratio was lower this formula produced higher values of C_T than field data and the predicted power output was as shown in Fig.2.13. Fig.2.17a shows the predicted C_T variation given by Harris' formula. It can been seen that value of peak of C_T at tip-speed ratio 1.5 was too high.

In the present work, a C_T formulation was developed which was an appropriate dynamic model for the VAWT case. The main features of this formula are

1). A zero lift drag term C_{D0}, was added to the C_T formula to account for the effect of viscous friction.

2). Since the C_T formula is directly related to C_N, it was necessary to correct the C_N first before starting to further modify the C_T formula. In the Beddoes' model, a time lag in dynamic response is introduced to consider the dynamic effect in the form of an effective angle of attack α_E. This is used in the calculation of circulatory loading C_N^c and is given by

$$\alpha_E = \alpha_n - X_n - Y_n$$

where the X_n and Y_n are the deficiency functions which represent the time history effect due to the shed wake. These take the form

$$X_n = X_{n-1} \exp[-b_1(1-M^2)\,\Delta s] + A1(\,\alpha_n - \alpha_{n-1}\,) \exp[-b_1(1 - M^2)\Delta s/2\,]$$
$$Y_n = Y_{n-1} \exp[-b_2(1-M^2)\,\Delta s] + A2(\,\alpha_n - \alpha_{n-1}\,) \exp[-b_2(1 - M^2)\Delta s/2\,]$$

where Δs is the distance travelled by the aerofoil in semi-cords in time Δt and A1,A2,b1,b2 are constants.

In the Prescribed Wake Model the influence of shed vorticity is also taken into account. When these two models are coupled together, care should be taken to avoid accounting for this effect twice. Fig.2.14b gives the results from a dynamic model without consideration of the shed wake effect, i.e., the X_n and Y_n terms are removed from the α_E formula. Compared with field data, these results give a far too quick recovery in the up-stroke part and consequently a more linear normal force. This is because, not only the influence of the shed vorticity but also the dynamic effect of the shed wake, which is not considered by the Prescribed Wake model, are taken away from the dynamic model. The correct modelling technique is to remove the influence of the shed vorticity from the Prescribed Wake model. Fig.2.14a shows the results from a modified PSWM, in which the influence of the shed vorticity was taken away, plus the complete Beddoes' model. An improvement can be seen from Fig.2.14a, albeit the recovery in the up-stroke part is slower than in the field data. This effect is due to the values of the empirical constants in X_n and Y_n being in error.

The empirical constants in the Beddoes' model were obtained by curve fitting results from wind tunnel tests. There are, however, some differences between wind tunnel testing and actual Vertical-Axis Wind Turbines. In wind tunnel testing, the vortex shed from blade is leaving it with an angle equal to its angle of attack , however, in the VAWT case the shed vortex leaves with an angle much larger than the angle of attack as seen in Fig. 2.15. When the contribution of the shed vorticity to the effective angle of attack, which is used to calculate the circulatory loading in the Beddoes' model, is considered the VAWT case should obviously be influenced less than the wind-tunnel test case. After numerical testing and comparison with field data, the constants A_1 and A_2 in the formula to calculate X_n and Y_n were

reduced from the original values of 0.3 and 0.7 to 0.24 and 0.56, respectively. The results using the new A_1 and A_2 values are also shown in Fig.2.14c) and are much closer to the field data.

3). As mentioned above, formula (2.1) under-predicted the C_T value. In fact, under dynamic stall conditions there are two loads not included in this formula which should contribute to the variation in pressure distribution on the aerofoil surface. These are the impulsive loading and vortex force. These effects are present during experiments and should be taken into account in the C_T formula. To do this, the C_T formula was modified in the following way,

$$C_T = \Phi (C_N^c \sqrt{f} + C_N^I + C_N^V) \mathrm{Tan}(\alpha_E) - C_{D0} \qquad (2.3)$$

Fig.2.16 shows the differences between the C_T formulas with and without considering the contribution of vortex force and impulsive load. These results were calculated at RK = 0.15 (RK is a constant in exponent Φ). Fig. 2.16a gives the results from the original C_T formula without considering the contribution from C_N^V and C_N^I at all. If this prediction is compared with field data, it is found that the predicted power coefficient is too low. This is directly attributable to the absence of the vortex force and impulsive loading terms. Evidence for this viewpoint can be gleaned from Fig.2.16b where a formulation which includes the circulatory and impulsive loadings is used to predict the C_T variation. In this case, a small improvement in the overall C_p is achieved but the prediction still falls well below the field measurement. The effect of the vortex force is assessed in isolation from the impulsive load in Fig.2.16c where a formulation which includes the vortex force is used. In this case, the peak C_T is considerably increased indicating that the vortex force gives a much larger contribution than the impulsive loading. Finally, the result from the final version of the C_T formula is presented in Fig.2.16d. The corresponding C_p agrees well with the field measurement and the loading pattern is more credible than those produced by the preceding schemes. A further detailed study on the application of the C_T formula (2.3) was made to ensure the quality of solution. Fig.2.17b shows the results at two tip-speed ratios using formula (2.3) solely. However, it has found that there was an unexpectedly large negative C_T area in the solution the tip-speed ratio 2.0. This became more serious when the tip-speed ratio was reduced to 1.5. This occurred because the C_N and α_E terms in equation (2.3) have opposite sign in that area. That means that in the up-stroke part , when the C_N gradually becomes positive, the effective angle of attack is still negative due to the time delay. After flow reattachment the C_N changes linearly with α. In order to improve the results, the following formula was used to calculate C_T in this area,

$$C_T = C_N * \mathrm{Tan} (C_N / C_N^{\alpha}) - C_{D0} \qquad (2.4)$$

The final version of the C_T formula used in this research work is composed of two parts. The first part is equation (2.4) which is used in the region before dynamic stall onset and after flow reattachment. In the region after dynamic stall onset until flow fully reattaches, equation (2.3) is used. Fig.2.17c shows the results from the final version of the C_T formula.

The new dynamic version of the Prescribed Wake model as illustrated above and in Fig. 2.12 was applied to the VAWT 220 machine. In Fig. 2.18 the instantaneous normal and tangential force coefficients are presented for tip-speed ratios two and three. These

curves provide a particularly good illustration of the influence of dynamic effects on the loading characteristics of a vertical axis wind turbine. It can be seen clearly that the unsteady aerodynamic effects become important only at tip-speed ratios lower than three for this particular machine. The marked changes in the instantaneous tangential force coefficient from the dynamic mod at tip-speed ratio 2 resulted in an improvement in the Cp prediction. In addition, a large increase in the peak normal force coefficient value over the quasi-static prediction can be observed. This is due to the contribution of the vortex force that appears under dynamic stall conditions. An enhancement of the force imbalance experienced by blades on the upwind and downwind passes is also identified. In contrast, the dynamic loads for the tip-speed ratio 3 case are little different from the quasi-static results.

Figure 2.19 represents the predicted results in terms of power output against wind speed with and without dynamic effects, together with field data, for the above case. Again, it can been seen clearly that the dynamic effect has no significant influence on the predicted power output at wind speeds below 10m/s which correspond to a tip-speed ratio of about three. The quasi-static method significantly under-predicted the power, particularly at wind speeds over 13m/s, due to its failure to consider the dynamic nature of the flow. The dynamic version of the Prescribed Wake model with the new Ct formula gave very good agreement with field data over the range of wind speed considered.

2.3 A Study of the Influence of Blade Geometry on the Performance of an H-Configured Vertical Axis Wind Turbine

The quality of prediction obtained from the fully dynamic Prescribed Wake model detailed above presented a unique opportunity to study the influence of blade geometric characteristics on the instantaneous loading patterns experienced by a vertical axis wind turbine. A study was, therefore, initiated to identify the possible benefits, in terms of power output, reduced structural loadings and smoother torque distribution, which could accrue from a 'tailored' blade. Substantial modifications were made to the original computer code to provide the flexibility necessary for this work and the resulting scheme has the capability to include the effects of blade pitch, twist, taper and aerofoil section.

In the parametric study, the effect of varying each one of the above geometric features was examined in turn by comparison with a baseline configuration. This configuration was taken to be a vertical axis wind turbine with straight, untapered blades. The profile used for the blade cross section was the NACA 0015 aerofoil. The low tip speed ratio range is associated with the largest unsteady aerodynamic loads and, thus, was the obvious region in which to target this study. For this reason, most of the results presented relate to the $\lambda = 2$ case although some results are presented over the entire tip speed ratio range. Analysis of the results obtained indicated that there was scope to improve the aerodynamic performance of VAWT blades and that, as a consequence, significant structural benefits could be obtained.

2.3.1. The Effect of Pitch

The performance of an H-configured vertical axis wind turbine at tip speed ratio 2 was studied for various degrees of blade pitch. It was clear from the outset that large pitch angles would be detrimental to the overall performance of the machine and would result in a severe loading imbalance between the two blades. For this reason, the range of pitch angle considered was limited to six degrees on either side of the circumferential direction.

In Fig. 2.20, the predicted power coefficient is plotted against pitch angle for tip speed ratio 2. It is clear from this figure that, although the variation of blade incidence is non-symmetric around the azimuth, there is no gain achieved by pitching the blade and, consequently, the optimum power production corresponds to zero pitch. The aerodynamic loadings for pitch angles of 4 degrees on either side of the neutral position are compared with those corresponding to zero pitch in Fig. 2.21. The effect of pitch is clearly illustrated in the comparison of instantaneous upstream and downstream torques where it may be observed that an azimuthal shift in the loading patterns characterises the applied pitch. This figure also illustrates that substantial gains in instantaneous torque can be made at certain azimuthal locations when pitch is applied but, as indicated above, the integrated effect is a reduction in average torque. The diagrams of shear force, which is the sideways force on the support tower due to the blades, again show the characteristic shift associated with blade pitch. It should also be noted that the relative changes in shear force magnitude are accompanied by similar changes in torque.

In Fig. 2.22., the predicted bending moment at the blade/crossarm junction is presented for the three pitch cases. Of these, the -4 degree pitch case produces the largest peak bending moment. Additionally, the peak is sharper and, therefore, structurally undesirable. Pitching the blade in the opposite direction can, as shown, reduce the peak bending moment but at the cost of performance degradation. In this case the reduction in power coefficient associated with 4 degrees of positive pitch is around 6%.

Another feature of the turbine performance which is of interest from a structural viewpoint is the manner of blade stalling. This is particularly relevant in the low tip speed ratio regime where the blade stalls dynamically. The first tangible sign that the dynamic stall process has been initiated is termed dynamic stall onset. The location of dynamic stall onset may be considered as one boundary of a region in which the blade is subjected to a series of severe non-linear unsteady aerodynamic loadings. The other boundary of this region is provided by the point at which, after stall, flow reattachment occurs and the variation of normal force with blade incidence becomes linear. For structural reasons, it is desirable that this dynamic stall region is confined to a limited azimuthal range. One way in which this can be achieved is to have simultaneous stalling on the upstream and downstream blades. This has the added advantage that the unsteady shear loads produced by one blade can, to some extent, be offset by those from the other blade. The effect which blade pitch has on azimuthal location and the extent of the dynamic stall region is shown in Fig. 2.23. Generally speaking, applying pitch to a blade increases the size of the dynamic stall region on one side of the turbine but has the opposite effect on the other side. This can clearly be observed for the negative 4 degrees of pitch case where the size of the dynamic stall region is compressed on the upwind blade pass and increased on the downwind side. Another notable feature of this diagram is the possibility of eliminating dynamic stall at the blade tip. If the -4 degrees of pitch case is examined, it can be observed that the blade tips do not stall on the downwind pass. There is, however, an increase in the azimuth range for which the blade tip is stalled on the upwind pass.

The -4 degree pitch case is particularly interesting since the turbine blades stall simultaneously. This is illustrated in Fig.2.24. where the azimuthal angle between the upwind and downwind blade stall onset locations $\Delta\Phi$ is plotted against applied pitch. In this case, $\Delta\Phi$ is defined as

$$\Delta\Phi = 180 + \Phi_{\text{upwind stall onset}} - \Phi_{\text{downwind stall onset}}$$

Finally, in Fig. 2.25, power and power coefficient curves corresponding to moderate positive and negative blade pitch are compared with the baseline condition over a range of tip speed ratio. Examination of these power curves indicates that a small amount of positive pitch, whilst reducing the power output at low tip speed ratios, can be beneficial to performance at high tip speed ratios. Larger amounts of positive pitch, however, have

been found to degrade the performance over the full tip speed ratio range and so there is little scope for power regulation using pitch.

2.3.2 The effect of taper

The influence of blade taper was examined using a fixed blade area but varying the taper ratio between the blade tip and the cross-arm junction. Thus, any reduction in the tip chord length required a corresponding increase in the chord length at the centre span. In Fig. 2.26 the variation in power coefficient with taper ratio is plotted for the tip speed ratio 2 case. Unlike the previous case, it is clear that tapering the blade can lead to slightly increased performance. In this case, a power coefficient increase of around 2% is achieved with 50% taper. Lower taper ratios than 0.5 result in very high solidity in the region of the cross-arm junction and performance is adversely affected.

Examination of the detailed aerodynamic loadings associated with the different taper ratios indicates that there is little change in the torque and shear force components with applied taper. The main difference in loading pattern is observed in the root bending moment variation with azimuth position. This is shown in Fig. 2.27. From this figure, a significant reduction in bending moment is apparent over the full azimuth range when taper is applied. In addition, the increased blade chord at the root results in a considerable decrease in the bending stress in that area. This, coupled with the decreased bending moment from centrifugal loads which results from the reduced mass outboard of the cross-arm junction, produces an overall effect which is beneficial.

Again, as with the case of pitch, the location of dynamic stall onset is influenced by taper. In this case, however, the effect is to vary the manner in which stall occurs on the blade. This is shown in Fig. 2.28. where increasing taper delays stall at the blade root whilst advancing it at the blade tip. This effect contributes to the reduction in the bending moment by promoting earlier stalling and later recovery on outboard blade sections.

In Fig. 2.29 the power and power coefficient curves for various degrees of taper are presented and compared with the untapered blade. Generally, a modest increase in power is observed for the taper cases over the entire tip speed ratio range. This is particularly apparent in the power coefficient plots at high tip speed ratios.

2.3.3 The effect of twist

Twist may be considered as a prescribed span-wise distribution of pitch and so it would not be unreasonable to expect the characteristics exhibited earlier by the pitch cases to be present when twist is applied. In this study, twist was applied linearly to the blades with -3° of twist indicating that the blade tip chord was offset by -3° from the chord at the cross-arm junction.

Again, as for the pitch cases, the azimuthal variations in torque, shear force and bending moment all exhibit an azimuthal 'shift' associated with the applied twist angle. In this case, however, the magnitudes of the changes in average loads are not as great as in the case of pitch. This is highlighted in Fig. 2.30 where the power coefficient at tip speed ratio 2 is presented for various degrees of twist and pitch. One consequence of this result is that twist may provide an appropriate mechanism for the control of spanwise stalling at little loss to the overall performance. This is highlighted in Fig. 2.31 where the azimuthal locations of the dynamic stall regions for blades with -3°, 0 and 3° of twist are presented. It is clear from this figure that the effect of twist is to modify the spanwise stalling and recovery patterns, particularly in the tip region.

The overall effect of blade twist on power and power coefficient is assessed, for the full tip speed ratio range, in Fig. 2.32. As expected, similar characteristics to the pitching cases are observed with twist of 3° being almost equivalent to the 2° pitch case.

2.3.4 The effect of aerofoil section.

To examine the influence of blade aerofoil section on turbine performance, two aerofoil profiles were used. The baseline configuration of the rectangular blade with a NACA 0015 aerofoil profile was again taken as the reference. The second configuration consisted of a rectangular blade with the NACA 0015 profile at the tip and an earlier stalling GUAV 10 profile at the cross-arm with the aerofoil performance characteristics varying linearly between the two sections. The features of this GUAV 10 profile are discussed in more detail later in this report.

It was hoped that the second configuration would exhibit some degree of power regulation as a consequence of the earlier stall on the inboard blade sections. Indeed, Fig. 2.33 illustrates that earlier stall and later recovery are, in fact, achieved by the second configuration. The consequences of this are apparent in the azimuthal load variations shown in Fig.2.34 where the torque and shear force in the stall region are considerably reduced. A reduction in torque over such a significant azimuthal range inevitably affects the power produced by the turbine. This is illustrated in Fig. 2.35 where the power and power coefficient variations with tip speed ratio are presented for the two configurations. It is clear that the second configuration does display some degree of power regulation without significant effect at the higher tip speed ratios.

2.4 AEROFOIL DESIGN AND WIND TUNNEL TESTING

In the present study, three aerofoil sections appropriate to VAWT applications were tested in the Glasgow University Handley-Page wind tunnel under dynamic conditions. This wind tunnel is a closed return type with a 1.61m x 2.13m octagonal working section. The general arrangement of a model in the wind tunnel is illustrated in Fig. 2.36. The standard aerofoil models tested in this facility have chord length 0.55m and span 1.61m but the second model tested in this study had a reduced chord length of 0.275m. The reasons for this are outlined below.

The first model to be tested was a design based on the NACA 0018 aerofoil but was intended to give a sharper stall. This feature was considered desirable for the purposes of stall regulation.

The second aerofoil tested had a NACA 0015 profile and was not, as originally intended, a new design. This transpired because of the need to resolve two inconsistencies between data collected at Glasgow and those collected elsewhere. In particular, an anomaly existed in the rate at which the dynamic stall vortex was convected downstream. In tests at Glasgow the convection rate had been found to be, to a first order, independent of aerofoil motion. Other researchers had found that the convection speed was related to the reduced pitch rate of the model. Additionally, in ramp-down tests at Glasgow negative lift had been observed at positive incidence. This had never been reported before. It was considered that these two phenomena should be studied in more detail before any further testing of new designs was undertaken. It was essential that the possibility of these being caused by wind tunnel constraint effects should be eliminated. A high aspect ratio version of the NACA 0015 aerofoil was, therefore, built and tested to examine the constraint effect. The results showed that the Glasgow database, which contains a substantial volume of data on VAWT aerofoils, was not subject to significant constraint effects.

The third aerofoil design was carried out by a wind turbine company (VAWT Ltd) and was a sharp nosed 21% thick aerofoil. This profile was again intended to provide some measure of stall regulation.

The aerofoil design technique applied at Glasgow is described in the following section followed by the salient features of the results from the wind tunnel tests on the three aerofoils.

2.4.1 Aerofoil Design Technique

The aerodynamic design of a VAWT requires more than just an accurate performance prediction method. Tools to assist in the derivation of an appropriate detailed geometric configuration are also very useful.

To design a VAWT blade of varying cross-section the designer must have a method of selecting appropriate aerofoil sections. A useful tool in this process is, therefore, some form of aerofoil design technique which not only assists in the design process but provides estimates of aerofoil performance for input to the VAWT prediction method. Together, a structured aerofoil design method and a VAWT performance prediction scheme can form the basis of a design methodology for VAWT blades. It is this type of approach to the aerodynamic design of VAWT's that offers the best possibilities for future designs.

An aerofoil design method has been developed which takes the form of an integrated computer package for aerofoil synthesis. In the technique, either application of an inverse aerofoil design procedure or heuristic modification of a seed profile may be used to derive a new aerofoil shape. Indeed, to provide maximum flexibility, both techniques may be used sequentially.

The main components of the design package are the generation, geometry modification, and analysis modules. In addition, several utility and file handling algorithms provide interface with external computer codes and data sources.

As indicated above, the actual design process is carried out either in the primary generation module or in the geometric modification module. The generation module contains an inverse conformal mapping technique in which an aerofoil shape is derived from a specified velocity distribution. This type of approach to design is very effective but often requires some experience on the part of the designer.

The geometric modification module allows the designer to manipulate the geometry of a seed aerofoil to produce required characteristics. Several techniques are available to assist in this process from individual profile point modifiers to composite aerofoil construction algorithms. Design by geometric modification is an effective process when tackled by the experienced aerodynamics but can be used to great effect by even the most inexperienced designer.

Inherent in this above approach is the requirement for some form of aerofoil performance assessment scheme. For this purpose the current package contains a version of the prediction method of Coton and Galbraith. This scheme has been demonstrated capable of providing accurate performance estimates over a wide range of incidence and so is ideally suited to VAWT applications. Other quality assessment codes can, of course, be implemented with little alteration.

When dynamic characteristics of a particular aerofoil are required, the static prediction can be used to provide input to the dynamic model of Leishman and Beddoes or, alternatively, the correlation of Gracey can be used to predict the variation of the dynamic stall onset angle with reduced pitch rate.

This approach to aerofoil design was applied in the derivation of the shape of the first model tested in this study.

2.4.2 Model 1

For VAWTs, it is considered to be very important to increase the fatigue life of the blades while keeping a certain level of power generating efficiency. It is known that passive stall regulation could be forced to occur in the region of the crossarm (for H configuration) rather than at the tips, and the preferential location for the stall will reduce the bending moments and increase the fatigue life. To do this it is necessary to design an aerofoil section which has sharp stall characteristics without losing too much C_t. Physically, sharp stall generally results from the bursting of a separation bubble at a position where there exists a strong adverse pressure gradient near the leading edge. With this in mind, the current design effort concentrated on designing a new aerofoil section with a sharper nose. A currently favoured VAWT section, the NACA 0018 aerofoil, was taken as the reference aerofoil in the design process with the objective being the design of a new profile possessing the stalling characteristics mentioned above but having similar overall performance to the NACA 0018.

The GUVA3 aerofoil designed by Coton and Galbraith was taken as the starting point for the design synthesis. This aerofoil displayed sharp stall, but suffered an associated reduction in C_t over the operating incidence range which was unacceptable. Further development of an appropriate design was, therefore, necessary. In fact, six intermediate profiles were developed before the final design was established.

The intermediate sections (named GUVA 4 to GUVA 9) were developed using the inverse aerodynamic technique of Nonweiler. In this inverse method, five coefficients are required to specify the velocity distribution. Of these, one (A) governs the aerofoil section nose radius and a second (B) represents the percentage of chord forward from the trailing edge for which the difference in upper and lower surface slope is constant. Thus, smaller values of A and B would result in a sharper nose and a more cusped aft portion, and vice versa. The inverse design method parameters for generating the intermediate sections are listed in Table 2.1. along with the geometric characteristics of the profiles. For these six intermediate designs, the angle of attack at which the separation bubble bursts is almost the same, approximately 14°. Additionally, in each case, the static stall angle α_{ss} is in the range from around 10° to 11° and the maximum C_t is around 0.2.

Of the profiles in Table 2.1, GUVA 4 and GUVA 9 gave the most desirable static performance. An assessment of their dynamic performance was made by extracting pertinent information from curves representing the variation of the separation positions with angle of attack and using the correlation of Gracey. This approach yielded the variation of dynamic stall onset angle versus reduced pitch rate. This analysis showed that both the GUVA4 and the GUVA9 were prone to dynamic stalling at a significantly lower incidence than the NACA 0018 and were likely to produce some degree of stall regulation on a VAWT. Since, however, the GUVA4 had a very cusped trailing edge region it was considered an impractical design for an actual VAWT application and so was discarded.

In an attempt to improve the design even further, an attempt was made to extract the favourable features of the sharp-nosed GUVA9 whilst achieving closer general agreement with the performance of the NACA 0018. This led to the design of the GUVA10 which is a combination of the GUVA 9 and the NACA 0018 which uses the GUVA 9's nose and the rear part of the NACA 0018. The predicted static performance characteristics of this profile are shown in Fig.2.37 and comparisons of the inviscid pressure distributions at 10 degrees and the aerofoil profiles of the GUVA10 and the NACA0018 are shown in Fig. 2.38. From Fig. 2.37., it can be observed that the GUVA10 has a very sharp stall occurred at about 11° and the maximum C_t reached is

0.21. In comparison with the NACA 0018 the angle of dynamic stall onset is about 3 degrees lower. This section was finally chosen as the model to be tested in the wind tunnel. Its coordinates are listed in Table 2.2.

The separation position variation during static tests on the GUVA10 profile are compared with that of the NACA 0018 in Fig. 2.39. It is clear from the figure that, as intended, the GUVA10 does stall earlier than the NACA 0018 and also in a sharper manner. The uncorrected normal force and moment curves associated with a static test at a Reynolds number of 1.5×10^6 are shown in Figs. 2.40a and 2.40b for both the GUAV10 and the NACA 0018. These figures mirror the result presented in Fig. 2.39 with the GUVA10 possessing an earlier but sharper stall. The difference in the static stall angle is, as predicted, around two degrees.

Examination of the dynamic performance of the two aerofoils reveals that the incidence of dynamic stall on the GUVA10 is lower, over the full range of reduced pitch rates, than that of the NACA 0018. This is illustrated in Fig. 2.41 where the curves corresponding to the two aerofoils are compared. In Fig. 2.42. the original prediction of the Gracey correlation based on the predicted static performance of the GUVA10 is compared with the measured dynamic stall onset variation. The prediction is seen to give dynamic stall onset around two degrees earlier than the measured data. Given that differences exist between the static performance prediction and the wind tunnel test results, this estimate of dynamic performance is exceptional and indicates that the design procedure adopted is appropriate for unsteady applications.

The overall performance of this aerofoil matched the original design requirements and the potential of the design for stall regulation was successfully demonstrated in an earlier section. This particular case provided validation for the design process used at Glasgow and demonstrated the capability of the dynamic stall onset correlation of Gracey.

2.4.3 Model 2

Originally, after the first model had been tested, a second vertical axis wind turbine blade design was to have been attempted and the resulting profile tested under dynamic conditions in the wind tunnel. At this time, however, two anomalies between unsteady aerodynamic data collected at Glasgow and data collected elsewhere became apparent. The first anomaly arose from tests on seven aerofoil models at Glasgow, both helicopter and VAWT blade sections, which indicated that the rate at which the dynamic stall vortex convected downstream was, to a first order, independent of aerofoil motion (Fig.2.43.). Other researchers had found that this was not the case and that the convection speed was related to the reduced pitch rate. Additionally, results from Glasgow indicated that during ramp down experiments it was possible to generate negative lift at positive incidence. This had never been reported elsewhere and could not be accounted for by standard correction techniques.

These two anomalies cast some doubt on the validity of the results in the Glasgow University database, which contained data sets for several wind turbine profiles, and pointed towards possible wind tunnel interference effects. It became clear that it was necessary to establish, beyond doubt, that the data were not a consequence of the test arrangement but that the phenomena observed were natural features of the unsteady aerodynamic environment. To do this, a test model with half the chord length and twice the aspect ratio of all those on the database was constructed. Consequenlty, the geometric wind tunnel blockage associated with this model was half that of the previous tests.

To obtain a valid indication of the wind tunnel constraint effect, it was important that the new model had the same aerofoil profile as one of the original tests. For this reason, the NACA 0015, which had previously been tested for VAWT applications, was selected.

A comparison between the normal force coefficients measured in static wind tunnel tests on the two models at a Reynolds number of $1x10^6$ is presented in Fig. 2.44. It is immediately obvious that substantial agreement exists prior to stall. Such agreement, however, is not apparent in the stall incidence with the original model stalling around two degrees earlier than the short chord model. This difference in the stall angle was considered to be attributable to wake constraint/downwash effects and thus prompted further investigation of the dynamic performance of the two models.

A series of dynamic tests were conducted on the new model and the results compared with the original NACA 0015 tests. In Fig. 2.45., the results of a ramp-up test, in which the aerofoil incidence was varied linearly between zero and forty degrees at a reduced pitch rate r = 0.018, are compared with those from the low aspect ratio model. Again, the pre-stall behaviour of the two models is almost identical but there are marked discrepancies after the stall vortex has left the trailing edge. These discrepancies are accompanied by similar variations in tunnel dynamic pressure which result from the influence of the wake formation. If these dynamic pressure variations were accounted for, the discrepancies in the figure would be reduced. Thus, whilst an interference effect is undoubtedly present , the gross features of the results from the two tests are the same.

The convection speeds of the dynamic stall vortex for the two cases were then compared for a range of reduced pitch rate. This comparison is presented in Fig. 2.46. where it may be observed that, although the results from the new model indicated slightly higher convection speeds than the old model, there was no evidence that the vortex convection speed was linked to the aerofoil motion. Additionally, the range of scatter on the original test was such that the difference in convection speed between the two tests was not significant. This led to the conclusion that wind tunnel constraints had no first order effect on the dynamic stall process in the previous tests and that it was not unreasonable to use the size of model that had previously been used for unsteady tests at Glasgow.

Finally, the ramp-down performance of the two models was examined. In Fig 2.47 the normal force coefficients of the two models are compared for a ramp-down test at reduced frequency r = 0.031. It can be observed that the gradient of the two curves is not identical and that the curve corresponding to the new model has a slightly higher average gradient than the original. This behaviour is repeated at all pitch rates. It is also apparent that the minimum normal force coefficients associated with the two tests are of different magnitudes and occur at different geometric incidence. These discrepancies may well be a consequence of the influence of wind tunnel constraints on the test environment but, as indicated in the figure, negative lift is apparent at positive incidence in both cases and is, therefore, considered to be a natural consequence of the unsteady flow environment.

2.4.4 Model 3.

There are considerable structural benefits which accrue from the use of relatively thick aerofoil sections on the blades of vertical axis wind turbines. In particular, the increase in cross-sectional area associated with these thicker sections can result in a reduction in the bending stress experienced throughout a blade. At Glasgow, several thick sections have, in the past, been tested for VAWT applications. Unfortunately, the static and dynamic stalling characteristics associated with thick NACA sections are not ideal and the overall performance of the aerofoils is, generally, inferior to profiles of moderate thickness. It was considered, however, that scope did exist to produce a thick aerofoil with characteristics appropriate for stall regulation and that, if successful, the structural benefits of such a design could be substantial.

The new aerofoil was generated using an inverse panel method and its performance was assessed using the viscous-inviscid interaction scheme of Coton and Galbraith. The resulting profile was 21% thick and had a relatively sharp leading edge.

In Fig. 2.48 a potential flow solution for this aerofoil at 5 degrees incidence is compared with the corresponding solution for the NACA 0021. The effect of the sharper leading edge is immediately recognisable in the form of an enhanced suction peak which is accompanied by a reduction of the adverse pressure gradient between the 15 and 30% chord location. It is clear from this figure, however, that the pressure gradient over the rear 60% of the aerofoil is little different to the NACA0021 and so similar initial separation point behaviour may be expected.

The static wind tunnel performance of the new aerofoil is presented in Fig. 2.49 at a Reynolds number of approximately 2.0×10^6. It can be observed that there is a well defined 'break' in the upper surface pressure coefficient traces corresponding to 26 degrees of incidence on the upstroke and 23 degrees on the downstroke. This 'break' also appears on the Ct trace and results in a rapid change of direction of the chordwise force. This behaviour corresponds to the desired sharp stall and can be contrasted with the performance of the NACA 0021 under similar conditions which is shown in Fig 2.50. In this case, the stalling characteristics are quite different and no clear break in Ct is achieved, even at 35 degrees incidence. Additionally, the NACA 0021 does not experience the Ct reversal which is essential if stall regulation is to be achieved.

The dynamic performance, under ramp-up conditions, of the new profile is considered in Fig. 2.51. Here, the aerofoil model is pitch linearly between 0 and 40 degrees in a given time period. In this particular case, the test results for a moderate reduced pitch rate of around 0.003 are presented, but it should be noted that VAWTs can experience reduced pitch rates of up to 0.3. The data clearly show that the Ct break occurs around 29 degrees and so is only slightly delayed by the aerofoil motion. In contrast, the equivalent data for the NACA 0021 are presented in Fig. 2.52. It is quite clear that, although the NACA 0021 does exhibit a Ct break, it occurs at a much higher incidence. In fact, the incidence of the full stall on the NACA 0021 is too high to be of any practical benefit for stall regulation on a VAWT. Thus,

The normal force coefficient variations experienced by the two aerofoils during the ramp-up tests are quite similar in form but it is noticeable that the new profile displays a more pronounced turn-over in Cn in the region of stall. This again is a desirable feature and reflects the success of the basic design philosophy.

2.4.5 Data archiving and storage

Throughout the period of this study the Glasgow University unsteady aerodynamic database has been maintained and updated. All new data sets collected in this study have been included on the database and existing routines have been upgraded to allow analysis and data-reduction in an ever more efficient manner. Glasgow University operates a set of standard procedures which permits updating of the database as and when required.

2.5 CONTRIBUTIONS TO VAWT ROTOR BLADE DESIGN AND FUTURE PROSPECTS

The work in this study has concentrated in two key technical areas. In the first of these, a comprehensive performance prediction scheme for vertical axis wind turbines has been developed. This technique, the unsteady Prescribed Wake model, is extremely

accurate and at least two orders of magnitude faster that comparable techniques. Its value as a design tool has been demonstrated with a parametric study to assess the influence of blade pitch, taper, twist and aerofoil section. This study has provided the basic guidelines for future blade designs and has shown that considerable scope does exist for the aerodynamic tailoring of VAWT blades.

The experimental work in this study has demonstrated the viability of aerofoil design for stall regulation and has provided validation for the design techniques which have been adopted. The influence of wind tunnel constraint effects has been examined and the results indicate a minimal effect on standard tests at Glasgow.

The performance prediction techniques developed in this study are now being extended to consider the modelling of horizontal axis wind turbines. Additionally, the new scheme will have the flexibility to calculate yaw and dynamic inflow cases.

13. Publication and Dissemination of Results

F.N.Coton & R.A.McD.Galbraith 'A Direct Viscid-Inviscid Interaction Scheme For The Prediction Of 2-Dimensional Aerofoil Performance In Incompressible Flow' G.U.Aero Report 8701

F.N.Coton & R.A.McD.Galbraith 'An Aerofoil Design Methodology For Low Speed Speed Aerofoil', Tenth Annual Wind Energy Conference

D.Jiang & R.A.McD.Galbraith 'A New Test Aerofoil Section For Vertical Axis Wind Turbines', G.U.Aero Report 9012,1990

B. Basuno, F.N.Coton & R.A.McD.Galbraith 'On The Aerodynamic Modelling Of Vertical Axis Of Wind Energy Convertors' London 1990.(IMECHE)

F.N.Coton, R.A.McD.Galbraith & B. Basuno 'An Aerodynamic Prediction Method For Use In Vertical Axis Wind Turbine', B.W.E.A. Conference, Swansea, 1991

D.Jiang F.N.Coton & R.A.McD.Galbraith 'A Fixed Wake Vortex Model for Vertical Axis Wind Turbine Including Unsteady Aerodynamics', Wind Engineering Vol.15 No. 6 1991

B. Basuno, F.N.Coton & R.A.McD.Galbraith 'A Prescribed Wake Aerodynamic Model For Vertical Vertical Axis Wind Turbines', Journal of Power and Energy Vol 206, 1992

D.Jiang F.N.Coton & R.A.McD.Galbraith 'The Inclusion of Unsteady Effects In An Aerodynamic Model For Vertical Axis Wind Turbines', Wind Energy Conversion, Proceeding Of The Fourteenth BWEA Wind Energy Conference 1992

R.B.Green & R.A.McD.Galbraith 'The Effect of Wind Tunnel Constraint on Unsteady on Unsteady Aerodynamics Experiments', ICAS Conference, Beijing ,1992

R.A.McD.Galbraith, M.W.Gracey & E.Leitch 'Summary Of Pressure Data For Thirteen Aerofoils On The University of Glasgow's Aerofoil Database', G.U.Aero Report 9221,1992

D.Jiang F.N.Coton & R.A.McD.Galbraith 'Detailed Blade Design Of An H-Configured Vertical Axis Wind Turbine', ECWEC 1993 Conference (in publication)

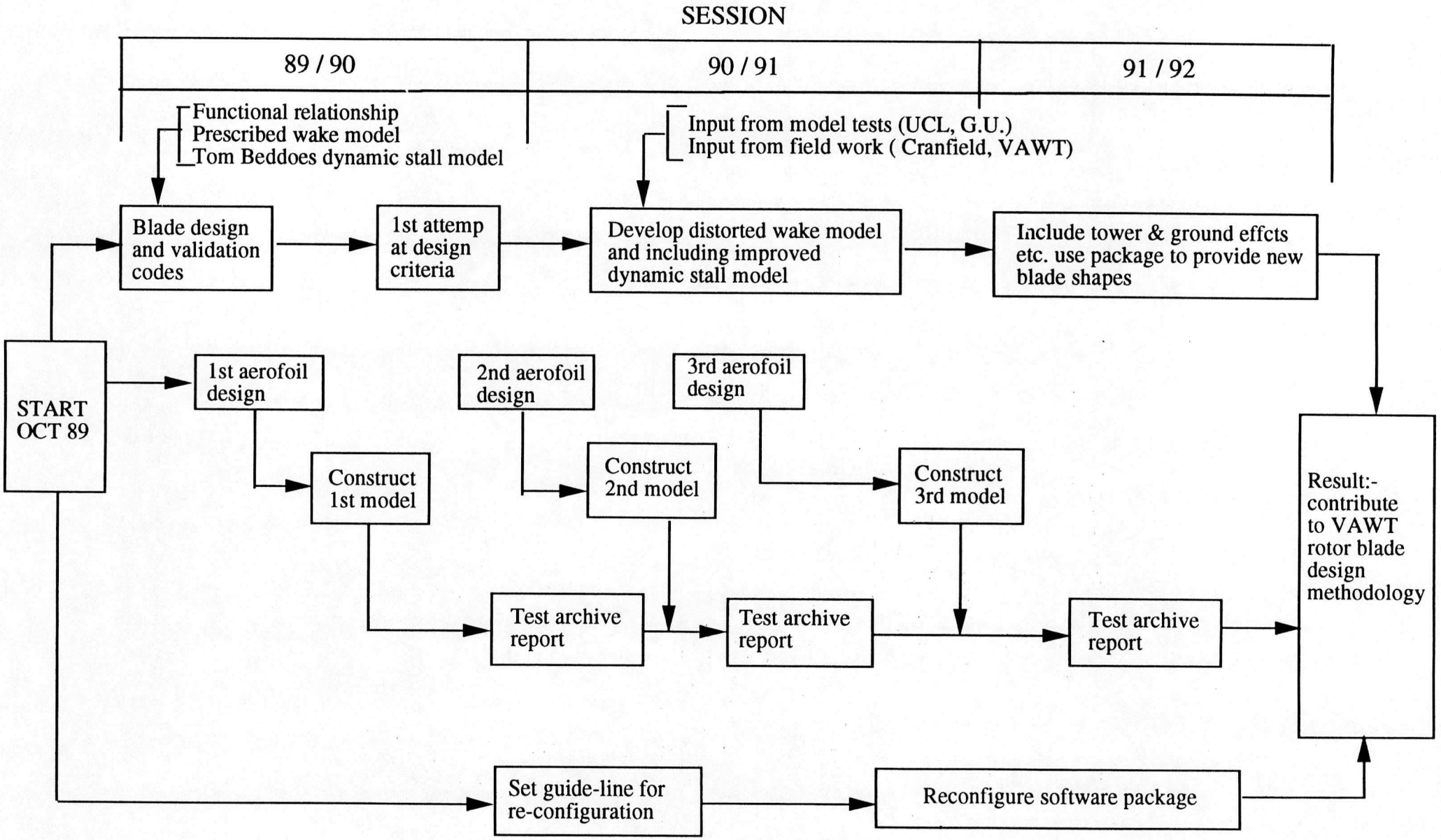

Fig. 1 PROGRAMME

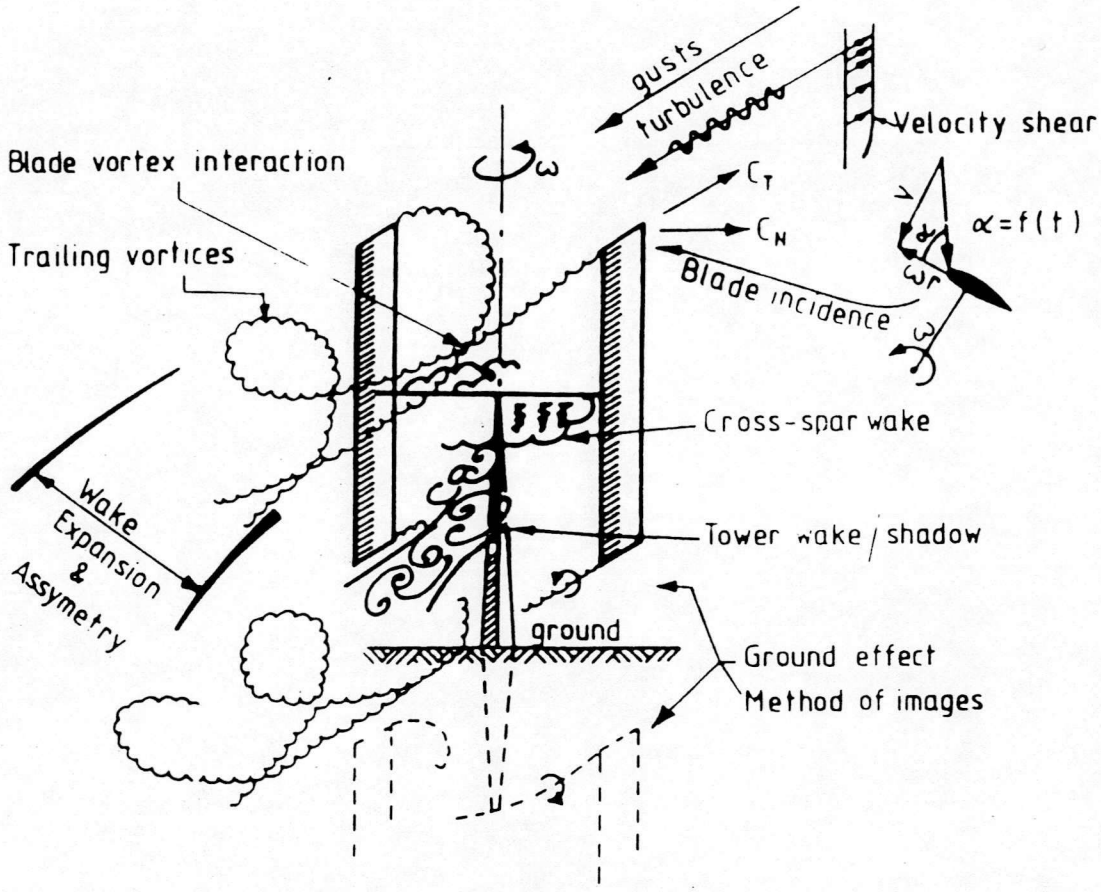

Fig. 2.1 Factors Influencing The VAWT Flowfield

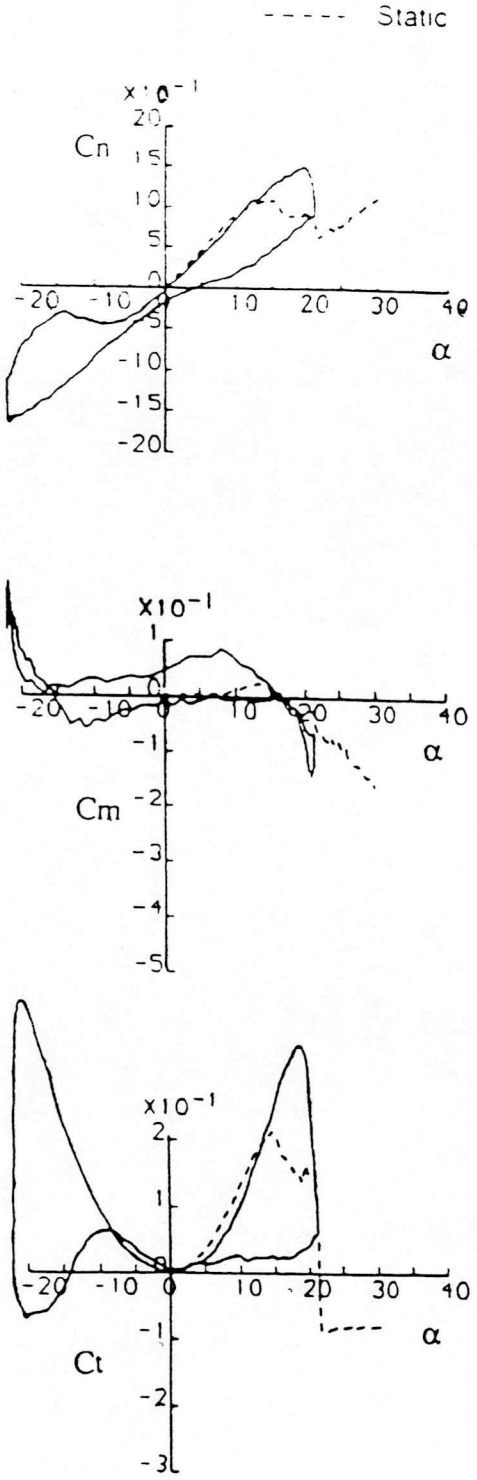

Fig. 2.2 Wind Tunnel Measurements Of Airloads On An Aerofoil Undergoing A VAWT Function in The Range $\alpha = \pm 22^{o}$

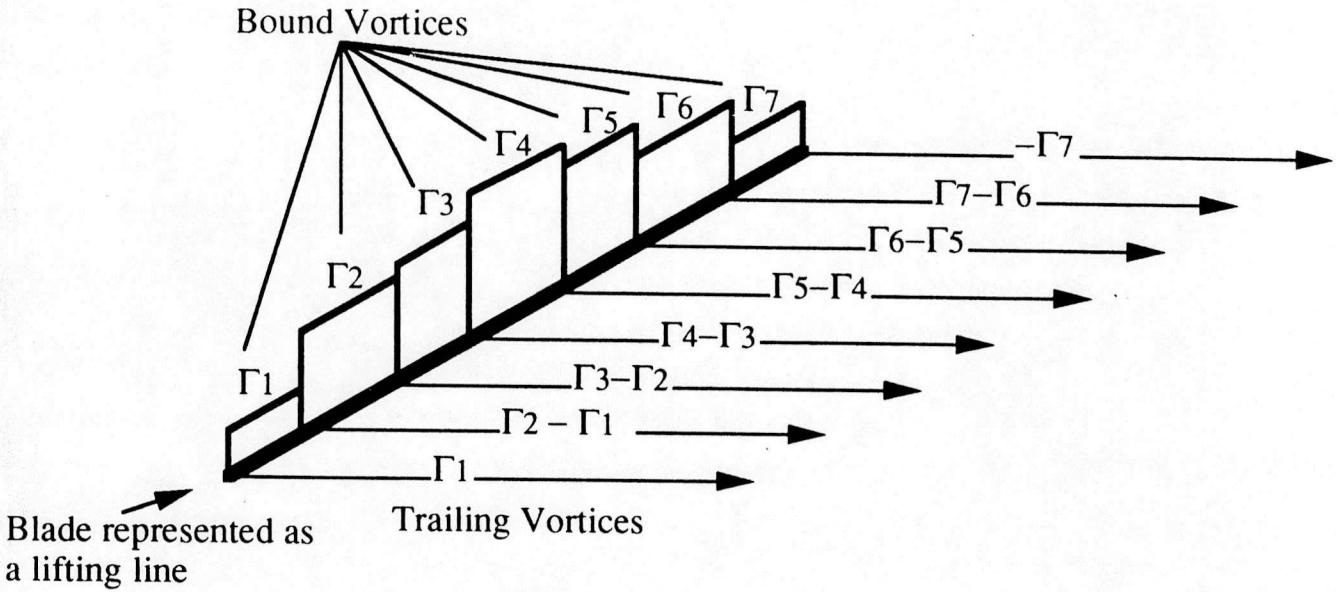

Fig. 2.3 Basic Vortex Model Of Turbine Blade

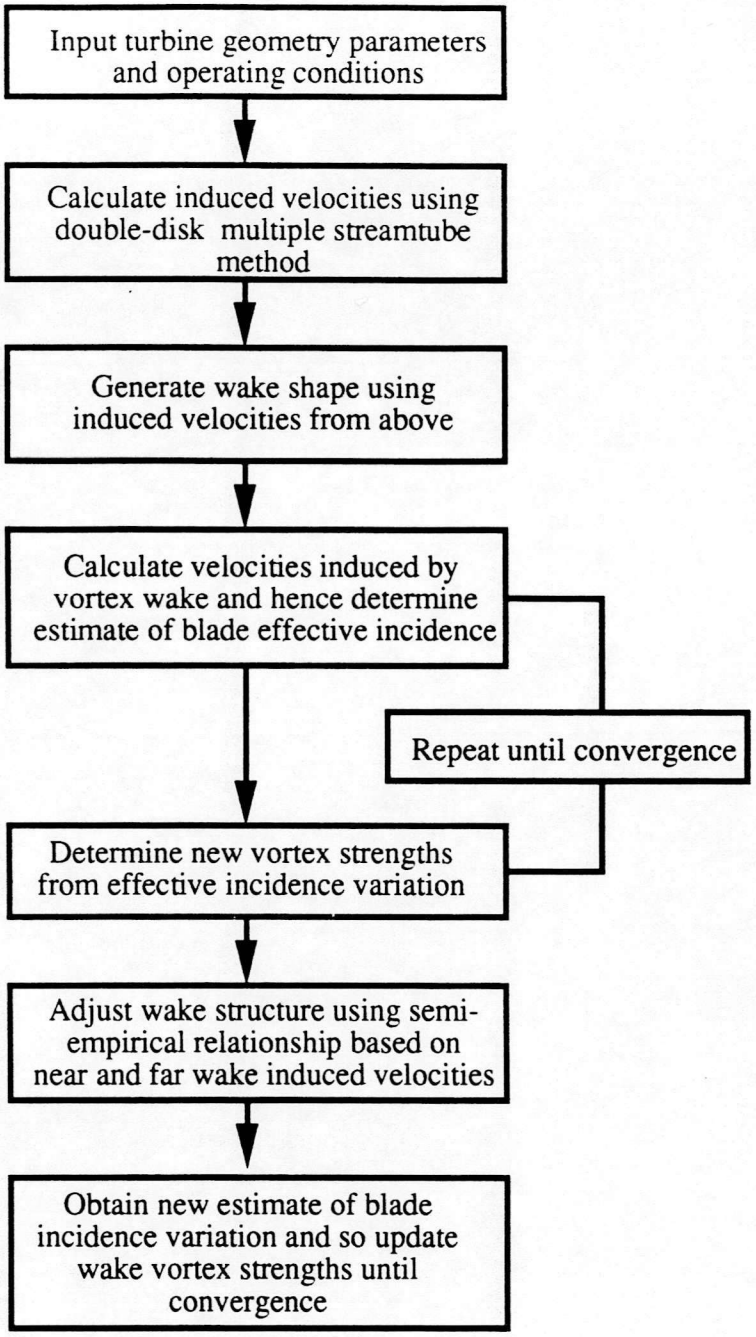

Fig. 2.4 Prescribed Wake Calculation Scheme

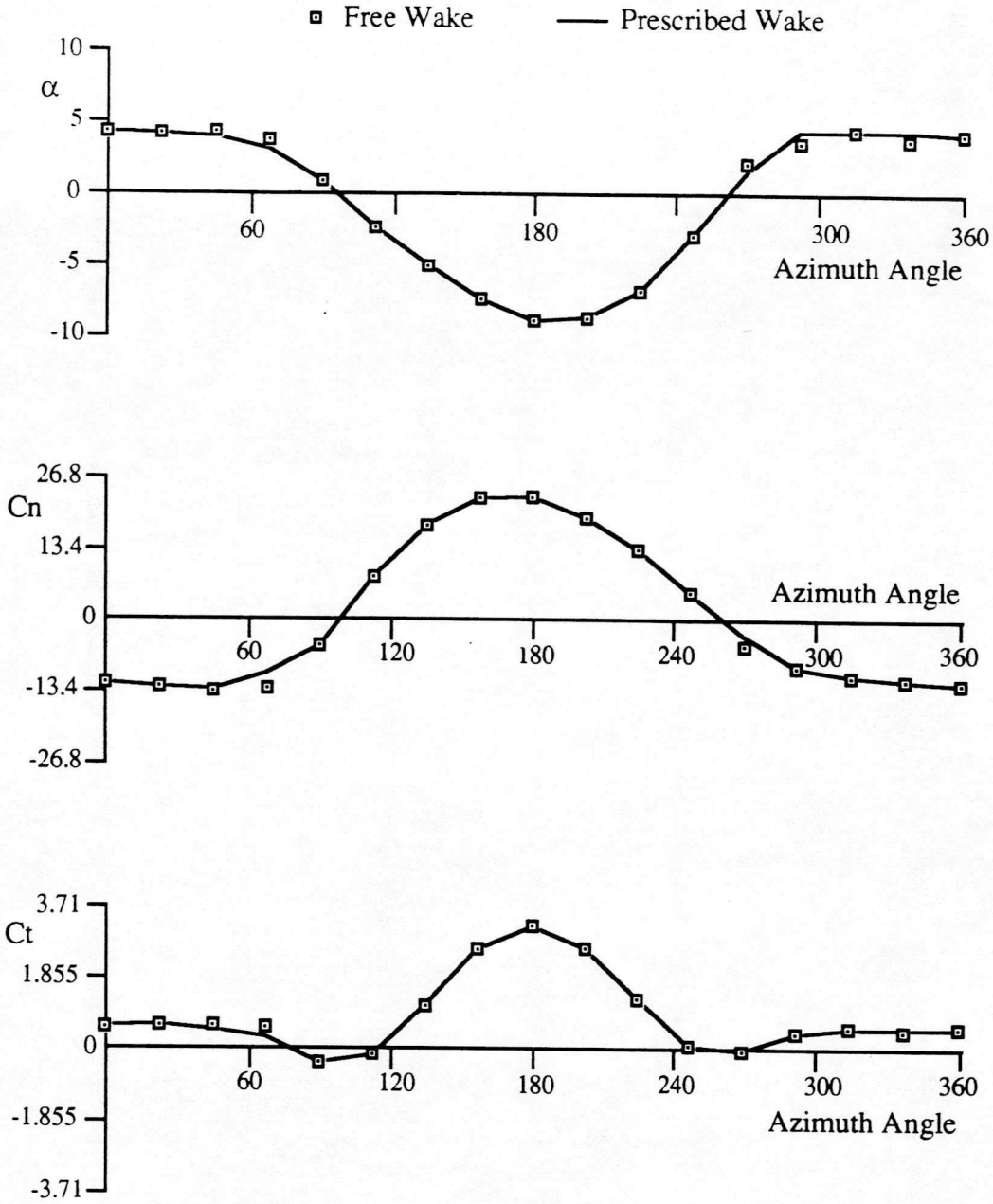

Fig. 2.5 Comparison Of Free And Prescribed Wake Vortex Methods At Tip-speed Ratio 5

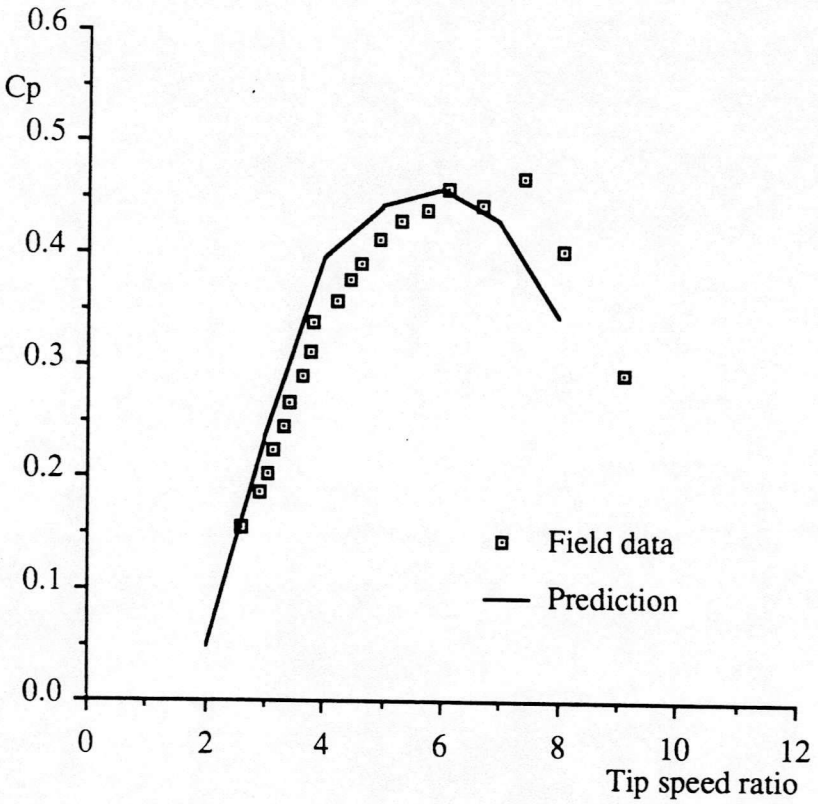

Fig. 2.6 Comparison Of Prescribed Wake Prediction With Field Data From 17m Sandia Turbine (38.7 revolution per minute)

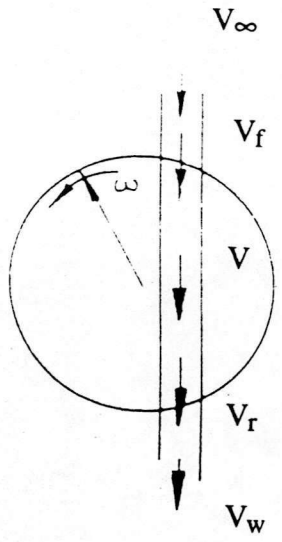

Fig. 2.7 Streamtube Representation Of The Flow Through A Vertical Axis Wind Turbine

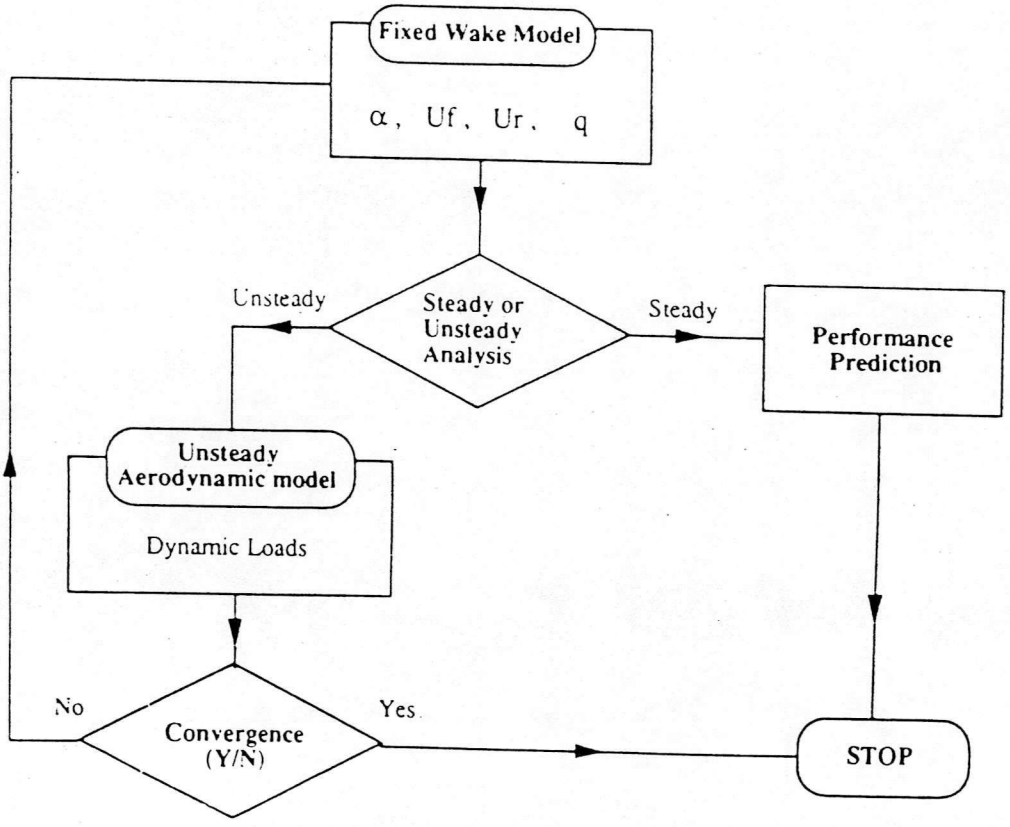

Fig. 2.8 Incorporation Of The Dynamic Stall Model Within The Fixed Wake Scheme

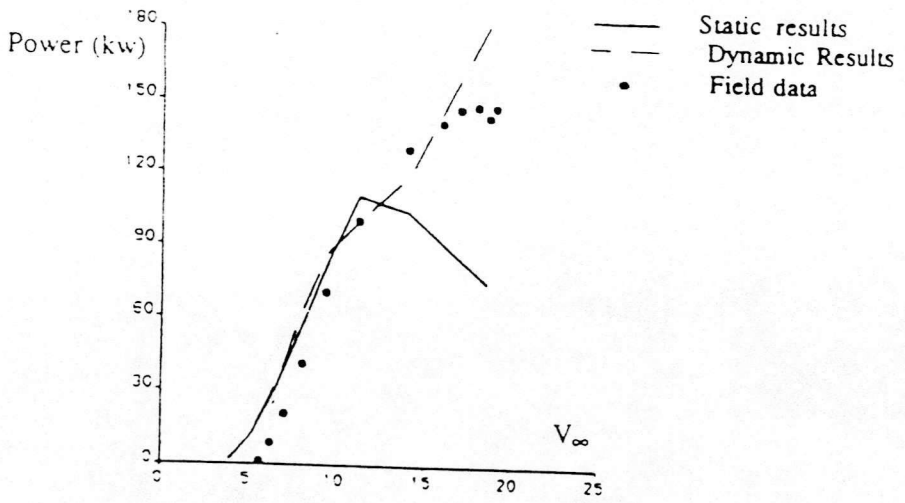

Fig. 2.9 Power Versus Wind Speed From The Fixed Wake Method

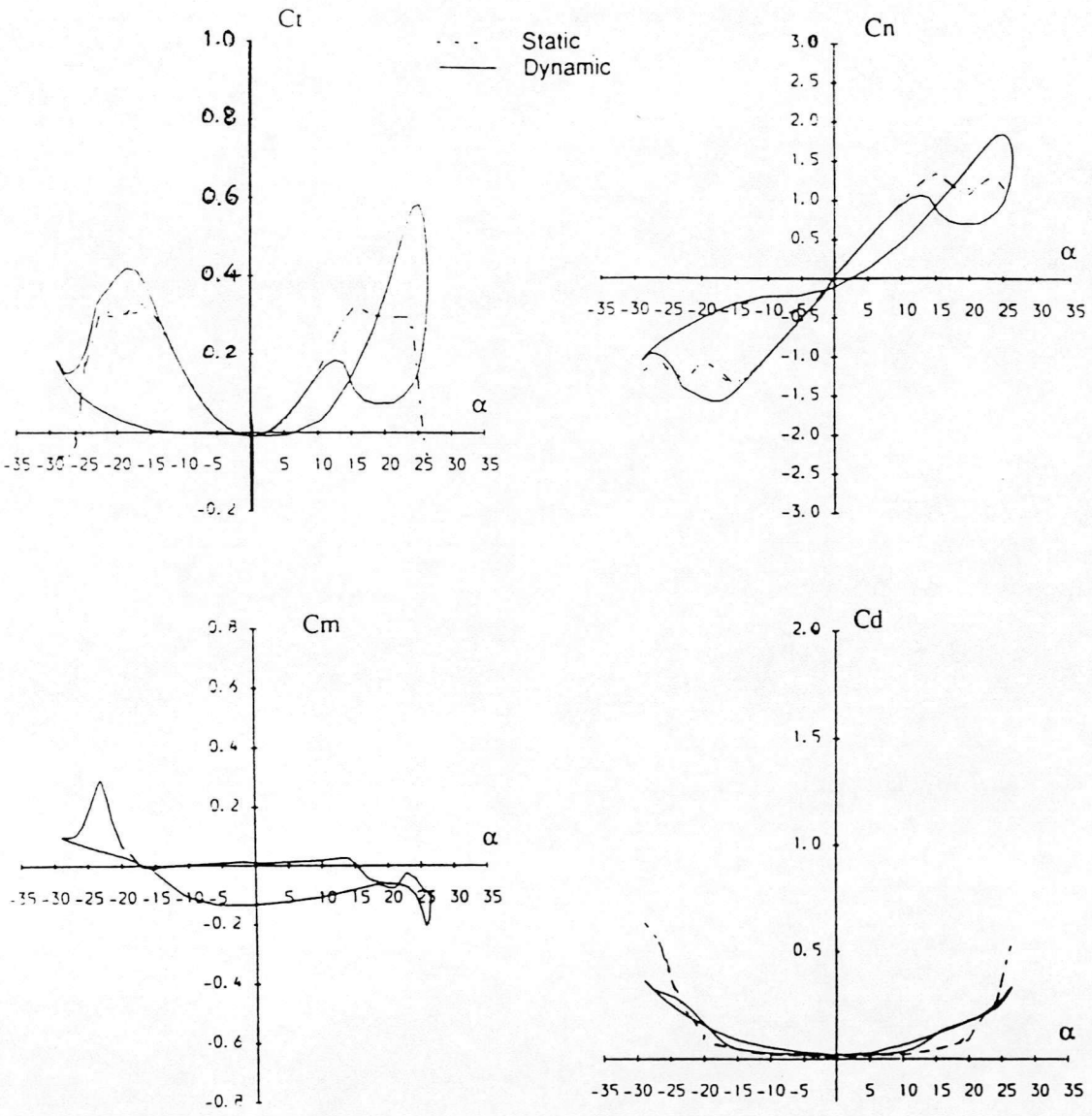

Fig. 2.10 Calculated Dynamic Airloads On The VAWT 220 At Tip-speed Ratio 2

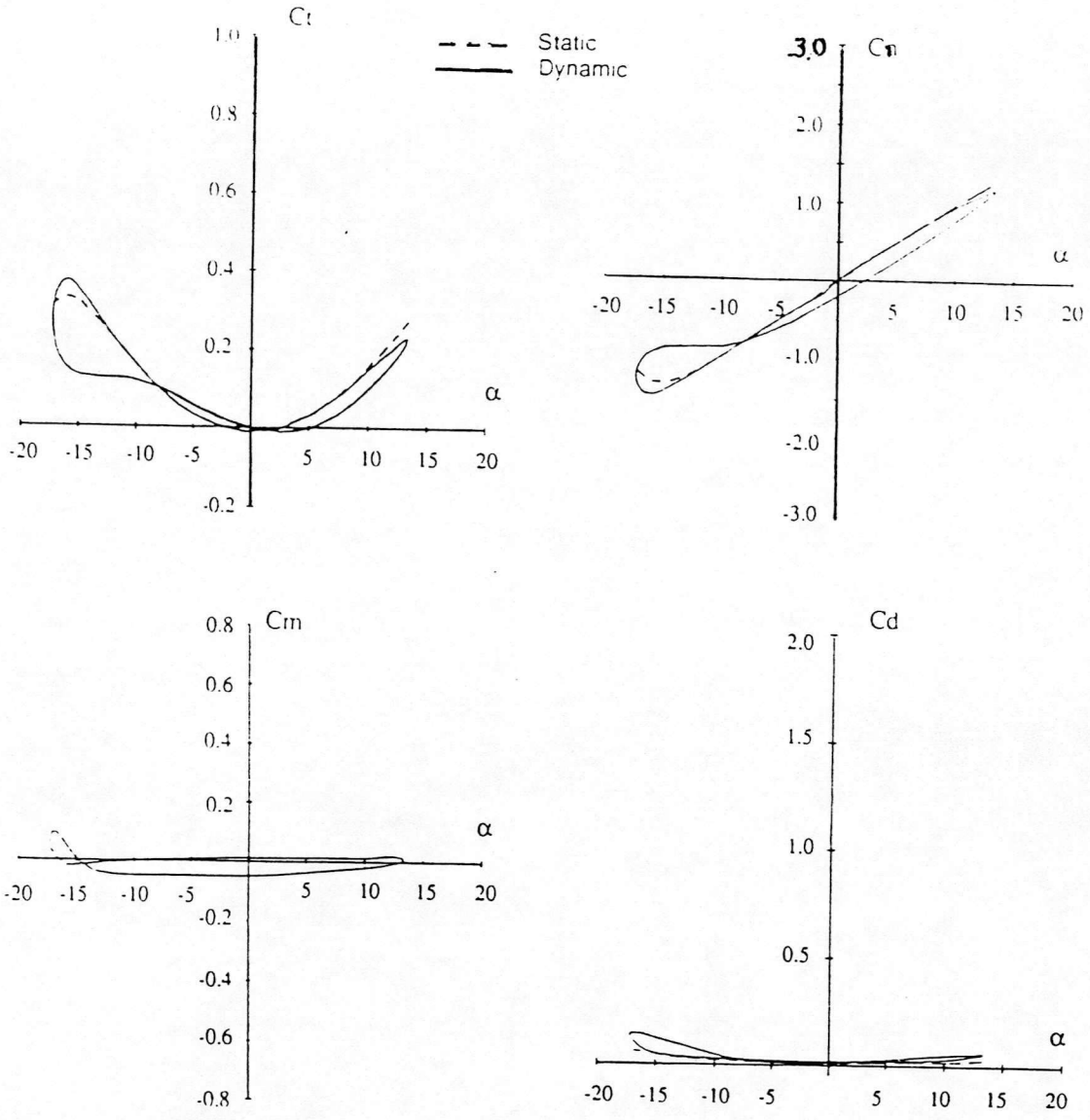

Fig. 2.11 Calculated Dynamic Airloads On The VAWT 220 At Tip-speed Ratio 3

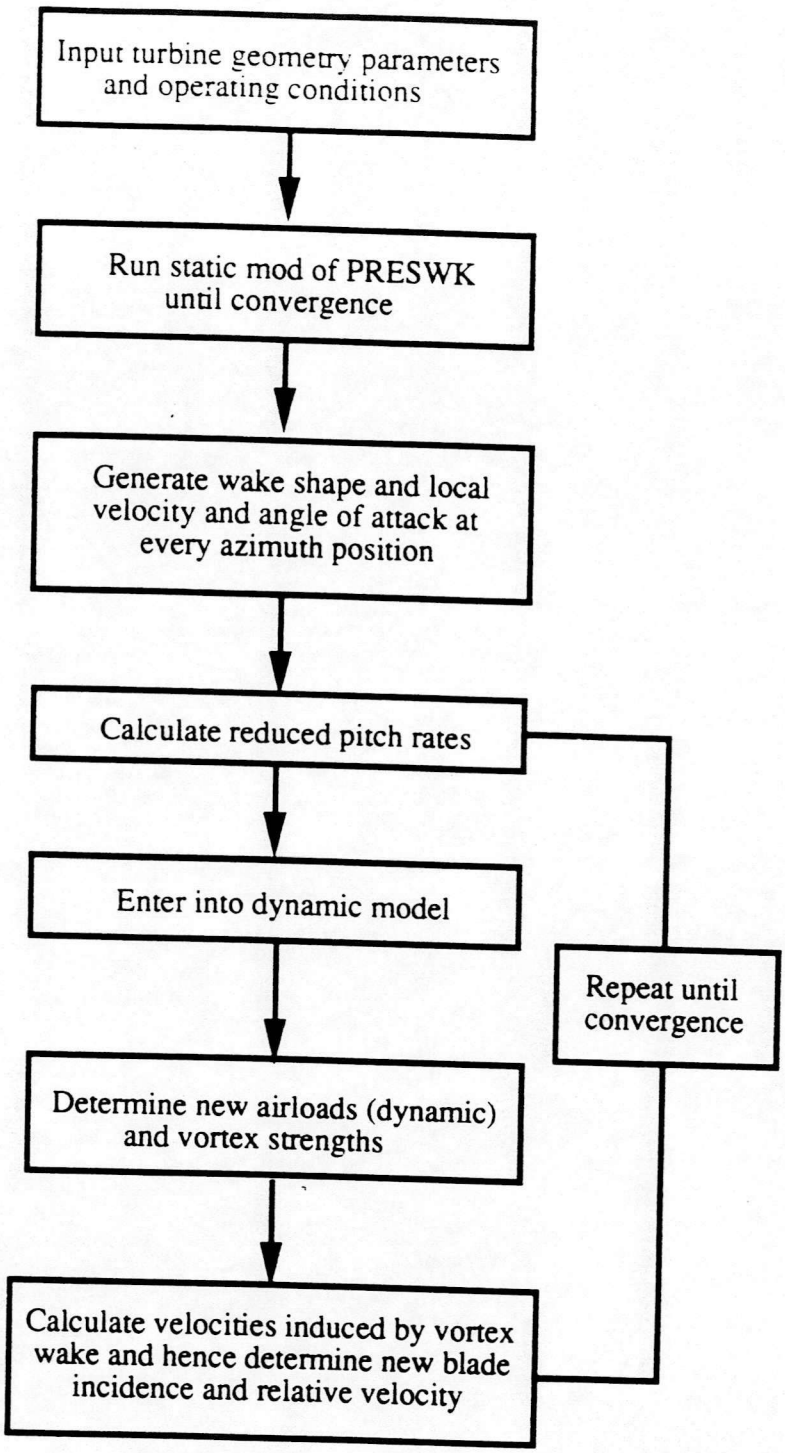

Fig. 2.12 Dynamic Mod PRSWK Calculation Scheme

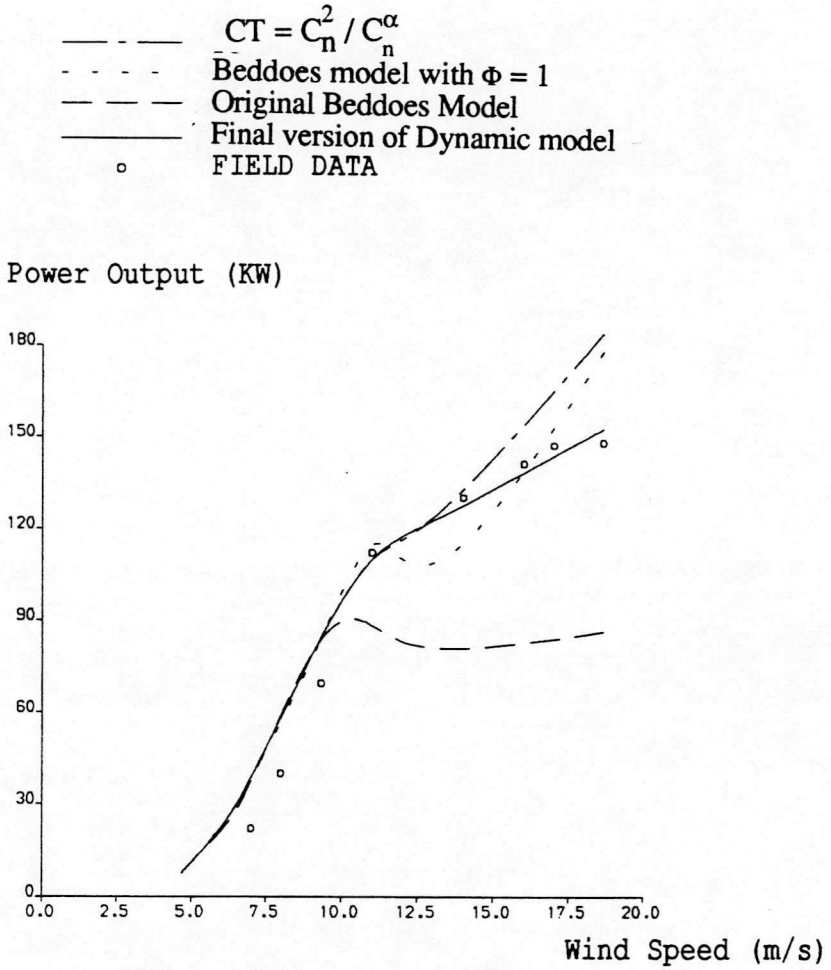

Fig. 2.13 Power Output Against Wind Speed

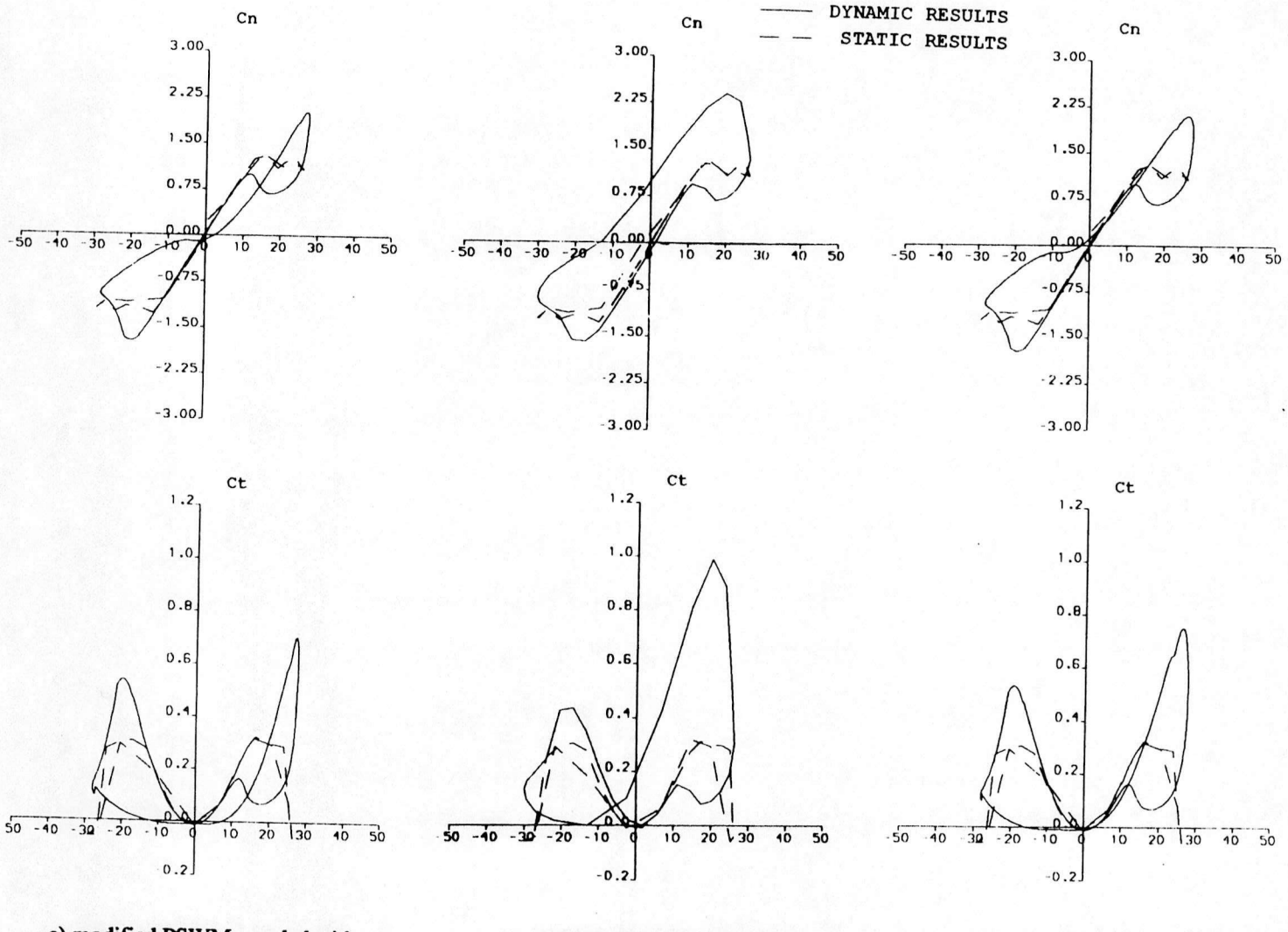

a).modified PSWM coupled with original Beddoes' model (tip-speed ratio 2.0)

b). PSWM plus dynamic model without the shed wake effect (tip-speed ratio 2.0)

c).modified PSWM plus the dynamic model with constant A_1 =0.21, A_2 =0.49 (tip-speed ratio 2.0)

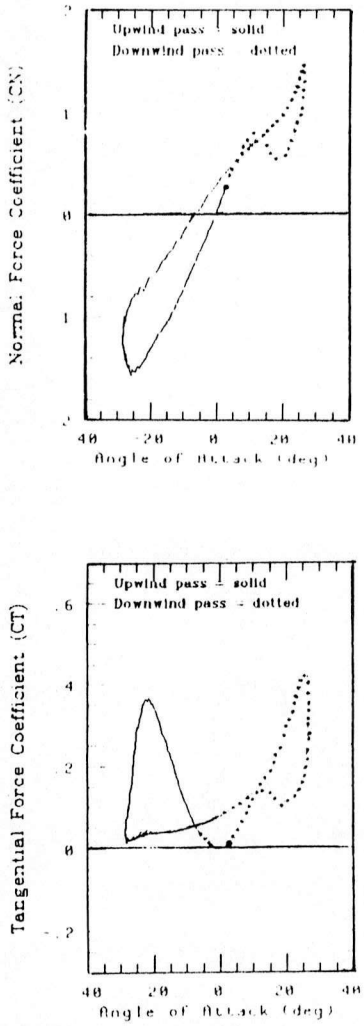

d). field data (tip-speed ratio 2.04)

Fig. 2.14 Comparison Of C_T Results From Different Models And Field Data

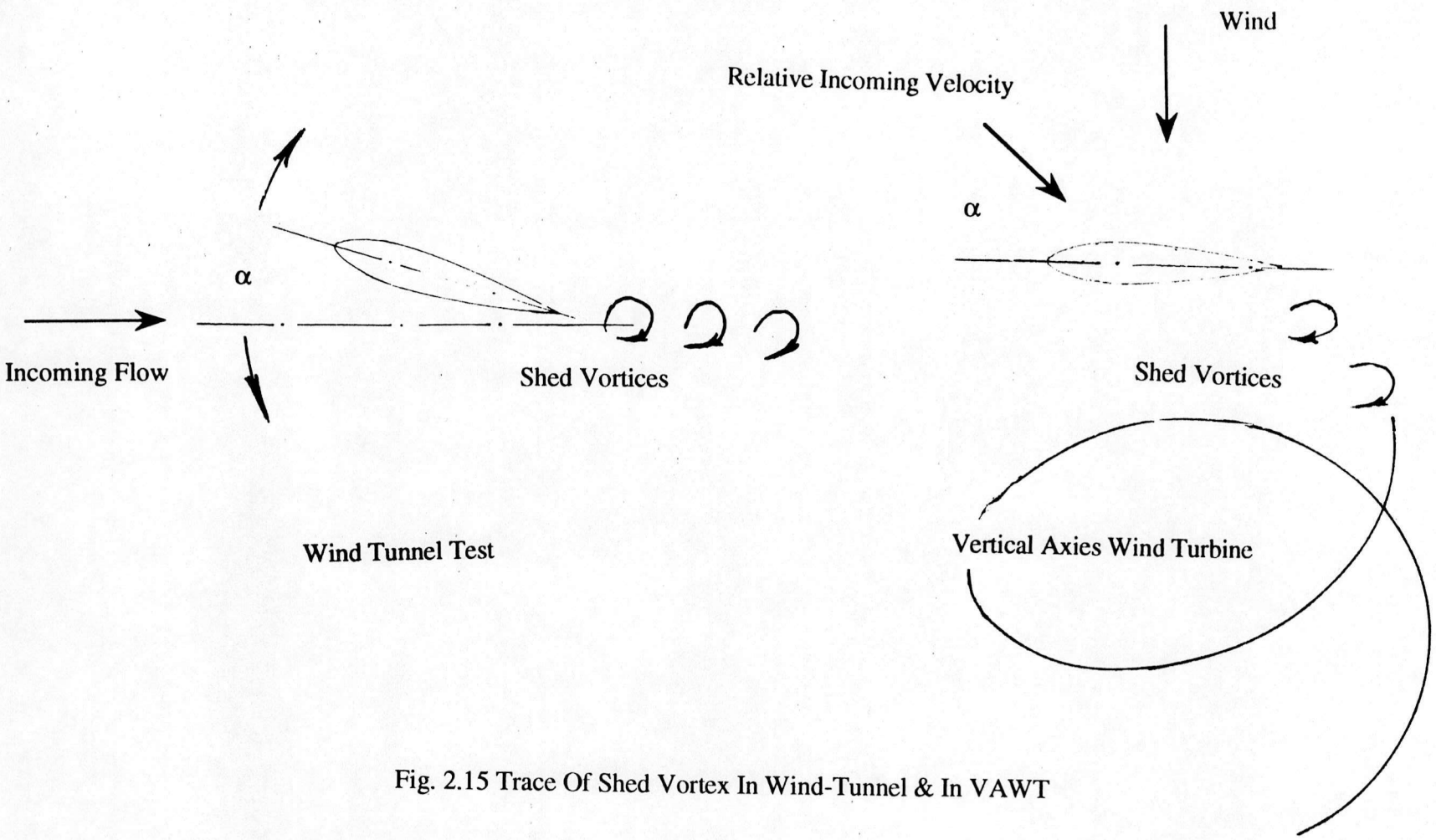

Fig. 2.15 Trace Of Shed Vortex In Wind-Tunnel & In VAWT

TIP-SPEED RATIO 2.0

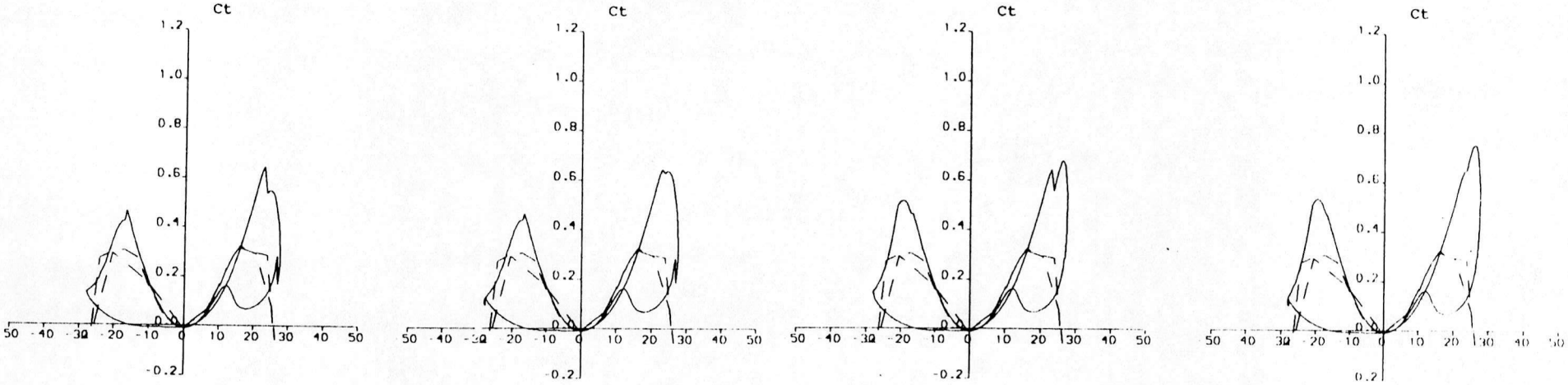

a).considering only C_N^C

b).considering the contribution both from C_N^C and C_N^I

c).considering the contribution both from C_N^C and C_N^V

d). results from the final version of C_T formula

Fig. 2.16 Contribution Of C_N^C, C_N^V and C_N^I to C_T

TIP-SPEED RATIO 1.5

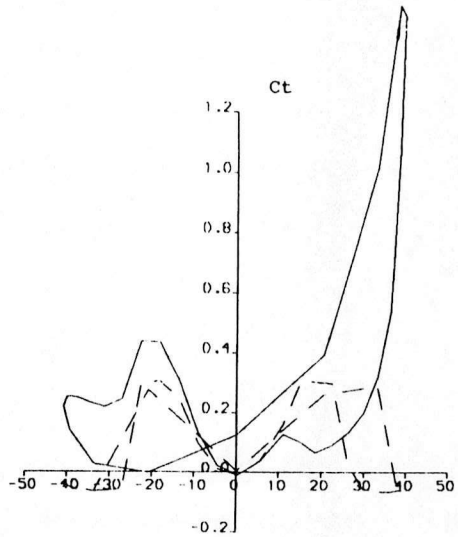

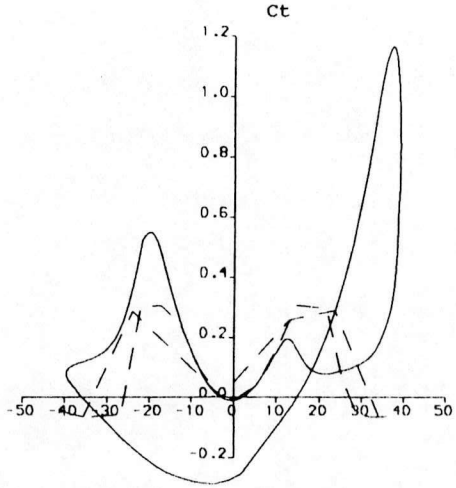

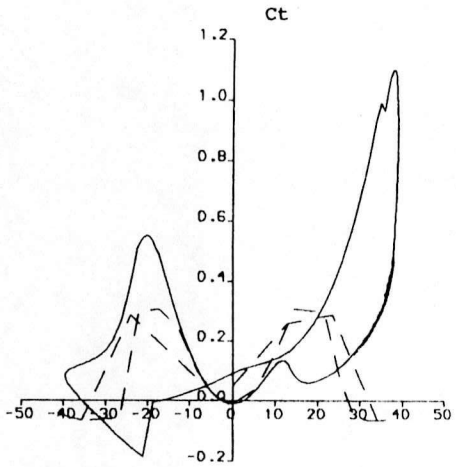

TIP-SPEED RATIO 2.0

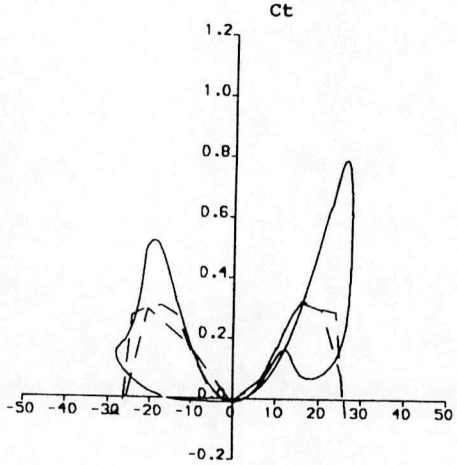

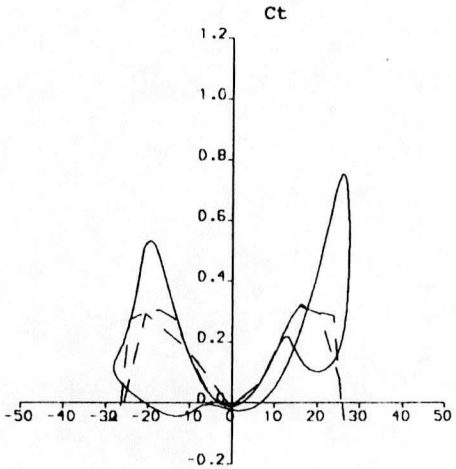

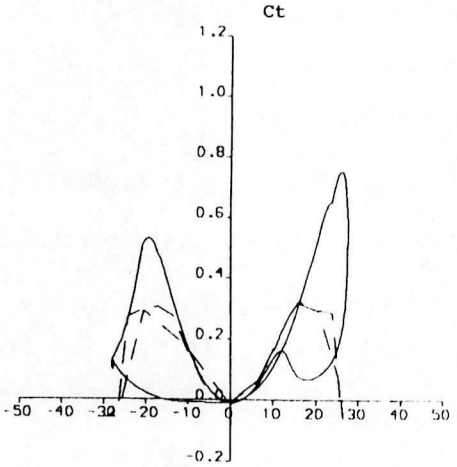

a). $C_T = C_N^2 / C_N^\alpha$

b). $C_T = \Phi (C_N^c \sqrt{f} + C_N^I + C_N^V) \mathrm{Tan}(\alpha_E) - C_{D0}$

c). final version of C_T formula

Fig. 2.17 Comparison Of Results From Different C_T Formulas

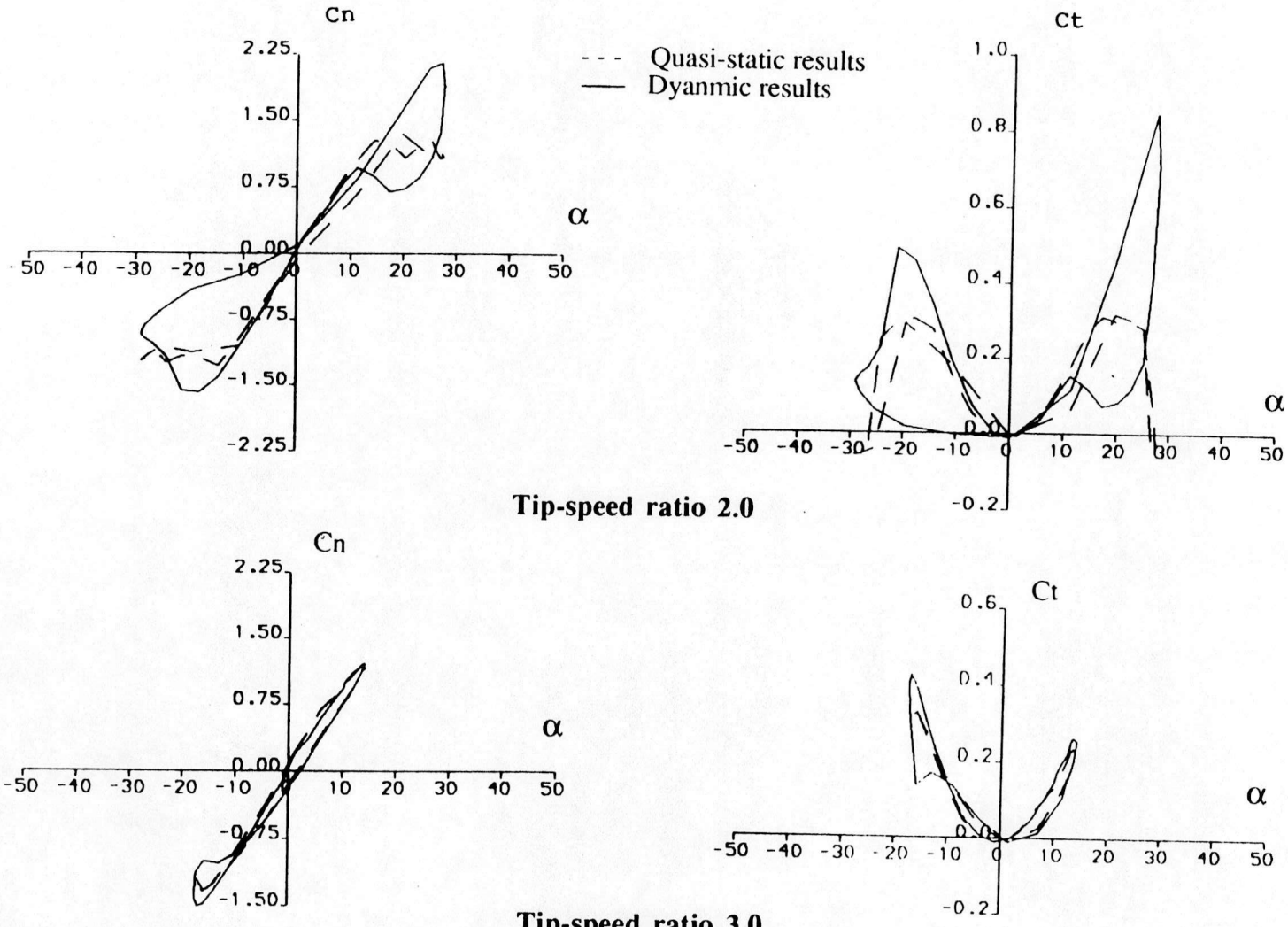

Fig. 2.18 Airloads On VAWT220 At Tip-speed Ratio 2.0 And 3.0

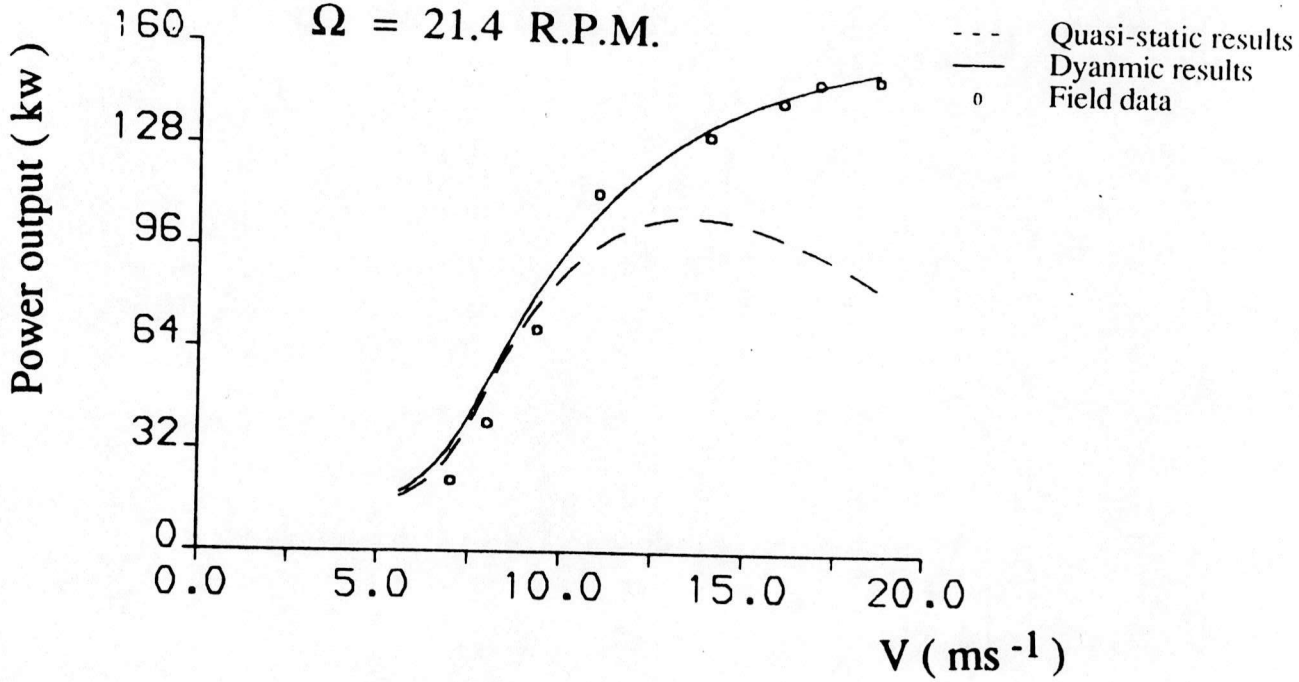

Fig. 2.19 Power Output Against Velocity From PRSWK

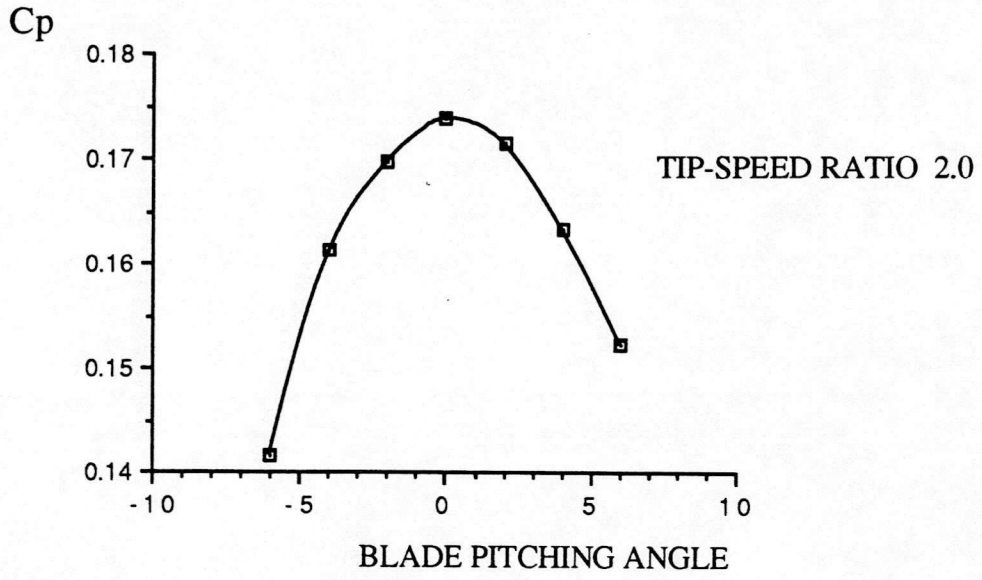

Fig. 2.20 Power Coefficient Against Blade Pitch Angle

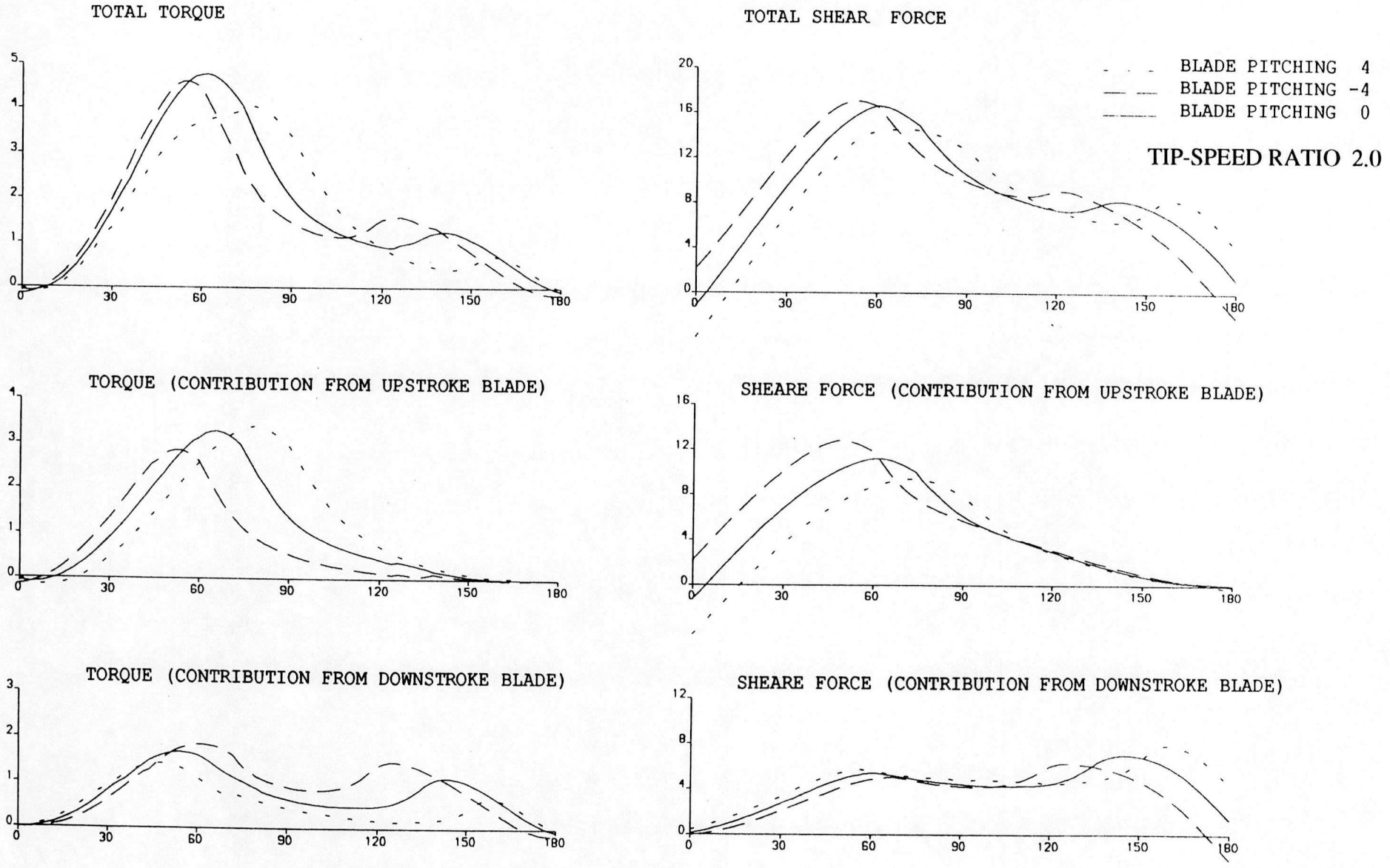

Fig. 2.21 Variation Of Total Torque and Total Shear Force with Azimuthal Angle At Different Blade Pitch Angle

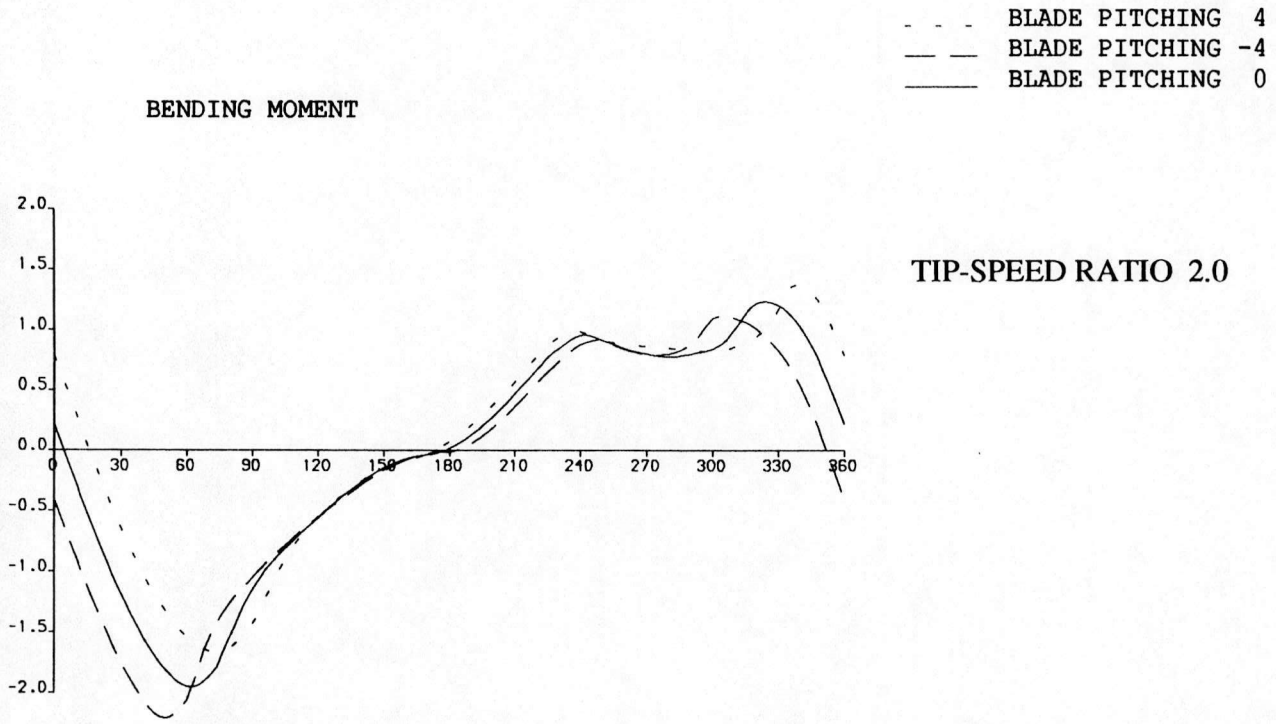

Fig. 2.22 Variation Of Bending Moment With Azimuthal Angle At Different Pitch Angle

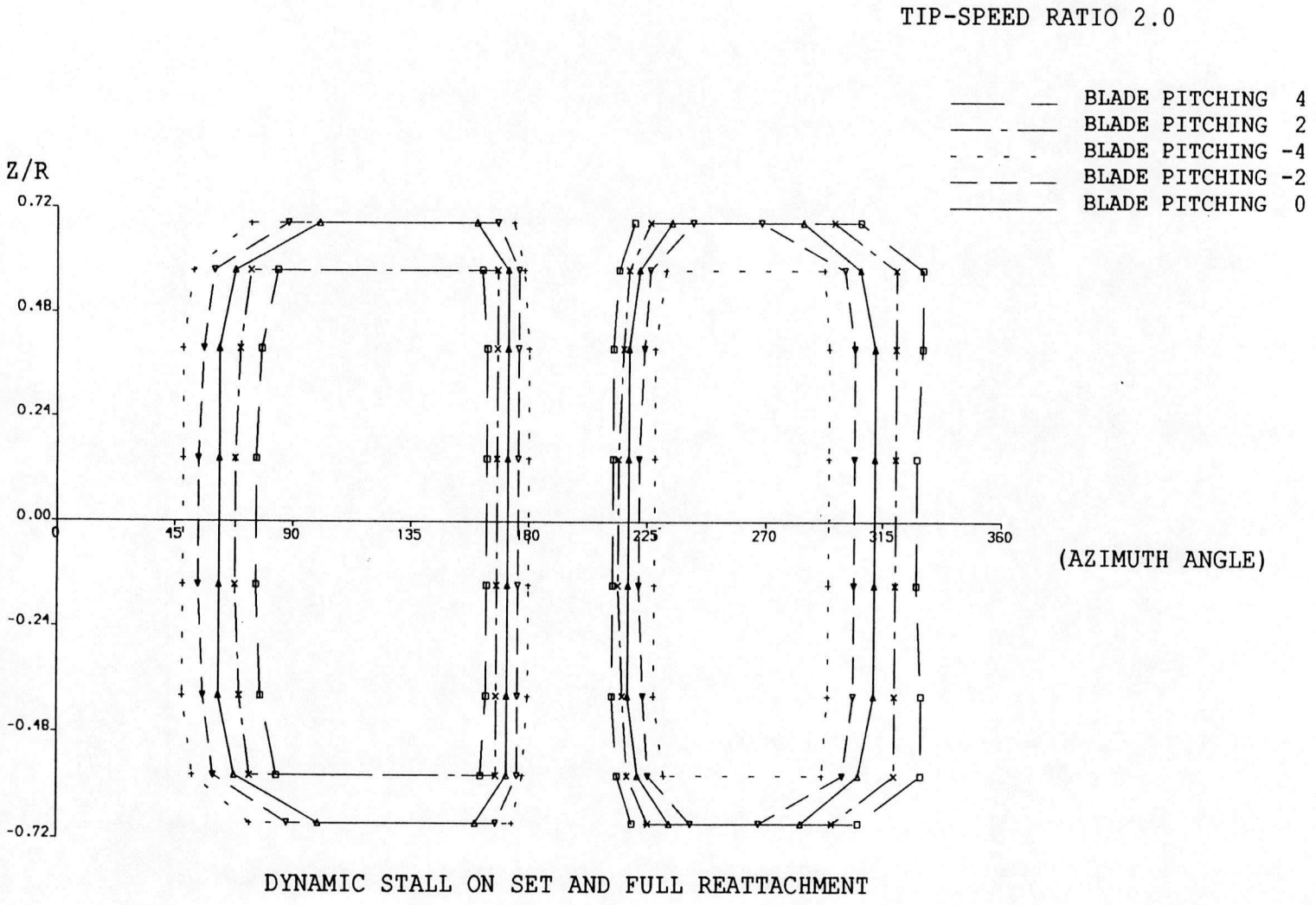

Fig. 2.23 Dynamic Stall Region In Blade Upwind Pass And Downwind Pass, Respectively, At Different Blade Pitch Angle

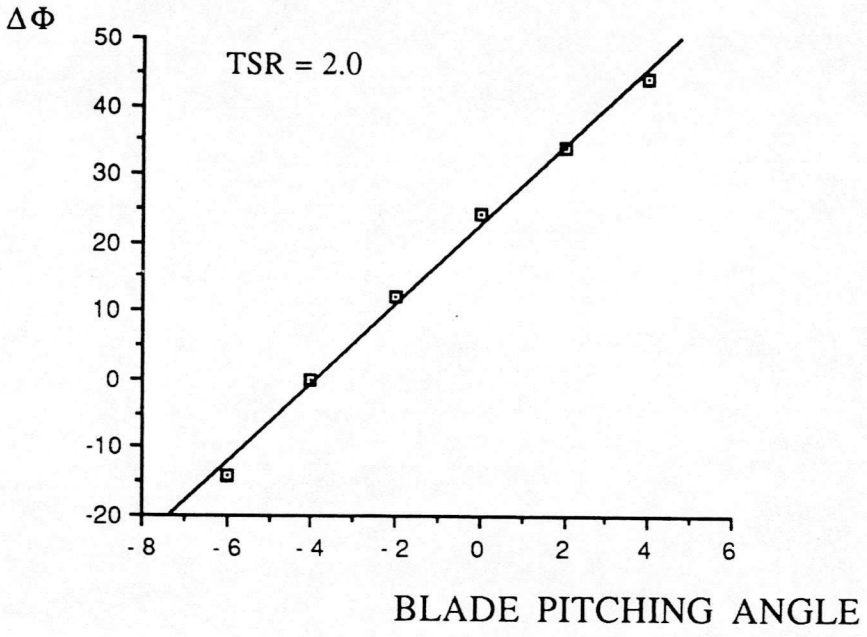

Fig. 2.24 Difference In Azimuthal Angle Of Dynamic Stall Onset Between Upwind Pass And Downwind Pass

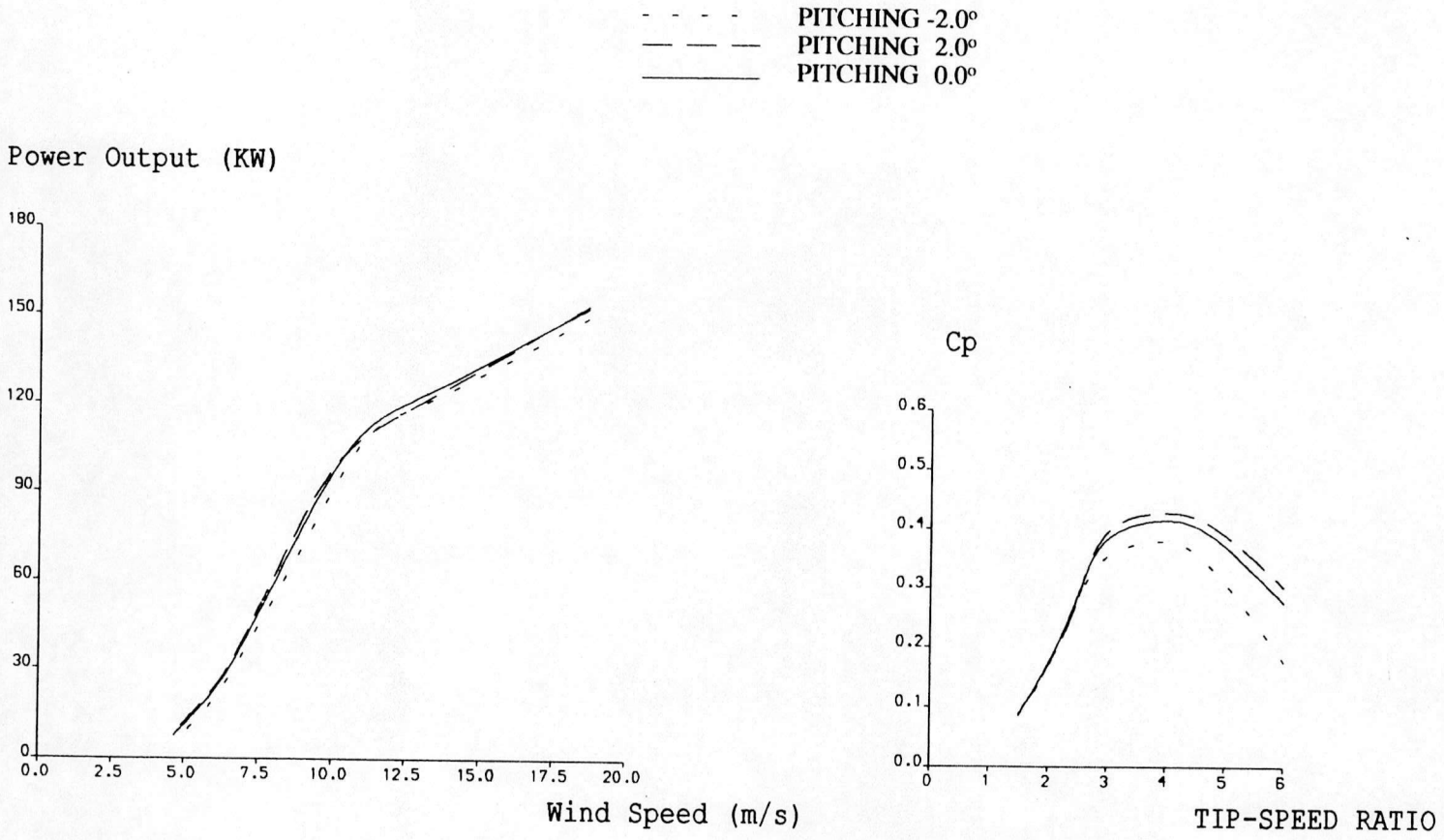

Fig. 2.25 VAWT Power Output And Power Coefficient
(R = 12.5m, ω = 21.4 R.P.M.)

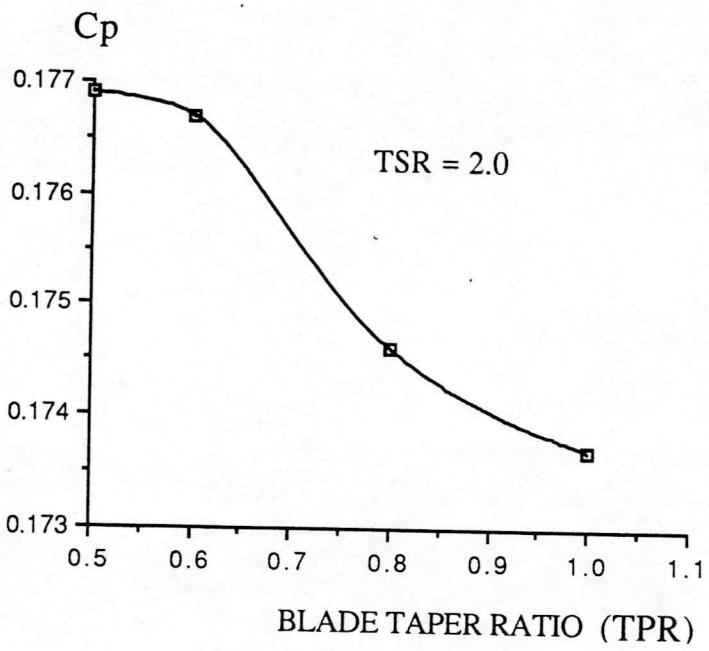

Fig. 2.26 Power Coefficient Versus Blade Taper Ratio

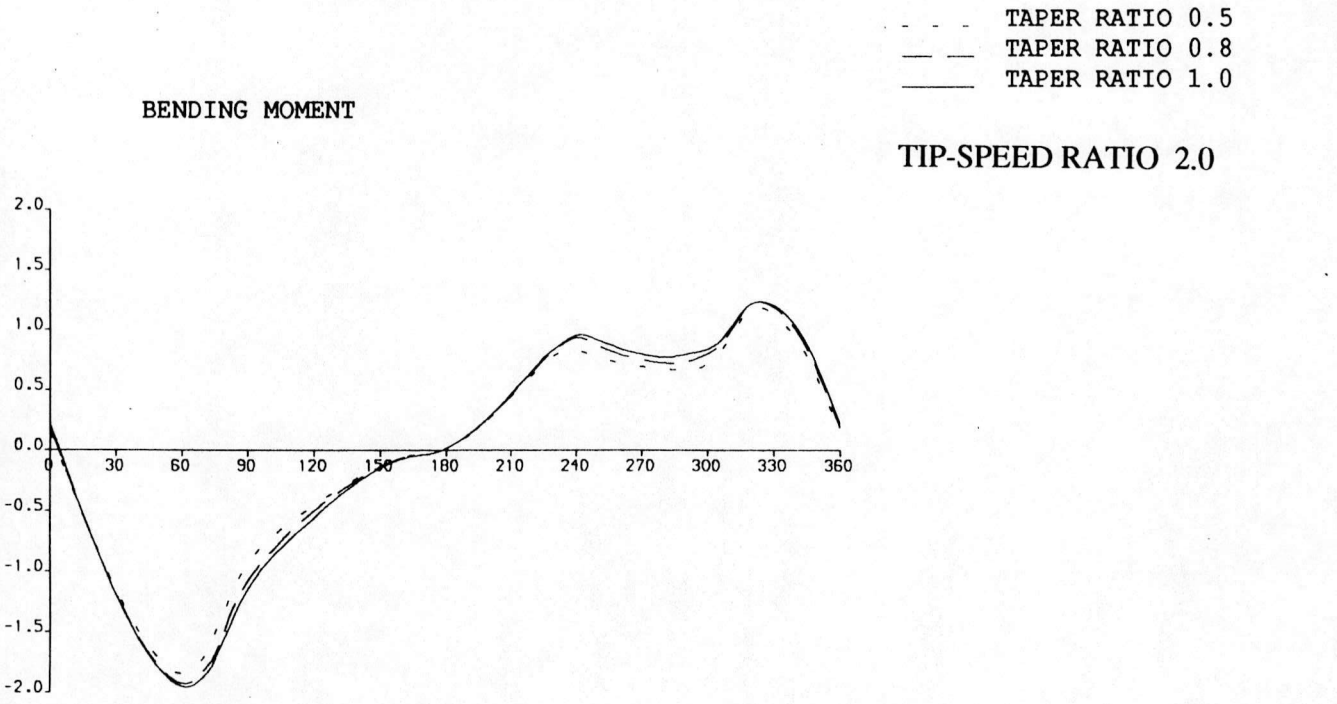

Fig. 2.27 Variation Of Bending Moment With Azimuthal Angle At Different Taper Ratio

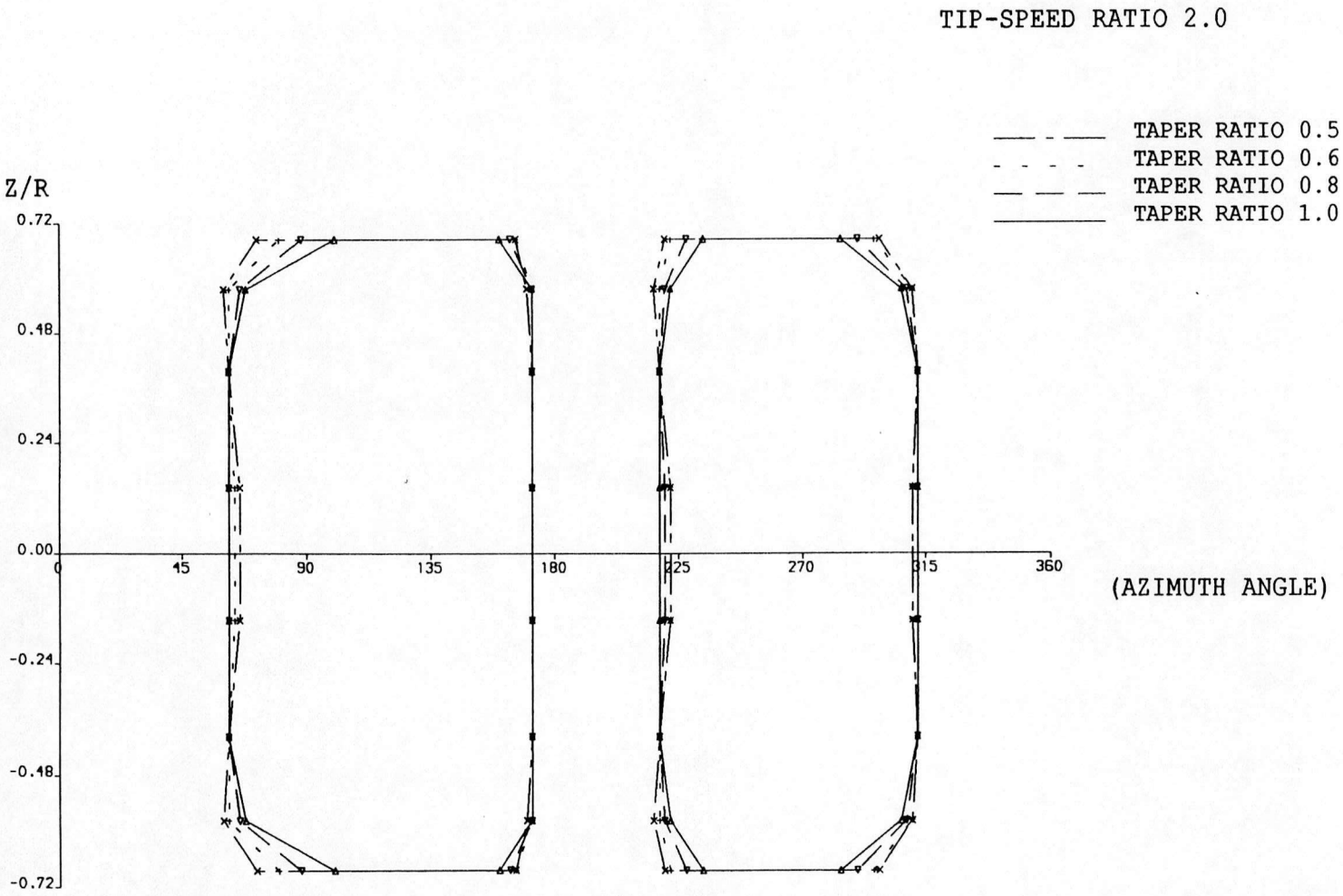

Fig. 2.28 Dynamic Stall Region In Blade Upwind Pass And Downwind Pass, Respectively, At Different Blade Taper Ratio

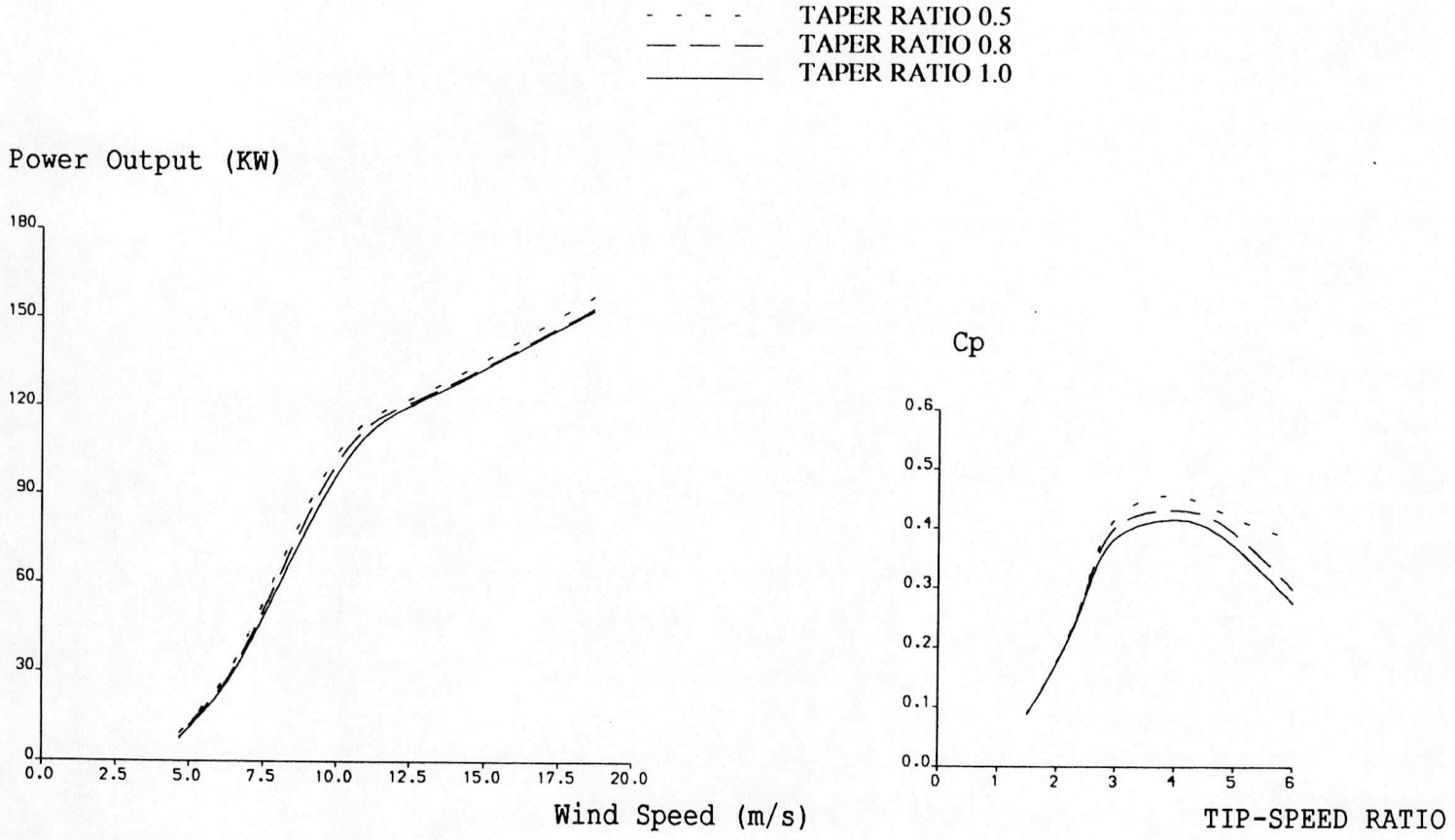

Fig. 2.29 VAWT Power Output And Power Coefficient
(R = 12.5m, ω = 21.4 R.P.M.)

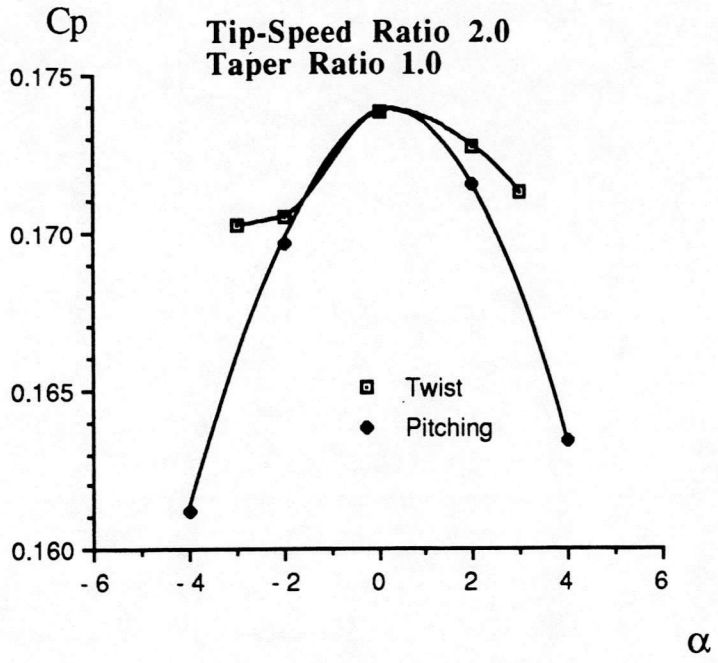

Fig. 2.30 Power Coefficient Against Blade Pitching Or Twist Angle

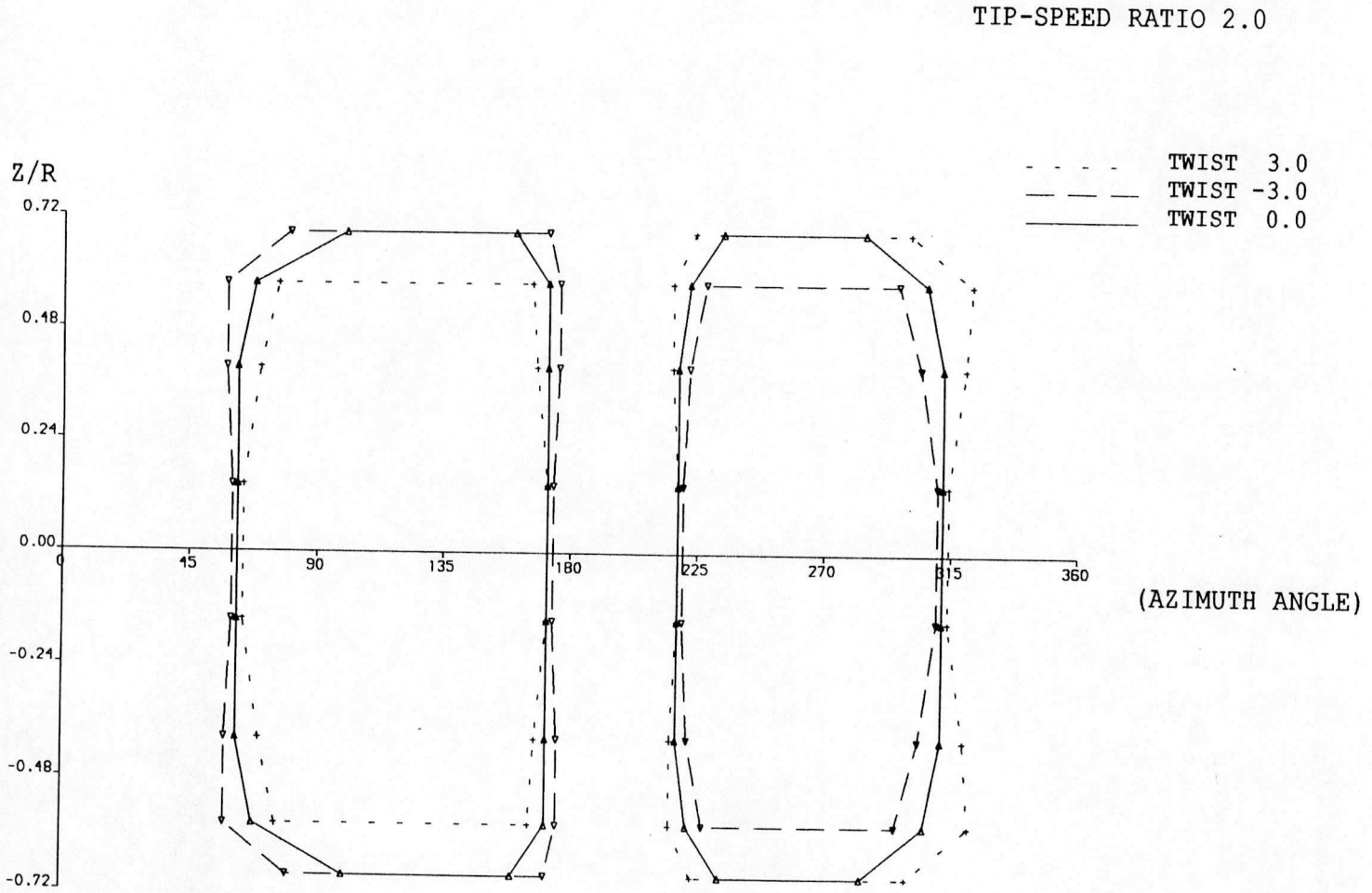

Fig. 2.31 Dynamic Stall Region In Blade Upwind Pass And Downwind Pass, Respectively, At Different Blade Twist Angle

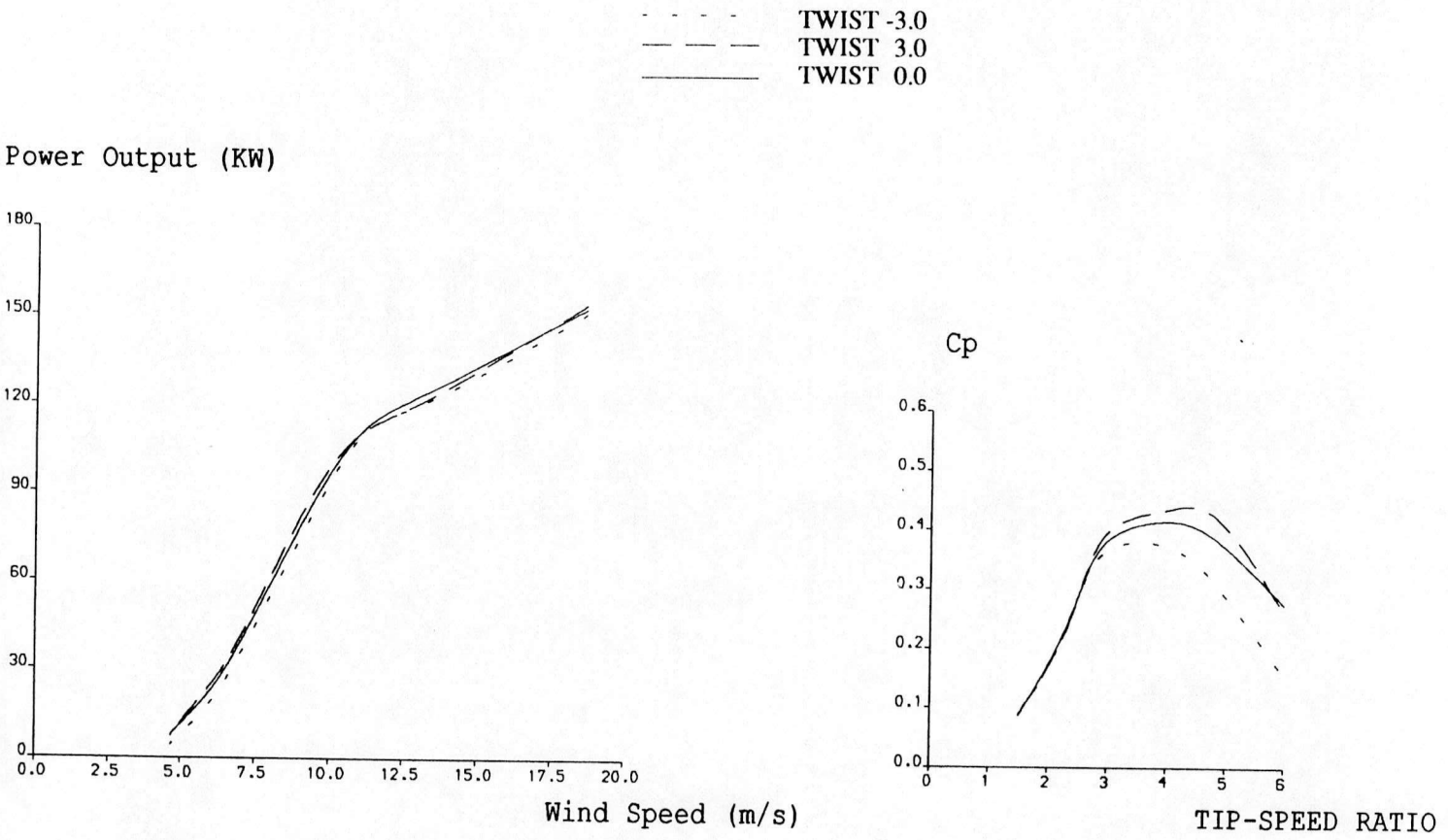

Fig. 2.32 VAWT Power Output And Power Coefficient
(R = 12.5m, ω = 21.4 R.P.M.)

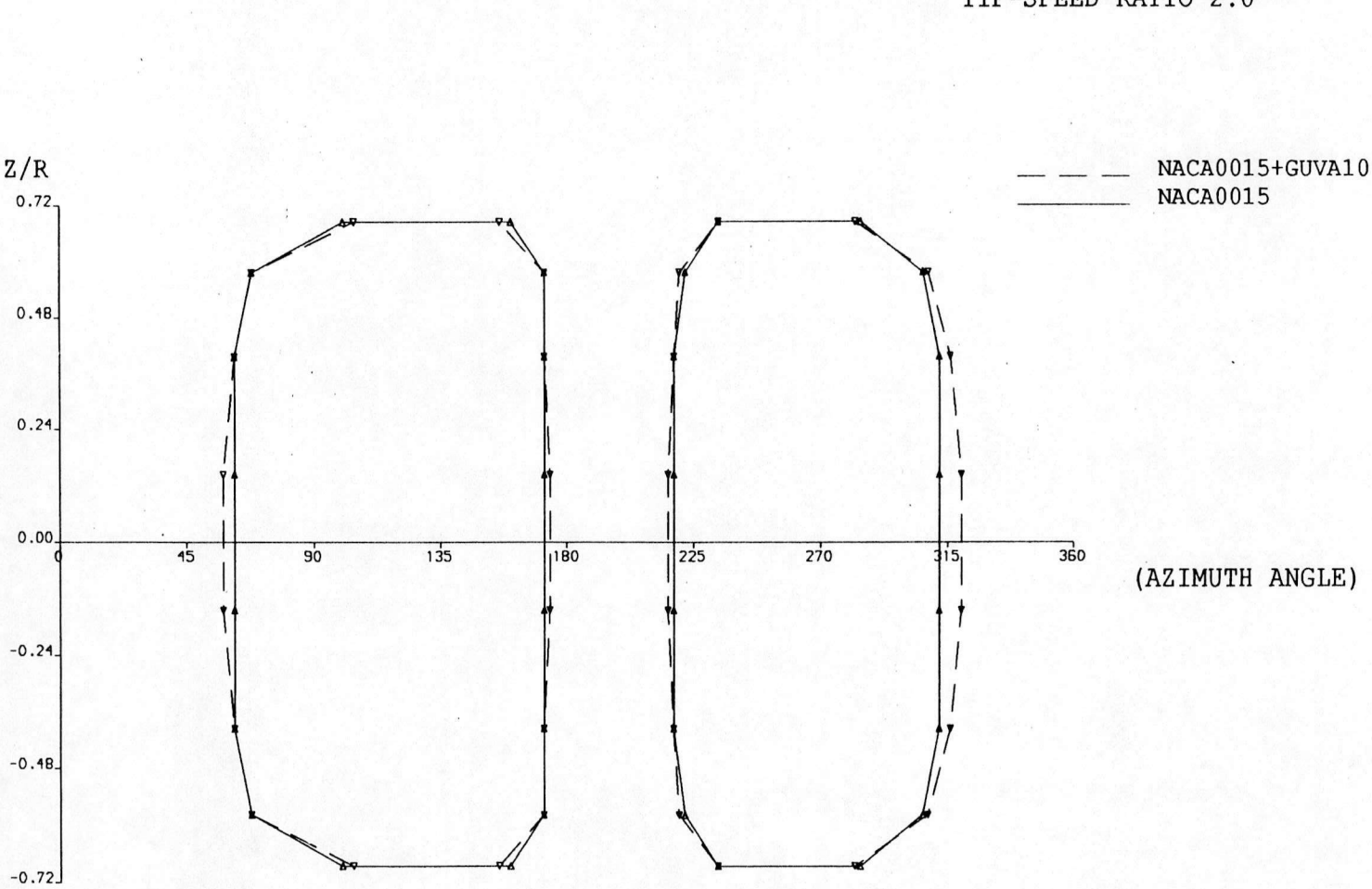

Fig. 2.33 Dynamic Stall Region In Blade Upwind Pass And Downwind Pass, Respectively,

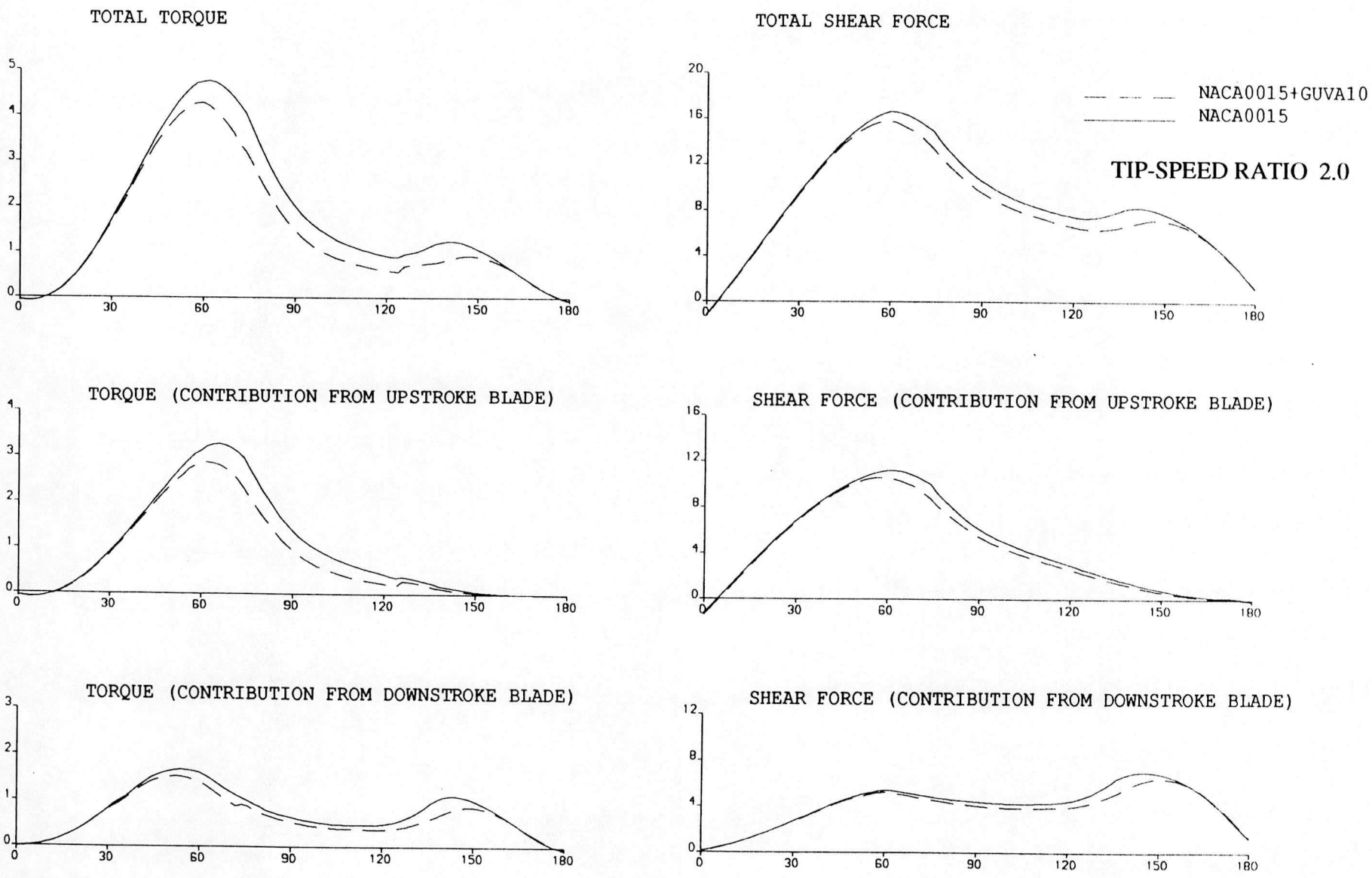

Fig. 2.34 Variation Of Total Torque and Total Shear Force Versus Azimuthal Angle

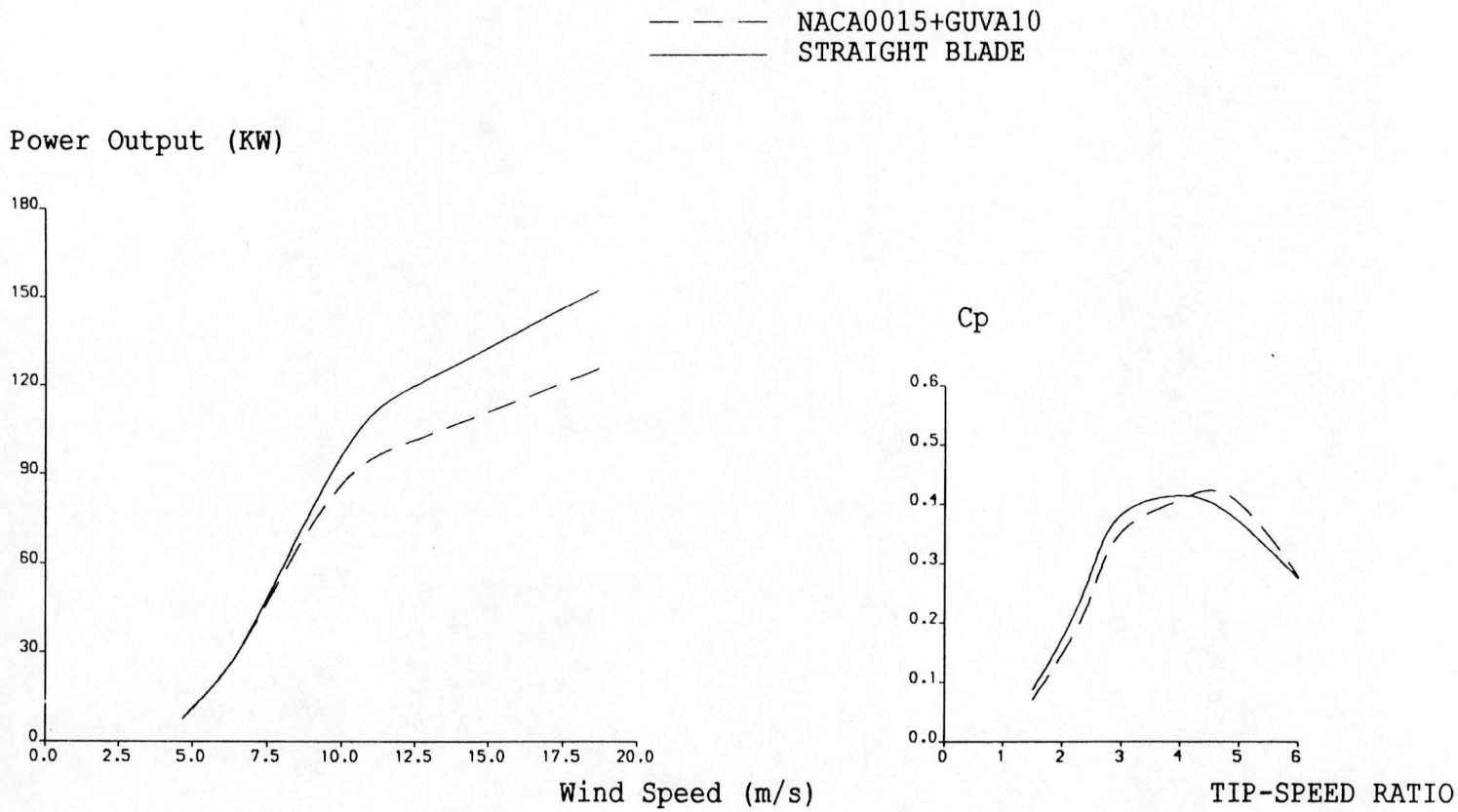

Fig. 2.35 VAWT Power Output And Power Coefficient
(R = 12.5m, ω = 21.4 R.P.M.)

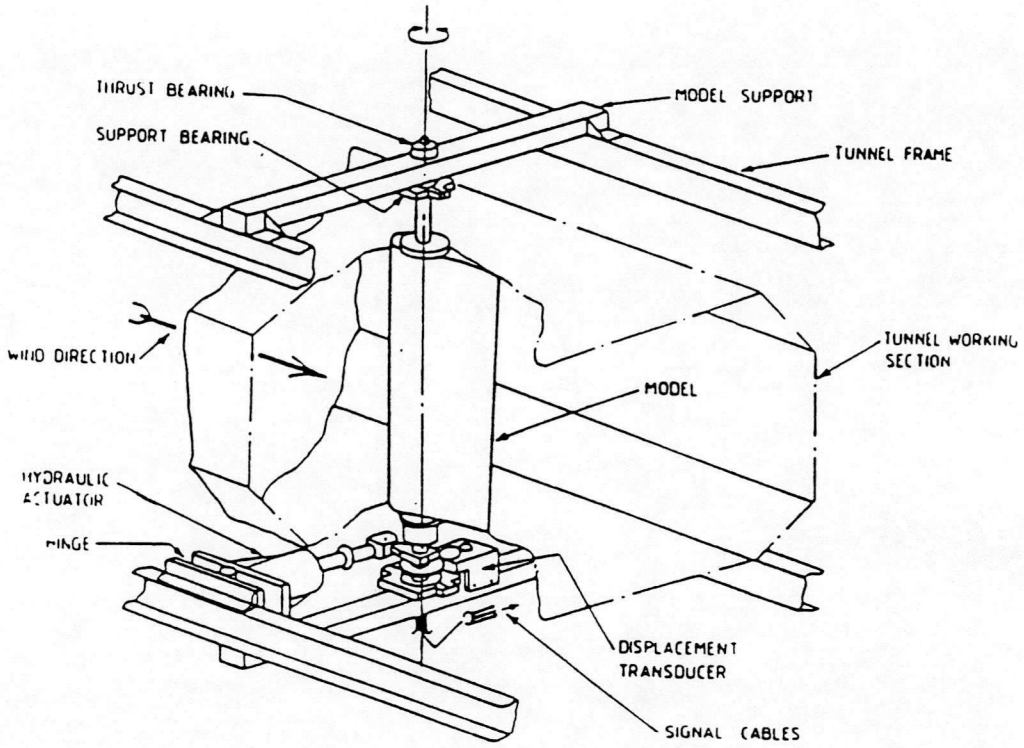

Fig. 2.36 The University Of Glasgow Handley-Page Wind Tunnel And Unsteady Aerodynamics Facility

C_L

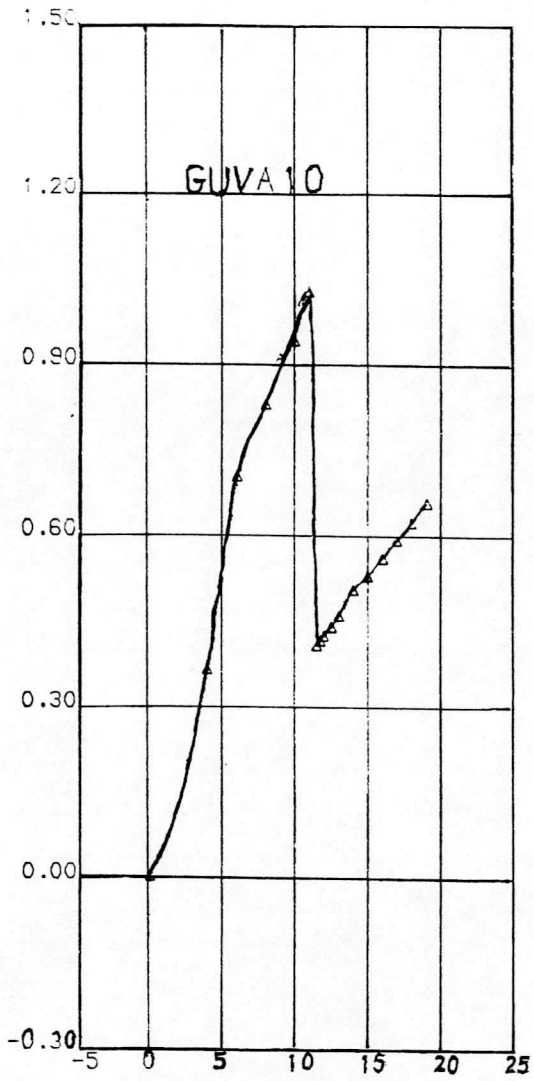

C_T

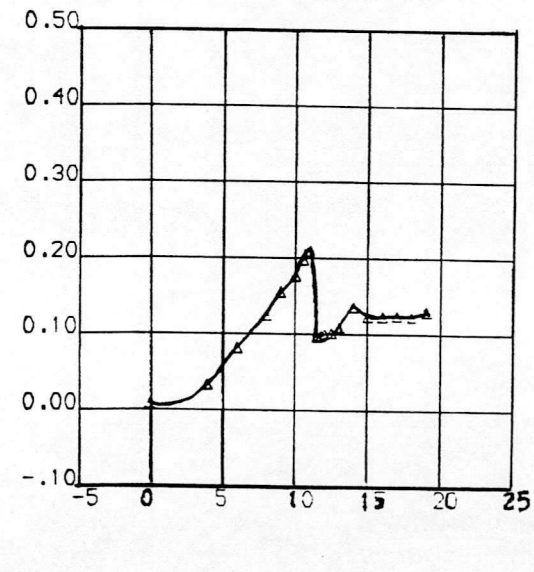

Fig. 2.37 The Static Aerodynamic Characteristics Of GUVA10

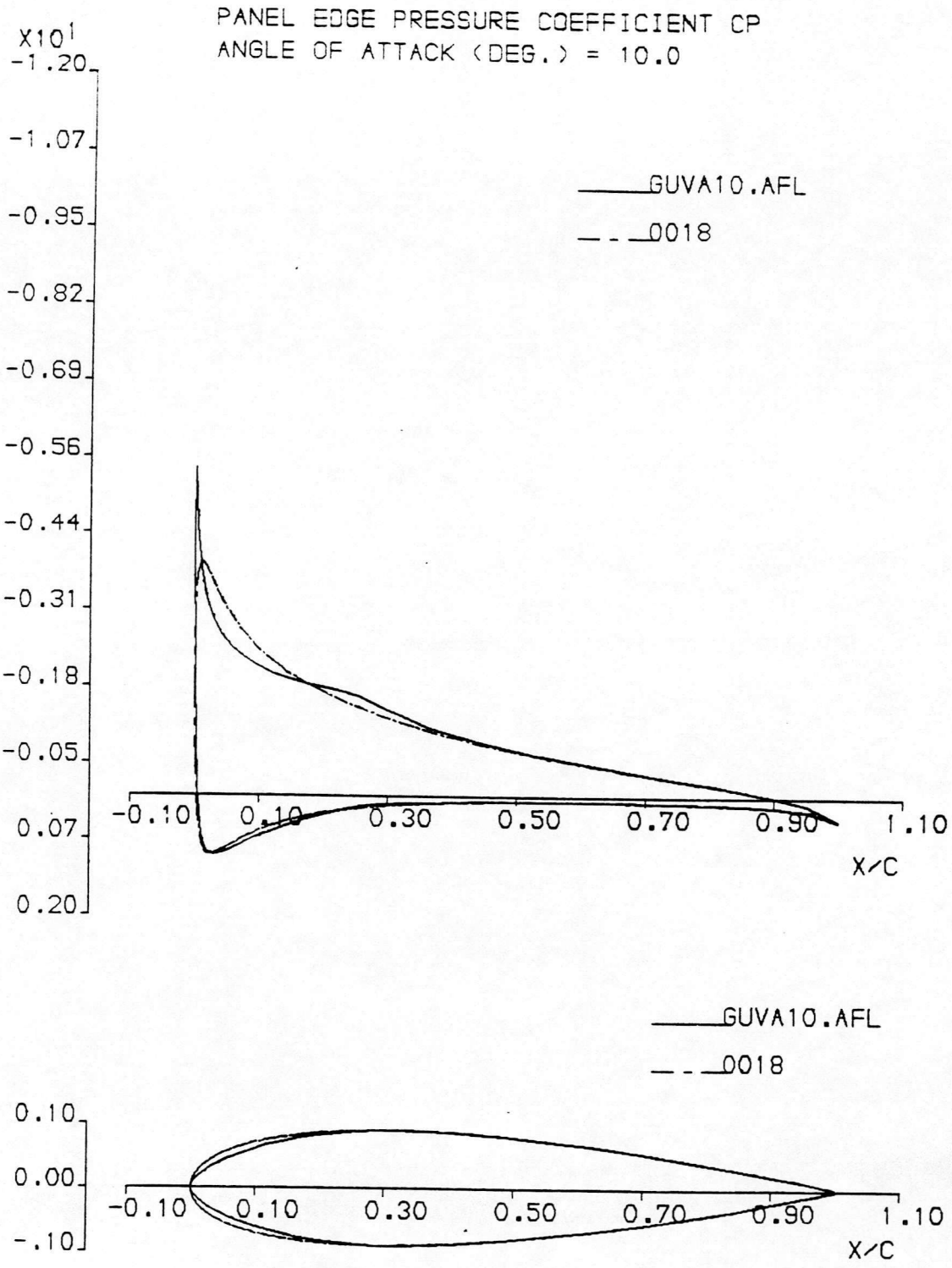

Fig. 2.38 The Presure Distribution On Panels Of GUVA10

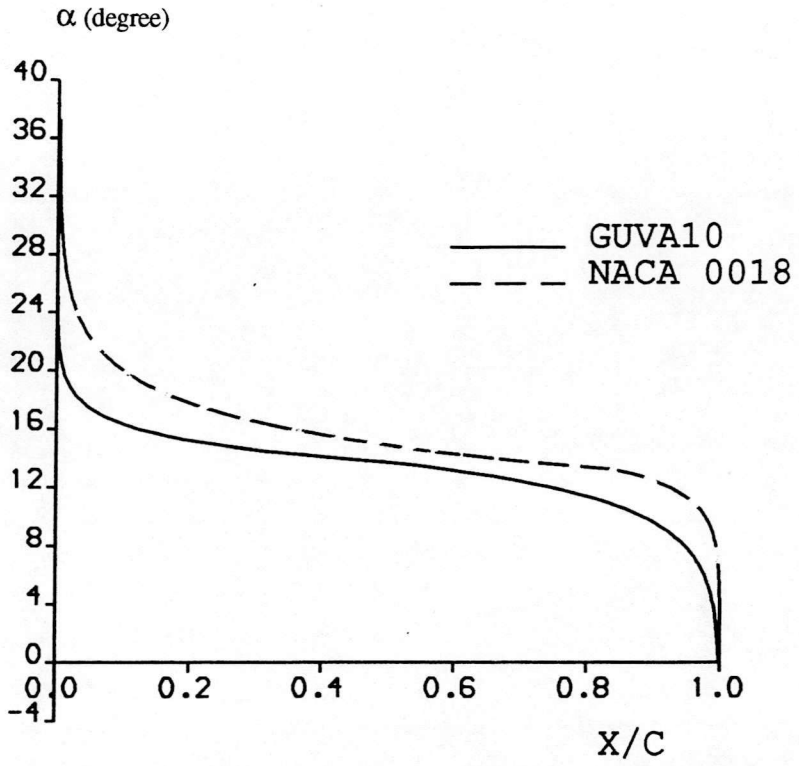

Fig. 2.39 Variation Of Separation Position With Angle Of Attack

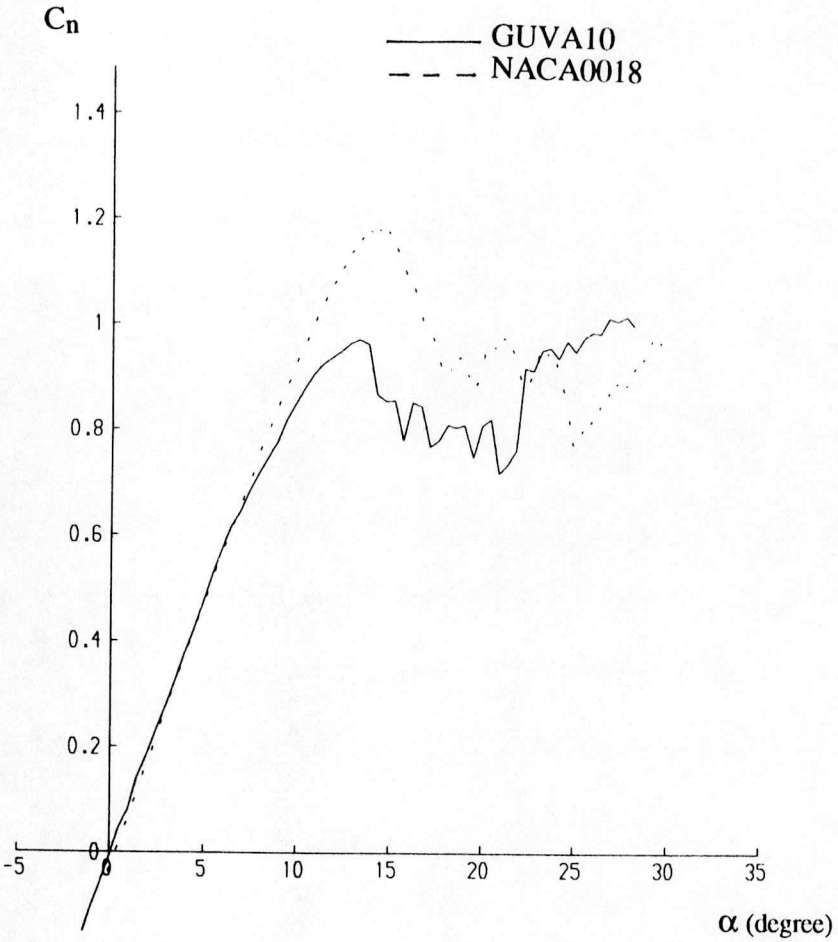

a). C_n Versus Angle Of Attack

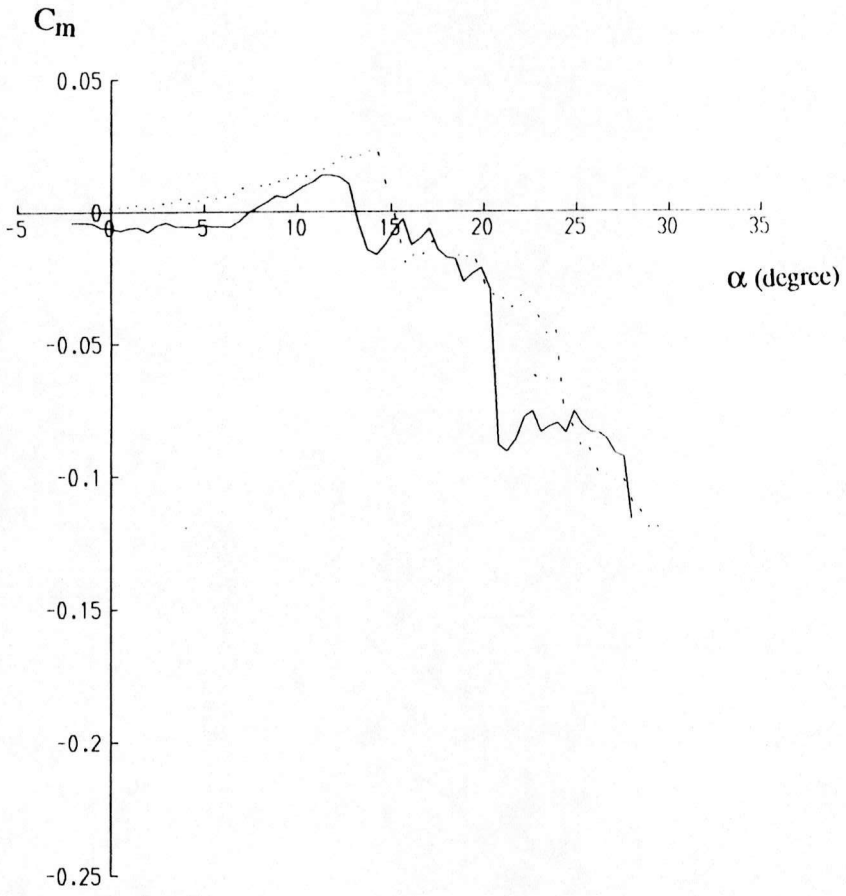

b). C_m Versus Angle Of Attack

Fig. 2.40 Comparisons Of Static Aerodynamic Characteristics Between NACA0018 & GUVA10 At Re = 1.5E6

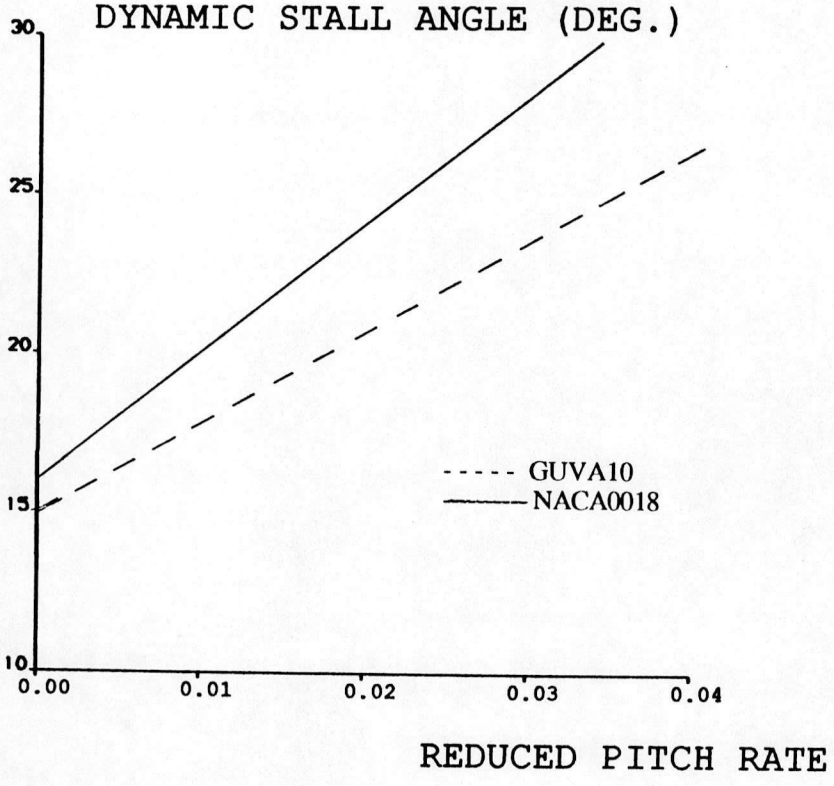

Fig. 2.41 Comparison of the variation of dynamic stall onset angle against reduced pitch rate between NACA0018 & GUVA10 (test results)

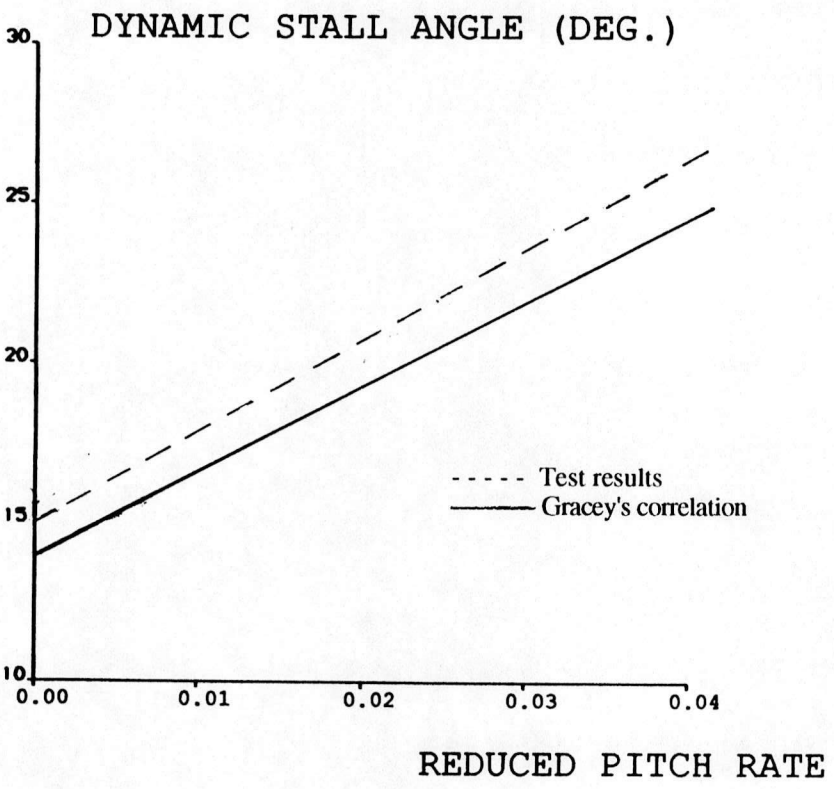

Fig. 2.42 Comparison of dynamic stall onset angle between Gracey's correlation & test results for GUVA10

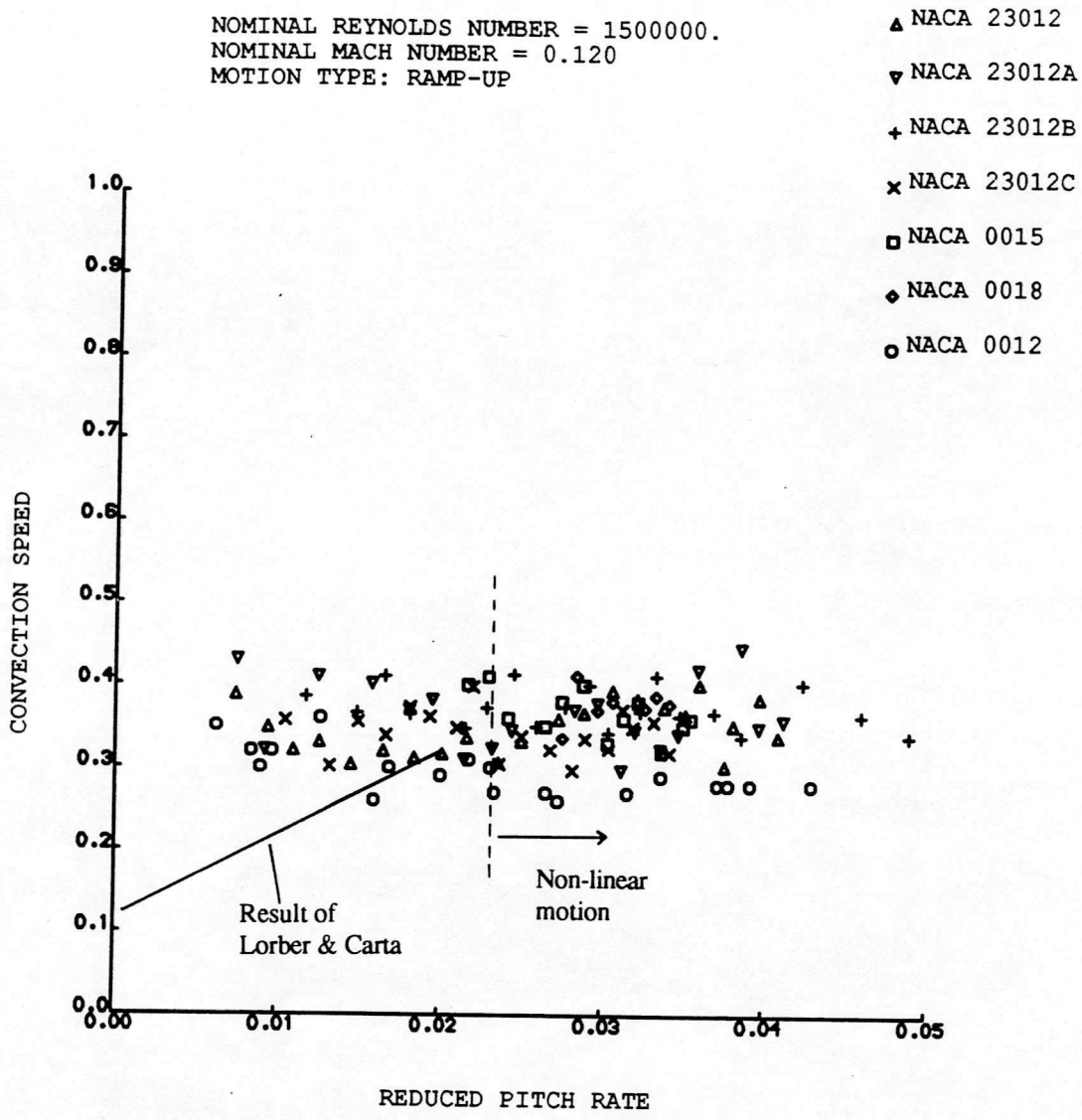

Fig. 2.43 The Collected Stall Vortex Convection Speed Data For Ramp-up Motion. Lorter & Carta's (1987) Results Is Shown By The Solid Line

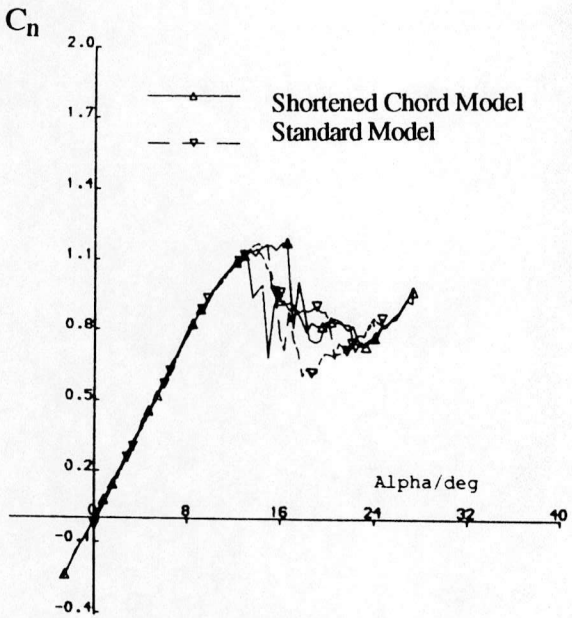

Fig. 2.44 C_n plotted against a static test for sandard model and shortened chord model at Re = 1.0 *10^6

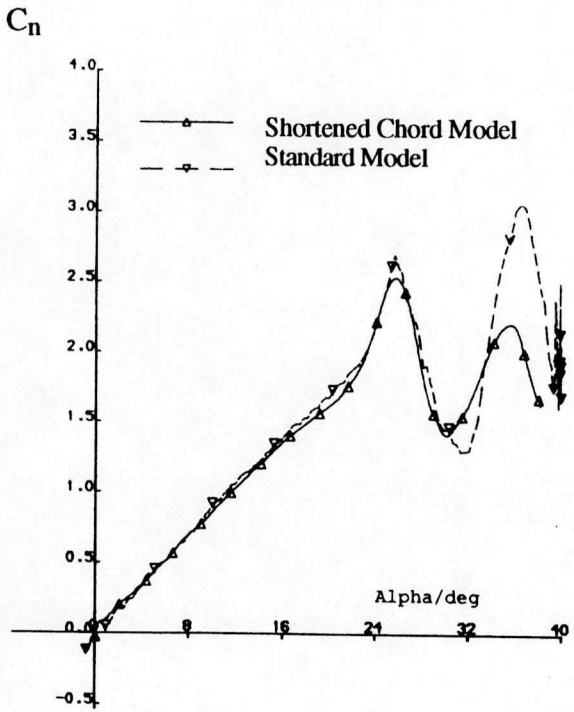

Fig. 2.45.a. C_n plotted against α for standard model and shortened chord model at Re = 1.0 *10^6 and reduced pitch rate 0.018

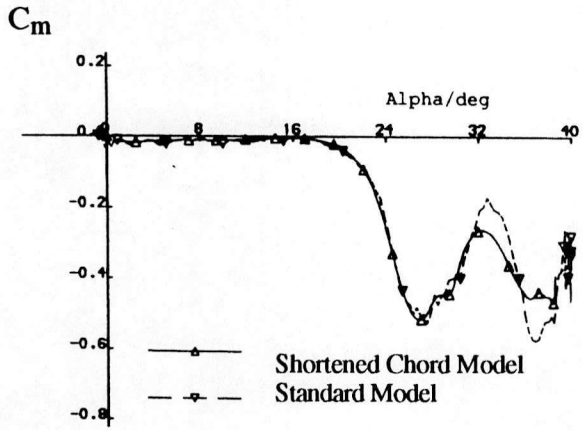

Fig. 2.45.b. C_m plotted against α test condition as for Figure a

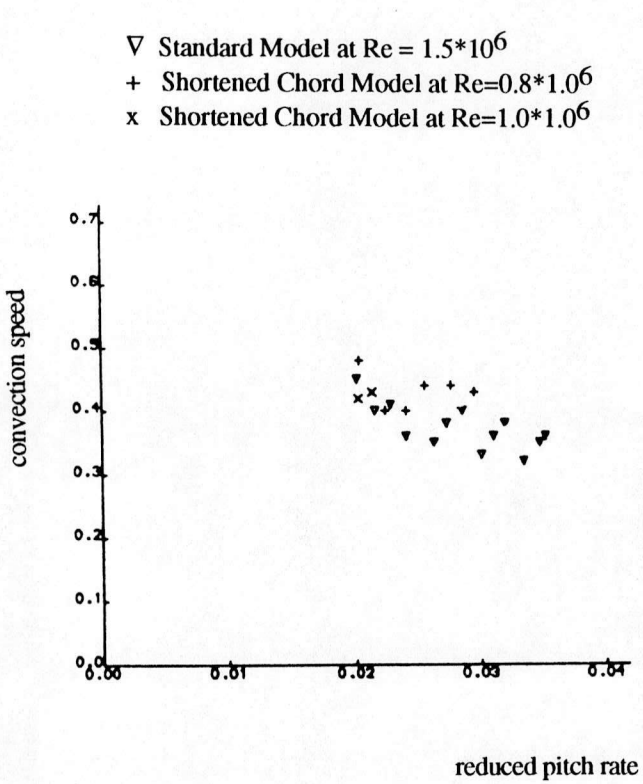

Fig.2.46 Small vortex convection speed plotted as a function of reduced pitch rate for the NACA 0015

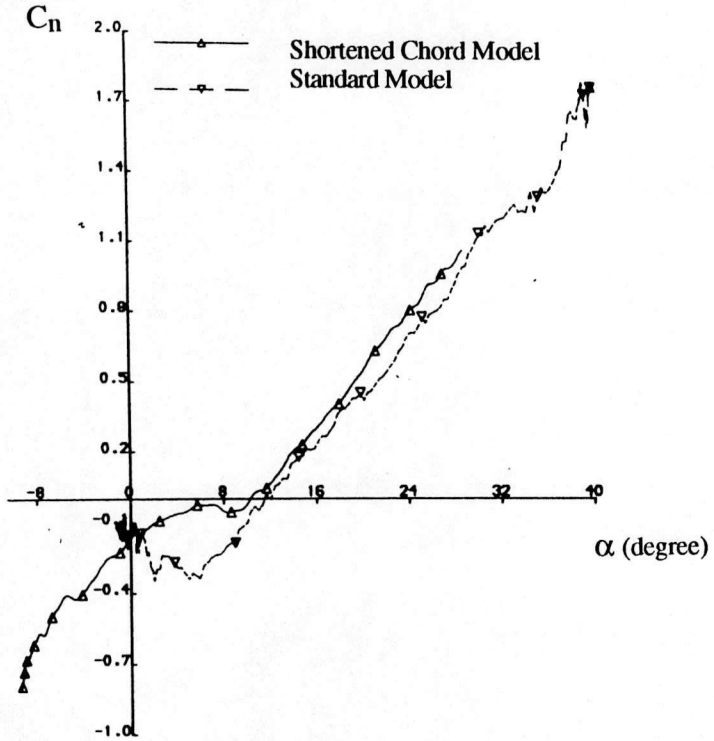

Fig. 2.47 C_n plotted against α for ramp-up motion at reduced pitch rate -0.031.standard model and shortened chord model at Re = 1.0 *10^6

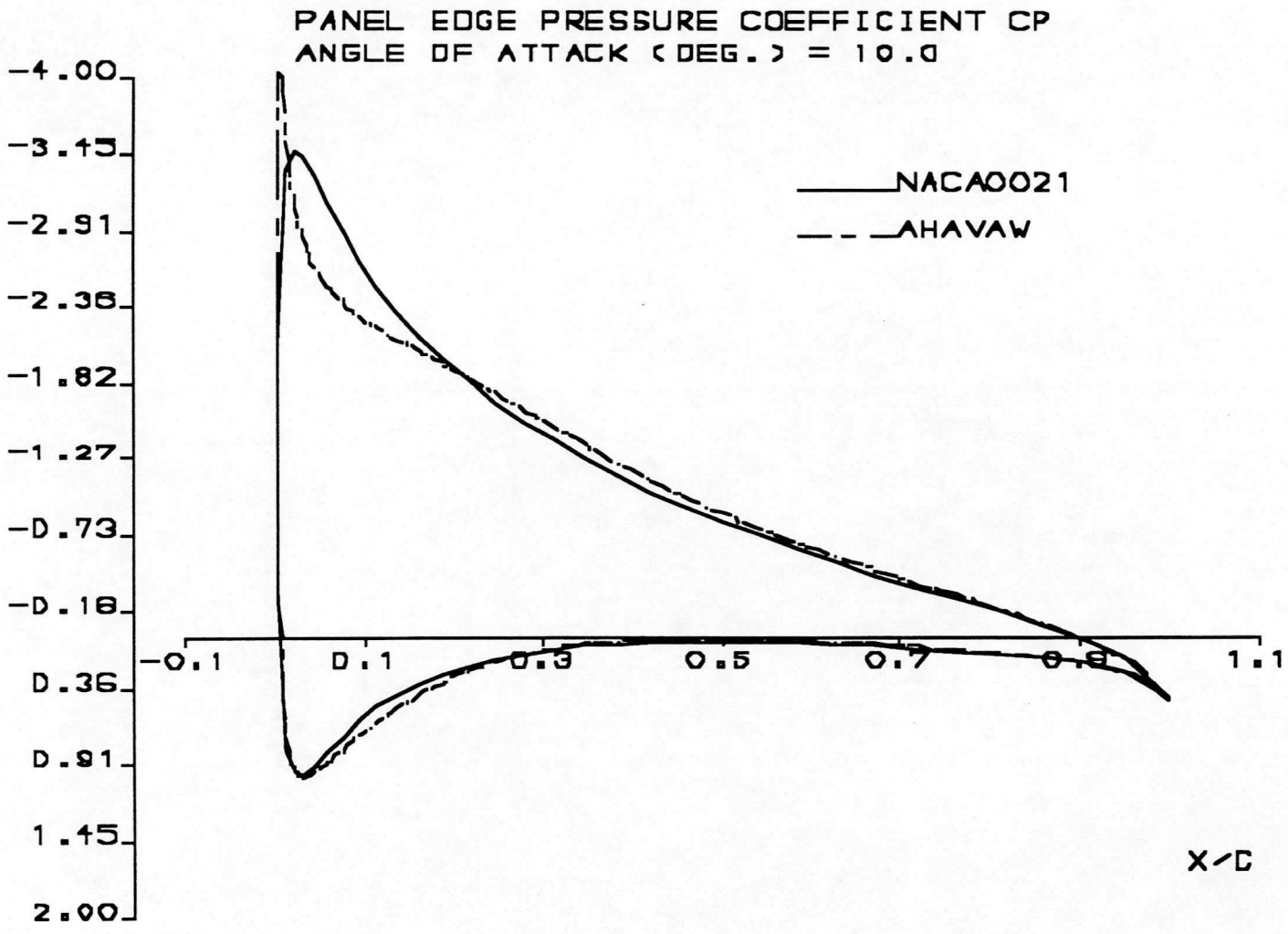

Fig. 2.48 The pressure distribution on panels of AHAVAW

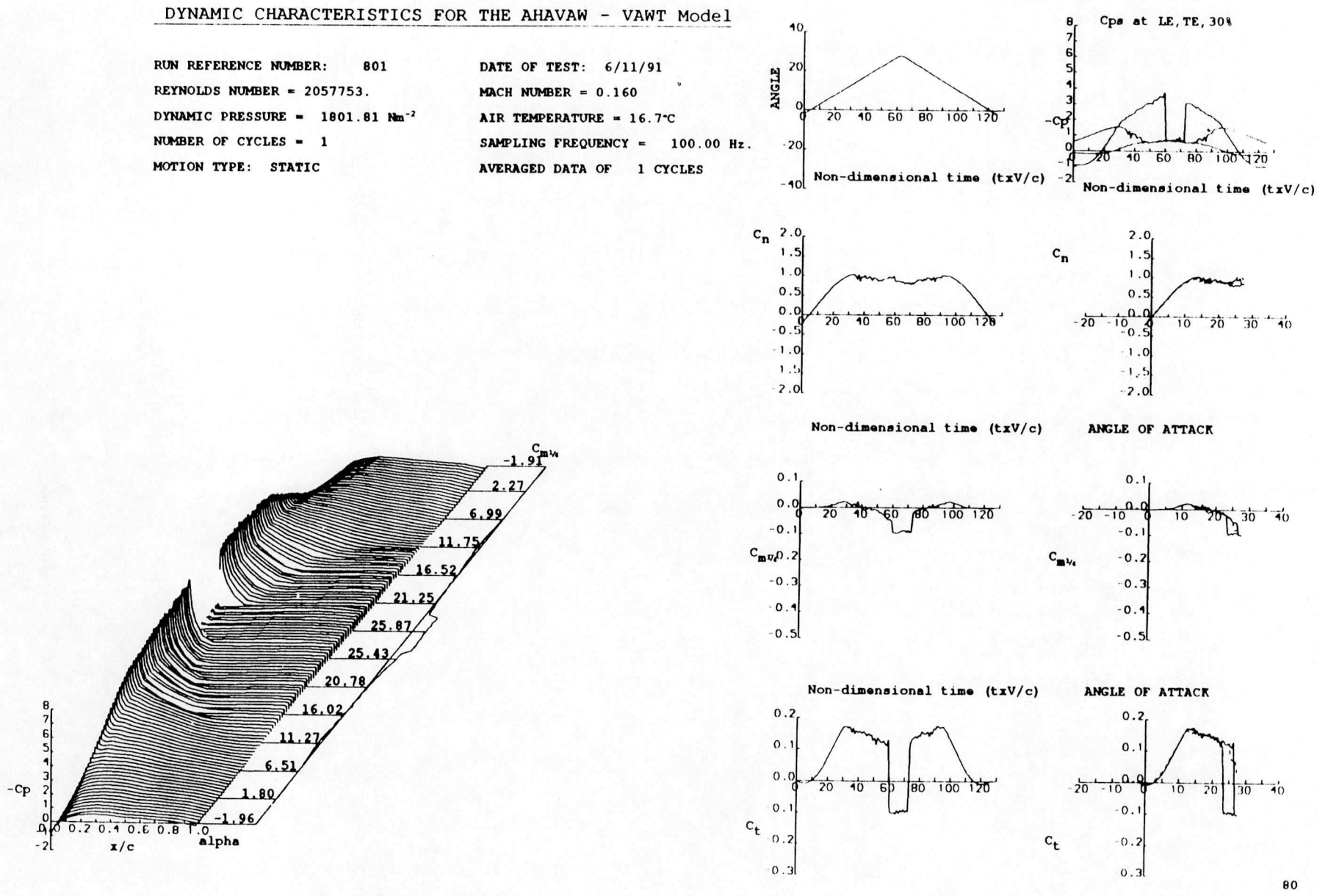

Fig. 2.49 Dynamic characteristics for the AHAVAW - VAWT model
(Static experiment)

DYNAMIC CHARACTERISTICS FOR THE NACA 0021

RUN REFERENCE NUMBER: 72
REYNOLDS NUMBER = 1893969.
DYNAMIC PRESSURE = 1724.46 Nm^{-2}
NUMBER OF CYCLES = 1
MOTION TYPE: STATIC

DATE OF TEST: 12/1/88
MACH NUMBER = 0.155
AIR TEMPERATURE = 26.2℃
SAMPLING FREQUENCY = 100.00 Hz.
AVERAGED DATA OF 1 CYCLES

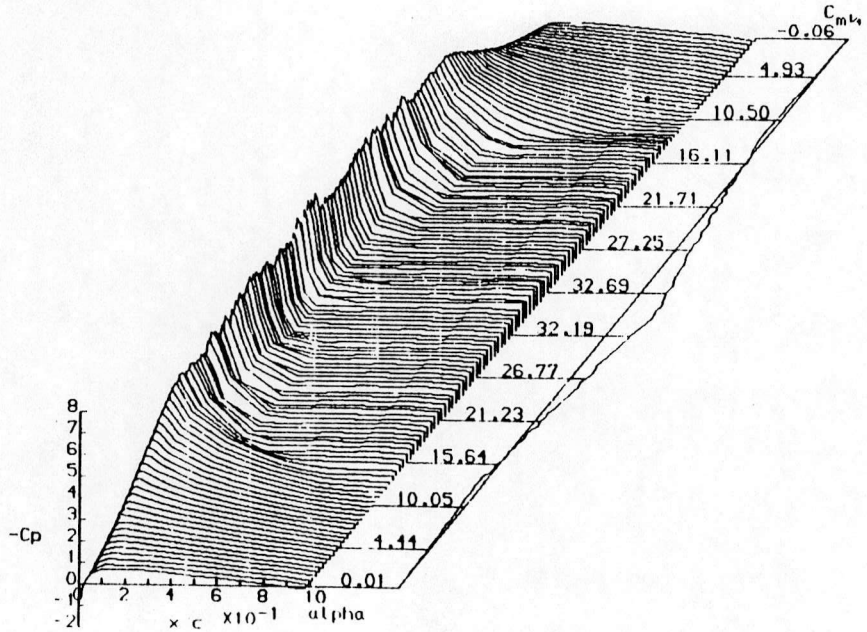

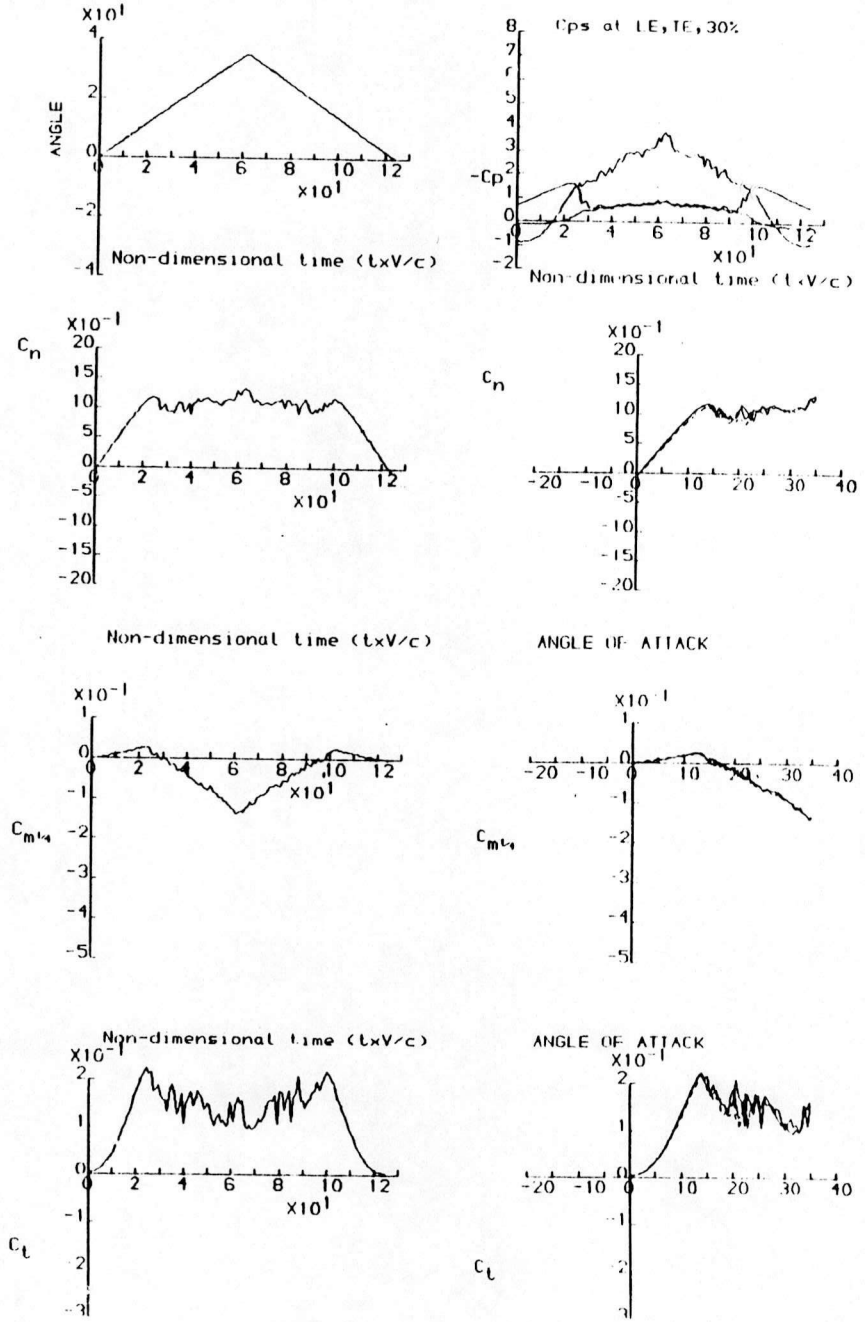

Fig. 2.50 Dynamic characteristics for the NACA0021 model
(Static experiment)

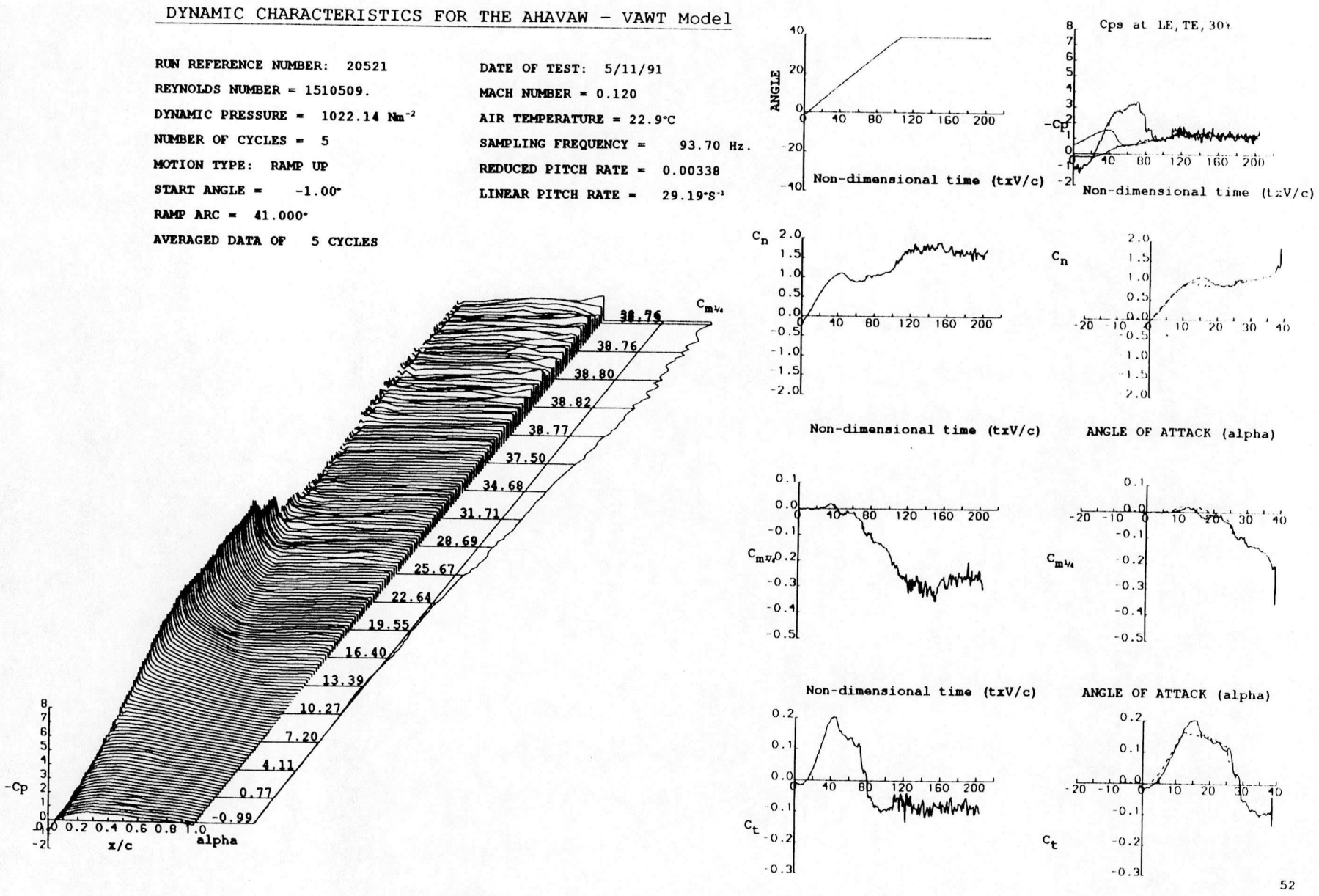

Fig. 2.51 Dynamic characteristics for the AHAVAW - VAWT model
(Ramp-up experiment)

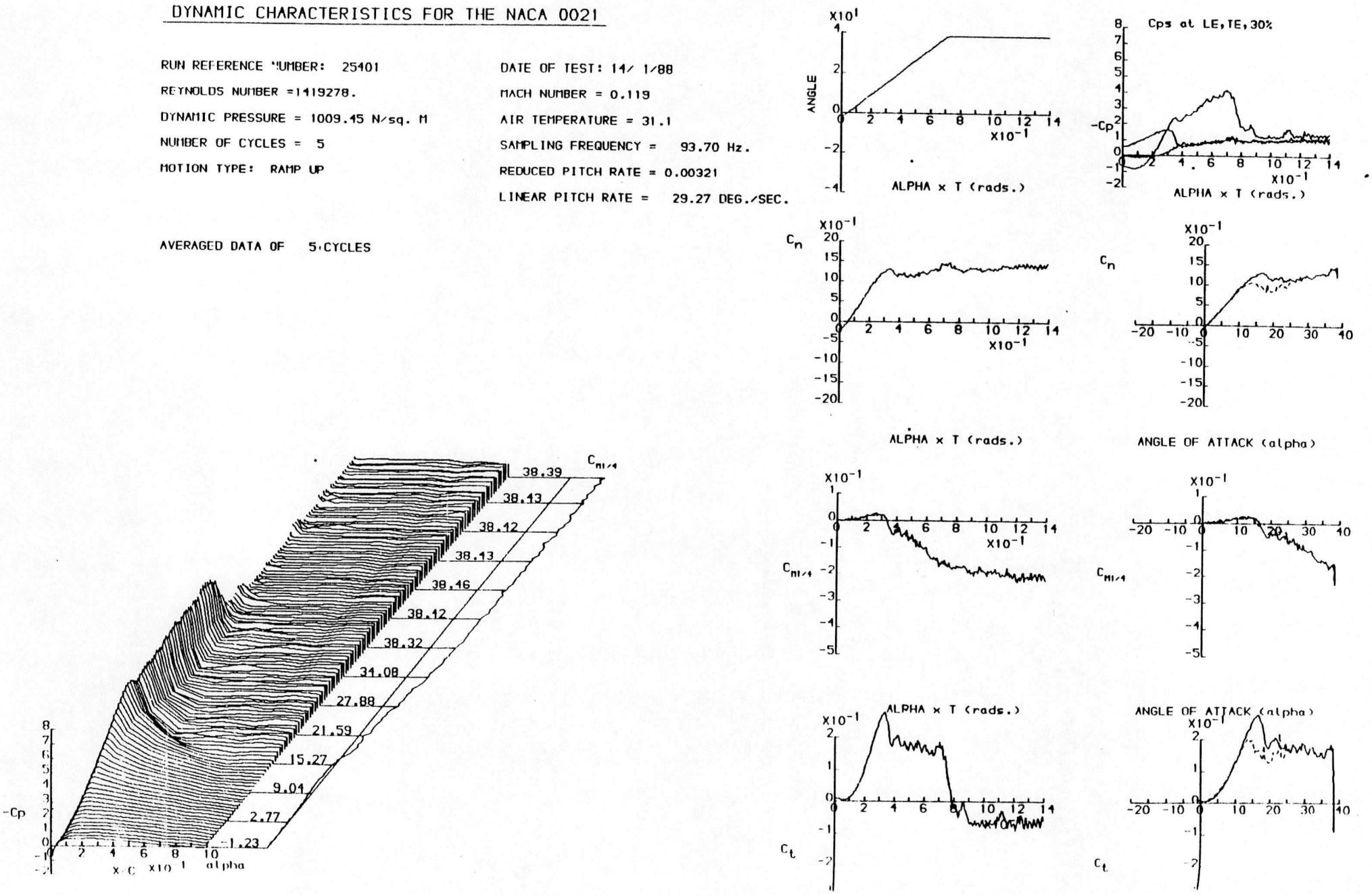

Fig. 2.52 Dynamic characteristics for the NACA0021 model
(Ramp-up experiment)

TABLE 2.1

Name of Aerofoil	NACA0018	GUVA3	GUVA4	GUVA5	GUVA6	GUVA7	GUVA8	GUVA9	GUVA10
velocity distribution parameter A	4	1.0	2.0	2	1.5	1.6	1.5	1.1	combination of GUVA9 & NACA0018
B	7	2	2	2	3.5	6.	7.4	7.45	
C	3.2	3	2.82	3.04	3	3	2.9	2.7	
D	0	0	0	0	0	0	0	0	
E	6	9.7	9	9 2	9.0	8.88	8.933	9.618	
T_{max}/C	0.18	0.18	0.18	0.18	0.18	0.18	0.18	0.18	0.18
X_{tmax}/C	0.3078	0.298	0.287	0.2978	0.300	0.309	0.3094	0.305	0.305
$dC_l/d\alpha$	0.1251	0.1237	0.1241	0.1238	0.1241	0.1244	0.1245	0.1245	0.1245
α_{ss}	13.0526	11.053	10.20	10.10	10.20	10.50	10.9500	10.50	11.20
S_1	0.60755	0.8363	0.4782	0.9092	0.8496	0.7398	0.9006	0.6146	0.3259
S_2	1.4166	1.950	1.115	2.120	1.981	1.725	2.100	1.433	0.76
$\triangle\alpha_{ds}$	0.000°	-1.5°	-3.5°	-2.25°	-2.25°	-2.25°	-1.63°	-2.83°	-3.0°
C_{tmax}	0.282	0.19	0.20	0.186	0.186	0.198	0.199	0.20	0.21

TABLE 2.2 Coordinates of NACA0018 and GUVA10

	NACA0018	GUVA10
X	Y	Y
1.00000	0.00189	0.00189
0.95093	0.01191	0.01191
0.90198	0.02134	0.02134
0.85327	0.03021	0.03021
0.80491	0.03853	0.03853
0.75702	0.04630	0.04630
0.70972	0.05353	0.05353
0.66311	0.06020	0.06020
0.61732	0.06628	0.06628
0.57244	0.07175	0.07175
0.52860	0.07657	0.07657
0.48590	0.08071	0.08071
0.44443	0.08413	0.08413
0.40430	0.08680	0.08680
0.36561	0.08868	0.08868
0.32844	0.08976	0.08986
0.29289	0.09001	0.08997
0.25905	0.08943	0.08887
0.22699	0.08801	0.08624
0.19679	0.08578	0.08232
0.16853	0.08275	0.07748
0.14227	0.07895	0.07193
0.11808	0.07442	0.06582
0.09601	0.06921	0.05928
0.07612	0.06337	0.05243
0.05846	0.05694	0.04537
0.04306	0.05000	0.03823
0.02997	0.04258	0.03112
0.01921	0.03475	0.02416
0.01082	0.02654	0.01750
0.00482	0.01799	0.01131
0.00120	0.00914	0.00567
0.00000	0.00000	0.00000